UNIVERSITA' DEGLI STUDI DI PADOVA
Department of Civil, Environmental and Architectural Engineering

MSc in Environmental Engineering

Soil, Water and Environment

Numerical investigation through OpenFOAM of an innovative anchoring solution of tethered ocean energy devices for design and environmental mitigation purposes

Supervisor: Ch.mo Prof. Ing. Luca Martinelli

Student: Carolina Ghezzo

ACCADEMIC YEAR 2021-2022

LIST OF CONTENTS

LIST OF FIGURES

ABSTRACT

The purpose of this thesis is to present a numerical survey, carried out using OpenFOAM, of an innovative anchoring solution of tethered ocean energy devices in order to evaluate design and environmental mitigation aspects.

The case examined is about the tidal energy converter GEMSTAR, placed in the Strait of Messina: the anchoring system proposed consists of a DWA, dead weight anchor, to which two tense cables are attached in order to bind the device to the anchor itself.

Thanks to the simulations carried out through OpenFOAM, it was possible to observe the hydrodynamics variations near the seabed due to the presence of the anchor, and consequently evaluate the possible repercussions in terms of actions of the current, which the structure on the bottom will have to withstand, and in environmental terms.

RIASSUNTO

Lo scopo di questa tesi è quello di presentare un'indagine numerica, realizzata utilizzando OpenFOAM, di una soluzione innovativa per l'ancoraggio di dispositivi di energia oceanica tirantati al fine di valutare aspetti progettuali e di mitigazione ambientale.

Il caso preso in esame è quello del convertitore di energia mareale GEMSTAR nello Stretto di Messina, per quale è stato proposto un sistema di ancoraggio costituito da una DWA, ovvero ancora a peso morto, alla quale sono fissati due cavi tesi che legano il dispositivo all'ancora stessa.

Grazie alle simulazioni svolte con OpenFOAM è stato possibile osservare le variazioni nell' idrodinamica nei pressi del fondale dovute alla presenza dell'ancora, e di conseguenza valutare le possibili ripercussioni in termini di azioni della corrente, che la struttura sul fondo dovrà sopportare, ed in termini ambientali.

Chapter I

TIDES

This chapter provides a brief overview on the theory of tide movements, specifically the main causes and the different types of tides will be dealt with.

1.Tides

Tide is the phenomenon consisting in the periodic rising and lowering of the level of the seas and oceans, caused mainly by the gravitational attraction of the Moon and the Sun on the water masses of the Earth and the rotation of the Earth itself.

Secondary factors that influence the tide are: the conformation of the coast, the width of the bay, the depth of the seabed, the winds and atmospheric pressure.

Tides originate in the oceans and progress toward the coastlines where they appear as the rise and fall of the sea surface, and two phases are distinguishable:

- **high tide:** the phase corresponding to the maximum elevation of the sea level;
- **low tide:** the phase corresponding to the maximum lowering.

The difference in height between the high tide and the low tide is called **tidal range**, while the horizontal movement of water that often comes with the rising and falling of the tide is called **tidal current**: precisely the flood current is the incoming tide along the coast and into the bays and estuaries; the ebb current is the outgoing tide.

In the open ocean, tidal currents are relatively weak. Near estuary entrances, narrow straits and inlets, the speed of tidal currents can reach up to several kilometers per hour.

To predict the actual tidal variations in sea level at any location, the amplitude (size) and phase (timing), also known as the tidal constants.

What Causes Tides?

Let’s see more in details what causes tides and which factors have an influence on them.

Equilibrium theory

Numerous theories exist to explain the origin of ocean tides, but one of the most known is the equilibrium theory by Issac Newton (1687).

Gravity is one major force that creates tides and Newton explained that through the law of universal gravitation. This law states that the gravitational attraction between two bodies is directly proportional to their masses, and inversely proportional to the square of the distance between the bodies. Therefore, the greater the mass of the objects and the closer they are to each other, the greater the gravitational attraction between them.

$$F = G\frac{m_1 * m_2}{r^2}$$

Tidal forces are based on the gravitational attractive force, and more precisely tidal generating forces are inversely proportional to the cube of the distance between the celestial body, which generates the tide, and the Earth, so the distance is usually more critical than their masses.

Knowing that the sun is 27 million times larger and 390 times further from the Earth than the moon, the sun's tidal generating force is reduced by 390^3 (about 59 million times) compared to the tide generating force of the moon.

Therefore, the sun's tide-generating force is about half that of the moon, and the moon is the celestial body that the most affects the Earth's tides.

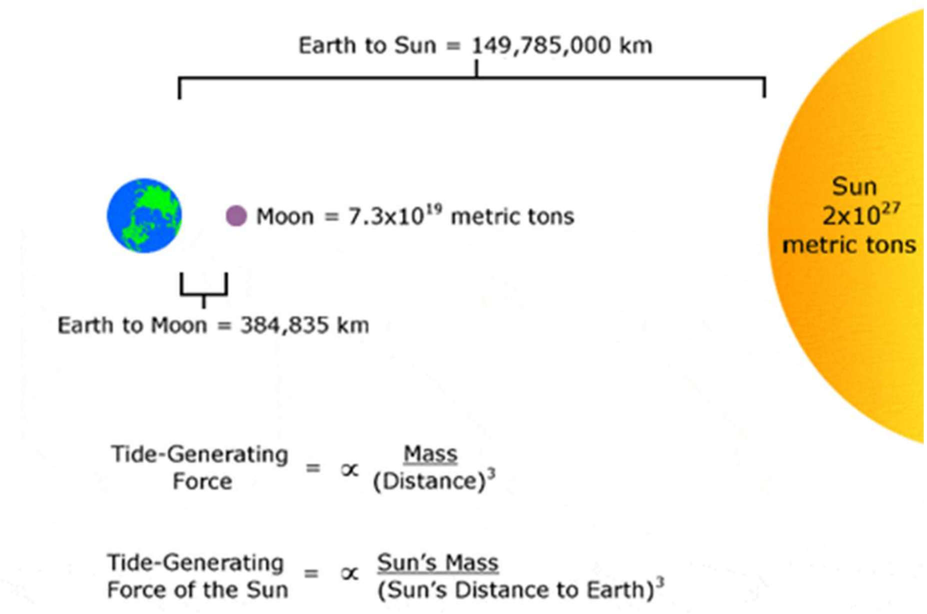

Figure 1:Masses and distances of the Earth-Moon-Sun system

Considering only the Moon-Earth system, it's known that the Earth and the Moon, while attracting each other, revolve around their common center of gravity. Due to the greater mass of the Earth, the center of gravity of the Earth-Moon system is located inside the Earth. Thus two types of force are produced:

- **Centrifugal force** that works outward from the center and it is due to the rotation around the common center of mass;
- **Centripetal force** that works towards the center and it's provided by the gravitational attraction between the Moon and the Earth.

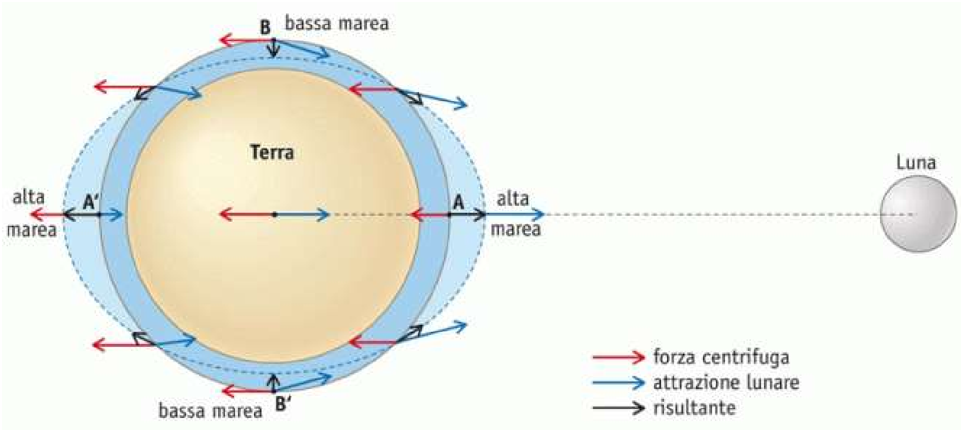

Figura 2:Scheme of the centrifugal and centripetal forces that characterize the Earth-Moon system

At the center of the Earth, the centripetal and centrifugal forces are exactly the same. The centrifugal force is similar at all points on the Earth's surface, while the gravitational attraction between the Earth and the moon varies and is strongest on the side of the Earth that faces the moon, because it is the closest. Since the gravitational force works by attracting the water closer to the moon and the centrifugal force attempts to hold the water in place, when the gravitational force overcomes the centrifugal force, the water is pulled towards the moon, causing a "bulge" of water on the side facing the moon (A). On the opposite side of the Earth, the farthest side, the gravitational attraction of the moon is less because it is further away, so the centrifugal force overcomes the gravitational force and a second bulge is generated (A ').

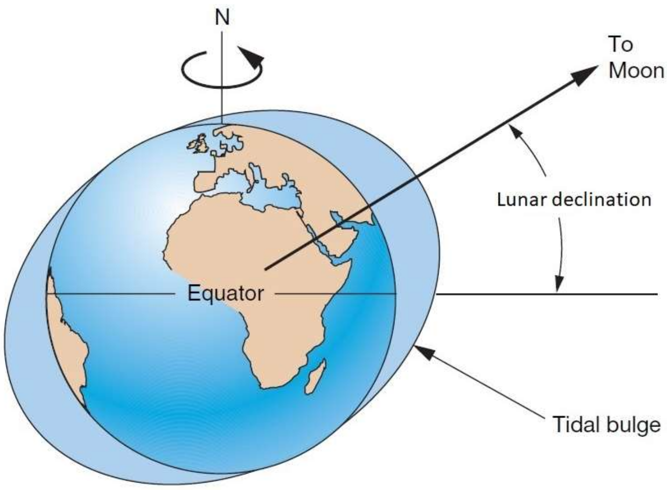

Figure 3:Scheme with lunar declination and the two "bulges" aligned with the Moon

Being the water a fluid, as the Earth rotates, the two bulges remain aligned with the moon. As the moon rotates around the Earth, its angle increases and decreases in relation to the equator: this is known as **lunar declination**, and the two tidal bulges follow the changes in the lunar declination by also increasing or decreasing their angles to the equator. Similarly, there is the **sun declination** because the sun relative position to the equator changes during a year as the Earth rotates around it, effecting seasons and tides. Hence as the angles of these two celestial bodies in relation to the Earth increase and decrease, so do the tidal bulges.

The Sun's influence

As previously said the moon is a major influence on the Earth's tides, but the sun also generates considerable tidal forces.

Solar tides are about half as large as lunar tides and are expressed as a variation of lunar tidal patterns, not as a separate set of tides.

During full or new moons, when the sun, moon, and Earth are in alignment, the solar tide has an additive effect on the lunar tide: the gravitational pull of the sun is added to the gravitational pull of the moon on Earth, causing the oceans to bulge a bit more than usual, and so creating extra-high high tides, and very low, low tides, both called **spring tides**. The position of the Sun, the Moon and the Earth in a straight line is called syzygy.

One week later, when the sun and moon are at right angles to each other, the bulge of the ocean caused by the sun partially cancels out the bulge of the ocean caused by the moon, producing moderate tides called **neap tides**, meaning that high tides are a little lower and low tides are a little higher than average. When Sun, the Earth and the Moon are in a position of a right angle, this position is called quadrature. Neap tides occur during the first and third quarter moon, when the moon appears "half full."

During each lunar month, two sets of spring tides and two sets of neap tides occur.

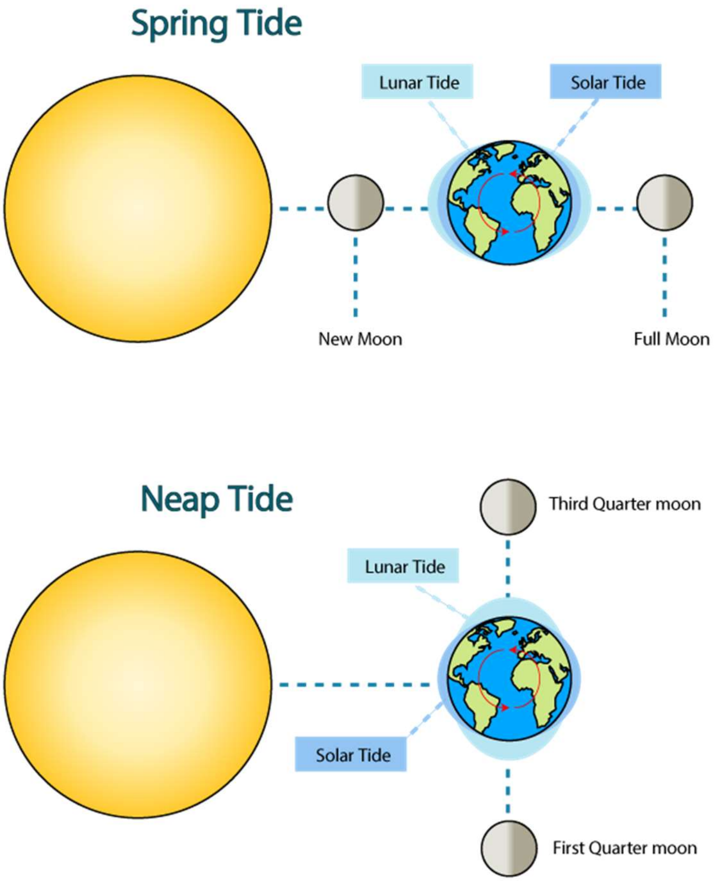

Figure 4:Spring tide and neap tide diagram

Perigee and Apogee tides

Another factor to take in consideration is the distance of the sun, moon and Earth between one another.

The elliptical orbits of the moon around the Earth and the Earth around the sun have a substantial effect on the Earth's tides. Once a month, at perigee, when the moon is closest to the Earth, tide-generating forces are higher than usual, producing above average ranges in the tides. About two weeks later, at apogee, when the moon is farthest from the Earth, the lunar tide-raising force is smaller, and the tidal ranges are less than average. Similarly, when the Earth is closest to the sun (perihelion), tidal ranges are enhanced. At aphelion, when the Earth is furthest from the sun, tidal ranges are reduced.

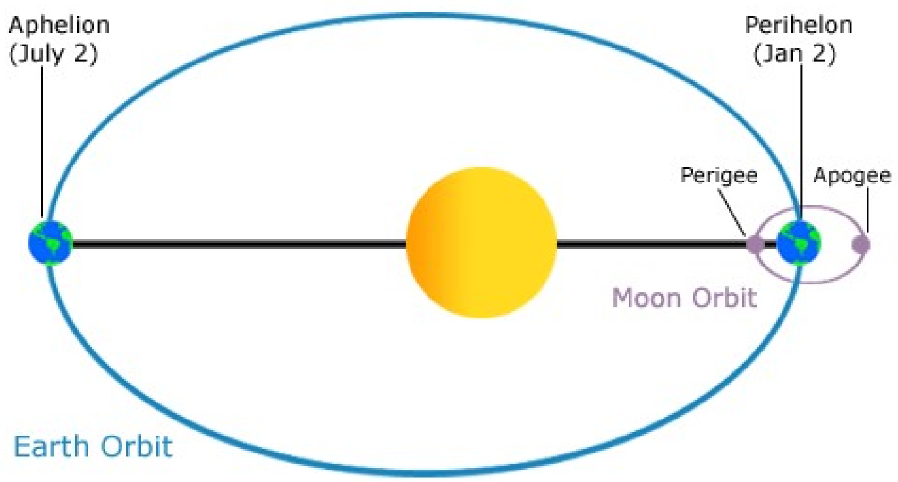

Figure 5:Apogee and Perigee tide diagram

Tidal frequency

Most coastal areas, with some exceptions, experience two high tides and two low tides every day. A lunar day lasts 24 hours and 50 minutes because the moon revolves around the Earth in the same direction that the Earth is rotating on its axis, and it takes the Earth an extra 50 minutes to catch up to the moon. Since the Earth rotates through two tidal "bulges" every lunar day, coastal areas experience two high and two low tides every 24 hours and 50 minutes. High tides occur 12 hours and 25 minutes apart, taking six hours and 12.5 minutes for the water at the shore to go from high to low, and then from low to high.

Types of Tidal Cycles

If the Earth were a perfect sphere without large continents, all areas on the planet would experience two equally proportioned high and low tides every lunar day. The large continents on the planet block the westward passage of the tidal bulges since the Earth rotates from west to east and hence the tide center shifts westward. Unable to move freely around the globe, the tides establish complex patterns within each ocean basin.

Three basic tidal patterns occur along the Earth's major shorelines:

- Diurnal tide cycle: an area that experiences one high and one low tide every lunar day. Many areas in the Gulf of Mexico experience these types of tides.
- Semidiurnal tide cycle: an area that experiences two high and two low tides of approximately equal size every lunar day. Many areas on the eastern coast of North America experience these tidal cycles.

- Mixed Semidiurnal tide cycle: an area that experiences two high and two low tides of different size every lunar day. Many areas on the western coast of North America experience these tidal cycles.

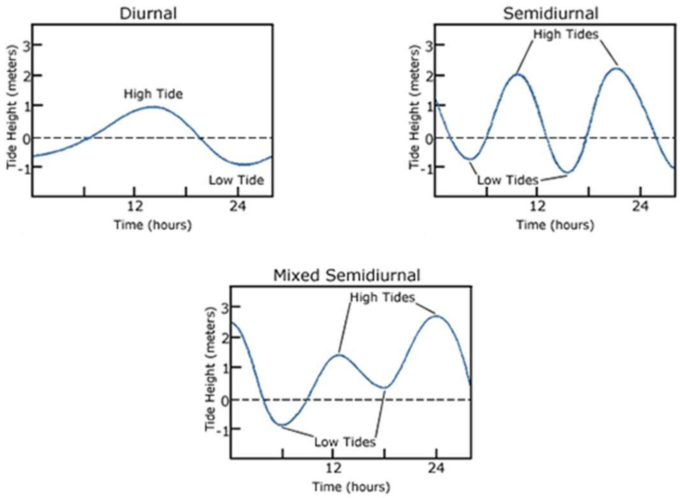

Figure 6:Diagram of the three basic tidal models: diurnal, semi-diurnal, mixed semi-diurnal tidal cycle

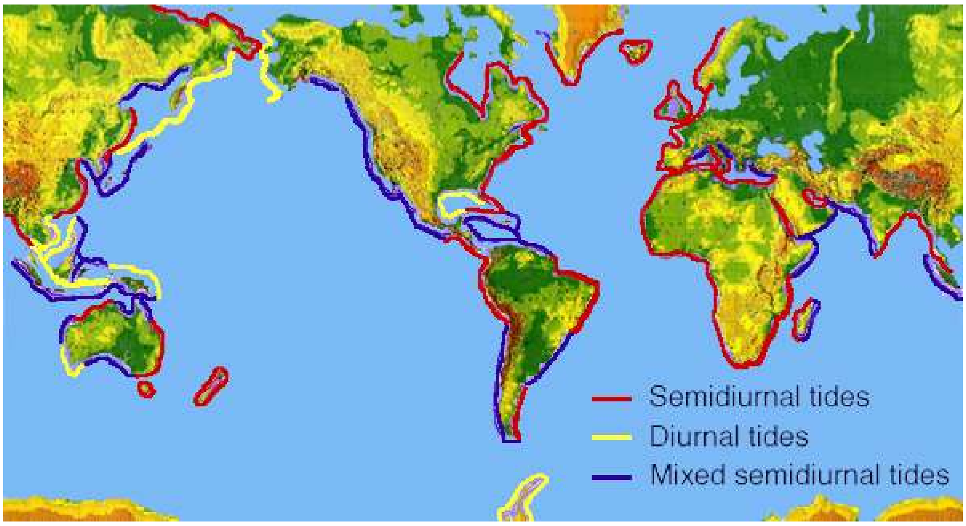

Figure 7:Planisphere of the distribution of the three types of tidal cycles on the coasts

Chapter II

TIDAL ENERGY CONVERTER (TEC)

This chapter provides a brief overview of the different types of tidal energy converters currently on the market. Particular attention will be given to GEMSTAR, SEAPOWER project, presenting its most important features and also providing a simple explanation of its operating principle.

2.Tidal energy converter (TEC)

Tidal energy is a form of hydropower that relies on the natural rising and falling of the sea levels.

This energy is a renewable source and one of its strength over other forms of renewable energy is that the process is entirely predictable, since the relative positions of the sun and moon can be predicted with complete accuracy, so can the resultant tide.

Tidal energy converts (TEC) are devices able to convert the energy gained from the tides into electricity. The field of tidal energy converters is still relatively young, but already a vast array of different devices and machine designs can be found on the market, each taking advantage of different principles to generate electrical energy.

There are basically two methods of generating electricity from the movement of the tides:

- **Tidal Range Devices:** these take advantage of the potential energy stored between the high and low tide levels;
- **Tidal Stream Devices:** these utilize the kinetic energy of moving water in tidal currents to generate electricity.

The main tidal energy converters are:

- Tidal barrages
- Tidal currents technologies
- Tidal fences
- Tidal kite

Let's analyze them more in details.

2.1 Tidal barrages

Tidal barrages are tidal range devices built across the mouth of a river or bay.

This technology uses a large dam structure, known as a barrage between the sea/ocean and the reservoir, that exploits the potential energy coming from the change in the height of the water level between high and low tides.

The bottom of this barrage dam is located on the sea floor with the top of the tidal barrage being just above the highest level that the water can get too at the highest annual tide. The barrage has a number of underwater tunnels allowing the sea water to flow through them in a controlled way by using "sluice gates" on their entrance and exit points.

Tidal barrages are able to generate electricity by creating a difference in the water levels either side of a dam and then passing this water difference through the turbines, fixed within the tunnels, either to fill or empty the tidal reservoir.

On incoming high tides, the water flows in one direction and fills up the tidal reservoir with sea water. On outgoing ebbing tides, the sea water flows in the opposite direct emptying it.

The three main tidal energy barrage schemes that use this water differential to their advantage are:

- Flood Generation: The tidal power is generated as the water enters a tidal reservoir on the incoming flood tide;
- Ebb Generation: The tidal power is generated as the water leaves a tidal reservoir on the ebb flow tide;
- Two-way Generation: The tidal power is generated as the water flows in both directions in and out of the reservoir during both the flood and the ebb tides.

Their environmental impacts are quite significant, not only for the landscape, but also for the substantial change in the path dynamics of the water, affecting the fish fauna of the zone. The first tidal barrage is "La Rance", situated in France.

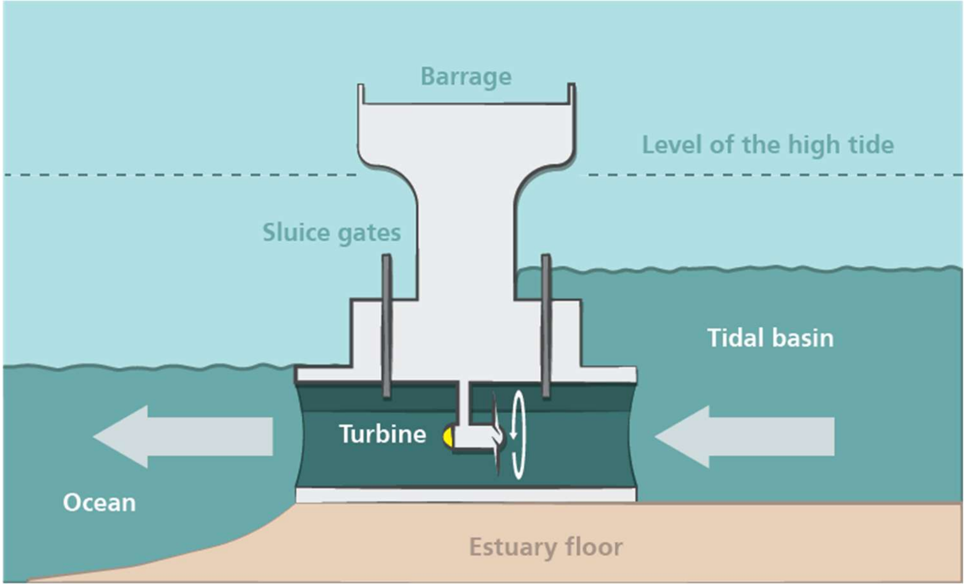

Figure 8:Section of a tidal barrage energy converter (above) and photos of the first tidal barrage, and also of the second largest tidal power station in the world, "La Rance", located in France (below)

2.2 Tidal current technologies

Tidal current technologies utilize devices that convert the kinetic energy of currents to electric power.

Tidal current devices are analogous to wind energy devices, generating energy from the rotation of a set of blades mounted on a rotor, moving thanks to the current of the fluid in which they are immersed in. The main difference is that water is 832 times denser than air and its flow speed is slower than air, so a higher amount of energy can be generated by smaller and slower turbines respect to the ones deployed for wind turbines.

Let’s see a more detailed classification of those devices:

Axial flow turbines: Axial flow turbines, also known as horizontal axis turbines, typically have two or three blades fixed on a rotor, which is oriented in the direction of flow. The axis of rotation is parallel to incoming water stream. Few examples are: SeaGEN, Open Center and Orbital O2.

Figure 9:SeaGEN (left) and Open Center (right)

Figura 10:Orbital O2

<u>Cross flow turbines</u>: Cross flow turbines, also known as vertical axis turbines, typically have two or three blades fixed on a vertical shaft which forms a rotor. The axis of rotation is perpendicular to incoming water stream. The incoming flow creates lift force to drive rotor, rotor then rotates the generator for producing power. An Italian device that utilizes this principal is the Kobold, from the company Seapower.

Figura 11:Schematic representation and photo of the Kobold TEC

<u>Oscillating hydrofoil/reciprocating devices</u>: Instead of using the rotational drive of turbine, it is also possible to capture tidal energy by using an oscillating hydrofoil. These devices make use of the lift/drag forces of the wing like hydroplane to move up and down. This mechanical energy is converted to electrical energy. Oscillating motion is controlled by changing the angle of attack relative to incoming water. Few examples are: Horizontal axis oscillating hydrofoil Stingray and Vertical axis oscillating hydrofoil BioStream.

Figure 12:Stingray (left) and BioStream (right)

To guarantee a correct functioning of the devices and an efficient production of energy, some considerations need to be done. Tidal current resources are generally largest in areas where a good tidal range exists, and where the speed of the currents are amplified by the local coastline and seabed, such as in narrow straits and inlets, around headlands, and in channels between islands, so it's necessary to find a place with favorable geographic conditions to reach an adequate range of values for the velocity of the water currents.

Additionally, the device needs to take into account the inhomogeneous distribution of velocity along the water body's depth and the current direction inversion, changing the tidal phase. The current velocity follows a logarithmic distribution along the depth: a null value at the seabed and then increasing until reaching the max value at the surface level, and to solve this issue smaller turbine blades are usually designed, in order that the current velocity's difference between the two extremities of the diameter of the turbine is not too high, or by deploying the device in deep water, with depths higher than 50 meters. Furthermore, similarly to wind turbines, the acoustic disturbance generated by the tidal current turbines devices is a problem, especially for the aquatic wildlife.

2.3 Tidal fences

The tidal fence is another form of tidal stream device. Tidal fences are composed of single vertical axis turbines that are mounted together within a single fence-like structure: tidal currents flow through the turbine blades, which in turn power generators creating electricity. Tidal fences do not block the flow of tidal water, allowing water to continually ebb and flow through it, making them cheaper to install and less impact on the environment than a solid concrete tidal barrage.

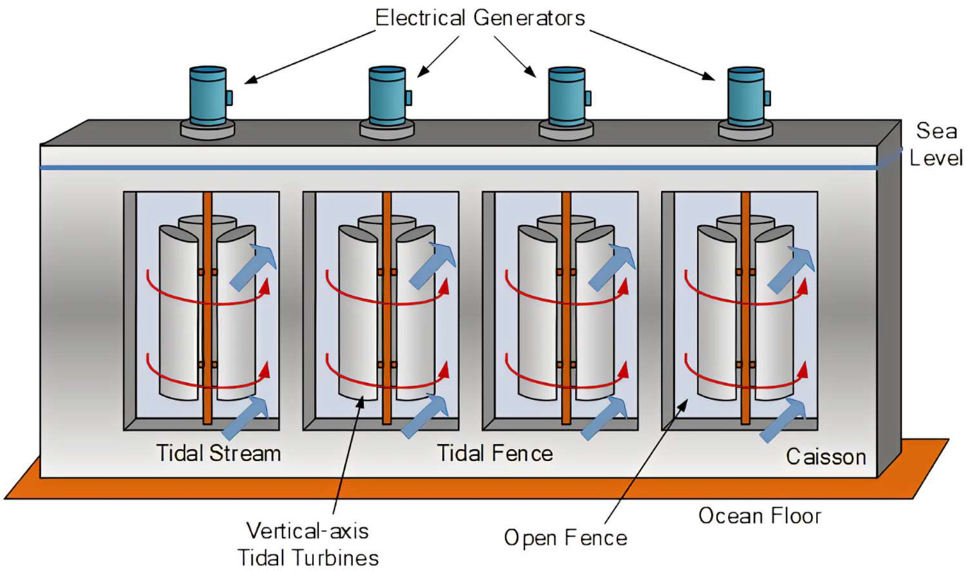

Figure 13:Tidal fence scheme

2.4 Tidal kite

Tidal kite device works in the same way as a conventional kite, but underwater. A tidal kite consists of a hydrofoil wing tethered to the seabed and which is allowed to “fly” along the oceans tidal currents. The flow of these tidal currents creates a lifting force on the wing, pushing the kite forward through the moving water. The tidal kite can be made to fly through the water, along a given trajectory, through a combination of tension in the kites tether and the use of a suitable rudder to aligning itself to the current controlling its direction. The mechanical energy of a small turbine, attached to the kite, is used to drive a generator to produce electrical energy as the kite flies through the seawater.

Other flying tidal power devices include those that resemble underwater airplanes with two counter-rotating turbines, connected to electrical generators, positioned symmetrically on either side of the body. The advantage of these types of technologies is that they are relatively cheap to produce, easy to maintain and service, have a relatively low environmental impact, and can be installed almost anywhere, sea or river. Two examples are: the Minesto tidal kite and the GEMSTAR.

Figure 14:Tidal kite Minesto

2.5 GEMSTAR

GEMSTAR (‘*Generatore Elettrico Marino, Sustainable Tethered Advanced Rotors*’) is an innovative water current energy conversion device suitable for the exploitation of tidal or ocean current energy, that has been developed in cooperation with University of Naples.

This ocean’s kite system is equipped with two fixed-pitch horizontal axis hydro turbines mounted on the sides of a supporting submerged structure that is stable in the surrounding flow during the power production. The submerged structure is supported by the buoyancy provided by a streamlined axial-symmetric floating body, placed at the top of the structure.

Figure 15:CAD Representation of GEMSTAR Single Cable Anchor (from SEAPOWER)

One of the major features is the self-alignment property of the system to the tidal current direction, meaning that the turbines’ axis are constantly and automatically kept parallel to the direction of the water flow to ensure the maximum efficiency and so being able to capture the tidal current energy in both directions of tide. This is also possible thanks to a tail that guarantee longitudinal and lateral-directional stability of the whole system.

Another peculiarity of the GEMSTAR are the two contra-rotating turbines, with three blades, attached to two electrical generators, symmetrically positioned on the two sides of the frame and two diffusers, mounted around the two turbines, shaped to double the power output.

The blades use a properly designed cavitation free airfoil section shape in order to achieve high efficiency in a wide range of operating conditions.

The electrical connection is provided through a power cable, that reaches an onshore grid connection point (or to batteries) and it is positioned along the singular or multiple mooring lines.

The GEMSTAR is held in position, at the desired depth, by means of a tethering system to the bottom.

During operation, the device behaves like a sort of submarine kite that remains fixed thanks to the balance between the thrust acting on the turbine and the structure, and buoyancy force of the hollow part of the structure. While for maintenance, GEMSTAR can be brought to the surface releasing the tension of the mooring line, allowing the floating structure to rise to the water level whilst being still attached to the mooring system.

In addition, a heading direction control system avoids the uncontrolled rotation around the vertical axis and the related possible excessive twisting of the mooring and power cables.

Thanks to the possibility of choosing the operational depth, GEMSTAR will always intercept the best quality of the current flow and its maximum velocity on the site, also allowing the vessel pass through. Detailed numerical analysis and many experimental tests have been carried on specific components to check the hydrodynamic, mechanical, and electrical performances.

Two different scaled models have been tested in the towing tank of the "Federico II" University of Naples.

Figure 16:Photo of the second 1:5 scale prototype of the GEMSTAR model

The first full-scale GEMSTAR prototype has been built by a consortium of Venetian companies and partially sponsored by Veneto Regional and has been deployed in the Venetian Lagoon on March 2012.

The final solution to be placed in the Messina Strait has a nominal power of 300 kW, that can be produced for wave currents of 2.0 m/s. For higher currents up to 3.0 m/s, the device will produce the same amount, while for extraordinary currents, the device would enter in a save mode. Globally the expected production is 900-1000 MWh per year.

Figura 17:Full-scale photo of the prototype in the Venice lagoon and detail of the turbine (from SEAPOWER)

Chapter III

AREA OF INTEREST

This chapter presents in the first part an overview of the main characteristics of the Strait of Messina. In the second part, the data on bathymetry, stratigraphy and the velocity field of the area provided by various field surveys, carried out in recent years, will be taken into consideration, in order to identify the best position in which to install GEMSTAR.

3.1 The Strait of Messina

The Strait of Messina is the marine branch that separates the island of Sicily from the Italian peninsula, precisely it is located between the eastern tip of Sicily and the western tip of Calabria. The strait is 70 km long and 10 km wide, with the narrowest passage about 3 km wide, and connects the Tyrrhenian Sea in the north with the Ionian Sea in the south (Figure 18).

The strait bottom has very irregular morpho-bathymetric features, with a shallower central saddle comprised between −70 and −90m of depth, which divides two wider and deeper subaqueous sectors. The northern Tyrrhenian exit of the strait is −100m to −400m deep, whereas the southern Ionian opposite exit reaches deeper depths to over −1000 (Figure 18).

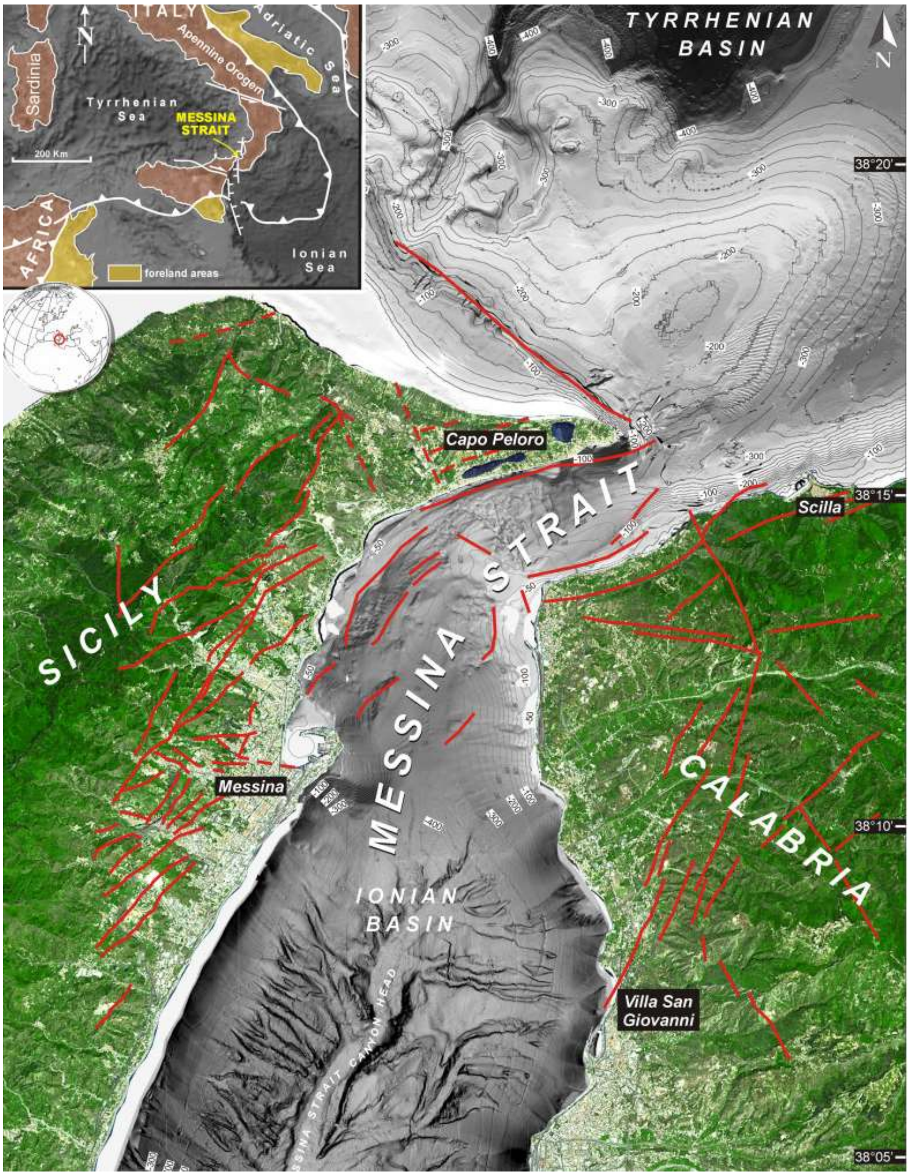

Figure 18:The Strait of Messina in the central Mediterranean Sea (inset), fault lines, revised bathymetric data of the strait floor and data for land areas

Since historical times, the Messina Strait (Figure 19A) was considered as one of the most important strategic passageway of the central Mediterranean, very well-known also because its sudden and violent strong currents, vortexes and sea-surface roughness often caused serious hazards for shipping (Figure 19B, C and D). These astonishing perturbations of the modern Messina Strait water surface inspired the myth reported in the Homer's ‘Odyssey’. Accordingly, Scylla was a six-headed sea monster hidden along the Calabrian coastal caves of the strait, whereas Charybdis was a whirlpool off the coast of Sicily. This mortal combination of the two enemies represented a dangerous passageway for brave sailors (Figure 19E).

Figure 19:(A) Panoramic-aerial view of the Strait of Messina seen from the south (B) During the inversion between the two opposite phases of flood and ebb, roughness of the sea surface can be observed in front of Capo Peloro in Sicily and further north (C), as well as vortices (D). (E) These phenomena have been attributed to sea monsters from Greek mythology

Let's see in detail some characteristic aspects of the strait.

Hydrodynamics of the strait

The tide, identified in the strait, is semi-diurnal. The strait is governed by bi-directional tidal currents flowing along the strait axis so that high tide in the Ionian Sea corresponds with low tide in the Tyrrhenian Sea and vice versa.

Every 5–6 h, a phase of high tide in the Tyrrhenian Sea corresponds with a phase of low tide in the Ionian Sea, generating ca. 17 cm/km of different elevation. This gradient of the water table between the two interconnected seas forces ca. 750.000–1.000.000m3/s of marine water to pass over the strait sill, from north to south and vice versa. The water mass is thus accelerated when it transits through the narrowest strait zone, which is also the shallowest (ca. –70m deep). This phenomenon is responsible for a specific case of tidal amplification, resulting in the generation of NE- and SE-flowing strong tidal currents in the Messina Strait with velocity picks up to $3ms^{-1}$.

Tidal currents cyclically accelerate passing through the strait central restriction and decelerate towards the strait exits, following reverse directions during each tidal phase. This hydrodynamics exert a great influence on the strait bottom, generating sediment erosion, transport and accumulation in specific subaqueous areas of the strait, shaping a great variety of subaqueous bedforms, which appear symmetrically distributed respect to the central sill.

The microtidal Messina Strait is one of the most energetic area of the central Mediterranean (Figure 20), whose complex hydrodynamics is mainly governed by the presence of a M2 amphidromic point, a point corresponding to zero tidal range of the Mediterranean Sea occurring right in the centre of the Messina Strait.

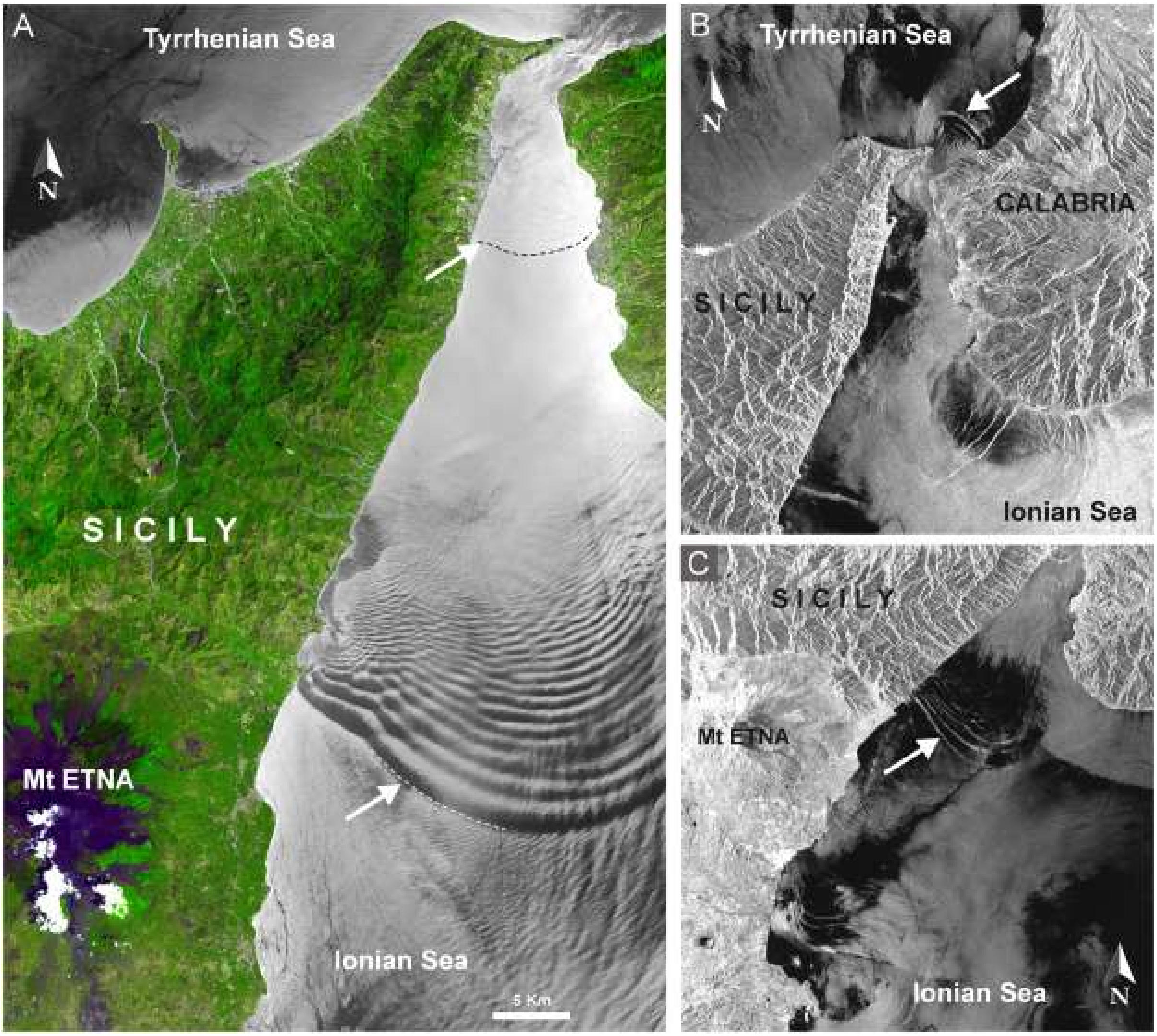

Figure 20:(A)Effect of southward tidal wave propagation on the sea surface of the Strait of Messina. The main front is indicated by the white arrow. Note a second more northerly incoming wave (arrow), separated by ca. 6 hours from the major. (B) Sea surface perturbations taken from the SAR ERS image 1 and acquired 20 minutes after the maximum northward tidal flow at Punta Pezzo (Calabria) and (C) during the opposite phase.

Water-mass stratification

The tidal hydrodynamics of the Messina Strait involves the entire water column, generating both superficial and subsurface processes. The bed-shear stress exerted by the currents on the sea bottom is unequal, due to a varied distribution of the main current vectors respect to the cross-sectional areas of the strait, as well to strong phenomena of water-mass stratification. This element is crucial in explaining the net gross sediment pathways in the Messina Strait bottom and relative bedform morphologies.

Instrumental measurements have shown differences in the water density between the Ionian and the Tyrrhenian seas: the Tyrrhenian Surface Water (TSW) is less dense than the Levantine Intermediate Water (LIW). Owing to their difference in temperature, after every semi-diurnal tidal cycle, the northward-directed LIW flood current spreads as a subsurface jet into the Tyrrhenian Sea, exerting a great potential bed-shear stress on the sediment bottom, while the southward-directed TSW ebb current propagates as a surface jet into the Ionian Sea, occupying a superficial interface layer.

Both flood and ebb flows transit across the narrowest and shallowest part of the strait with comparable average velocity values (2.1 and 2.4ms−1, respectively). However, this setting may invert during episodic seasonal stages, with the Tyrrhenian current flowing as subsurface jet beneath the Ionian one, as consequence of occasional and anomalous horizontal density distribution of the water masses.

In this setting, the north-directed flood current (LIW) represents the dominant flow controlling the strait sedimentary dynamics, over the south-directed ebb current (TSW) which, although reinforced by the tidal amplification during every passage through the strait narrowest centre, it is always weaker at the bottom than its opposite counterpart, because of the minor density. This difference impacts noticeably on the transport capacity of the two opposite flows and on their relative distance to the bottom: the LIW virtually flows in continuous contact with the sea bed, whereas the TSW interplays with the bottom during the ebb phases only in the northern reach of the strait or during episodic water-mass vertical inversions (Figure 22).

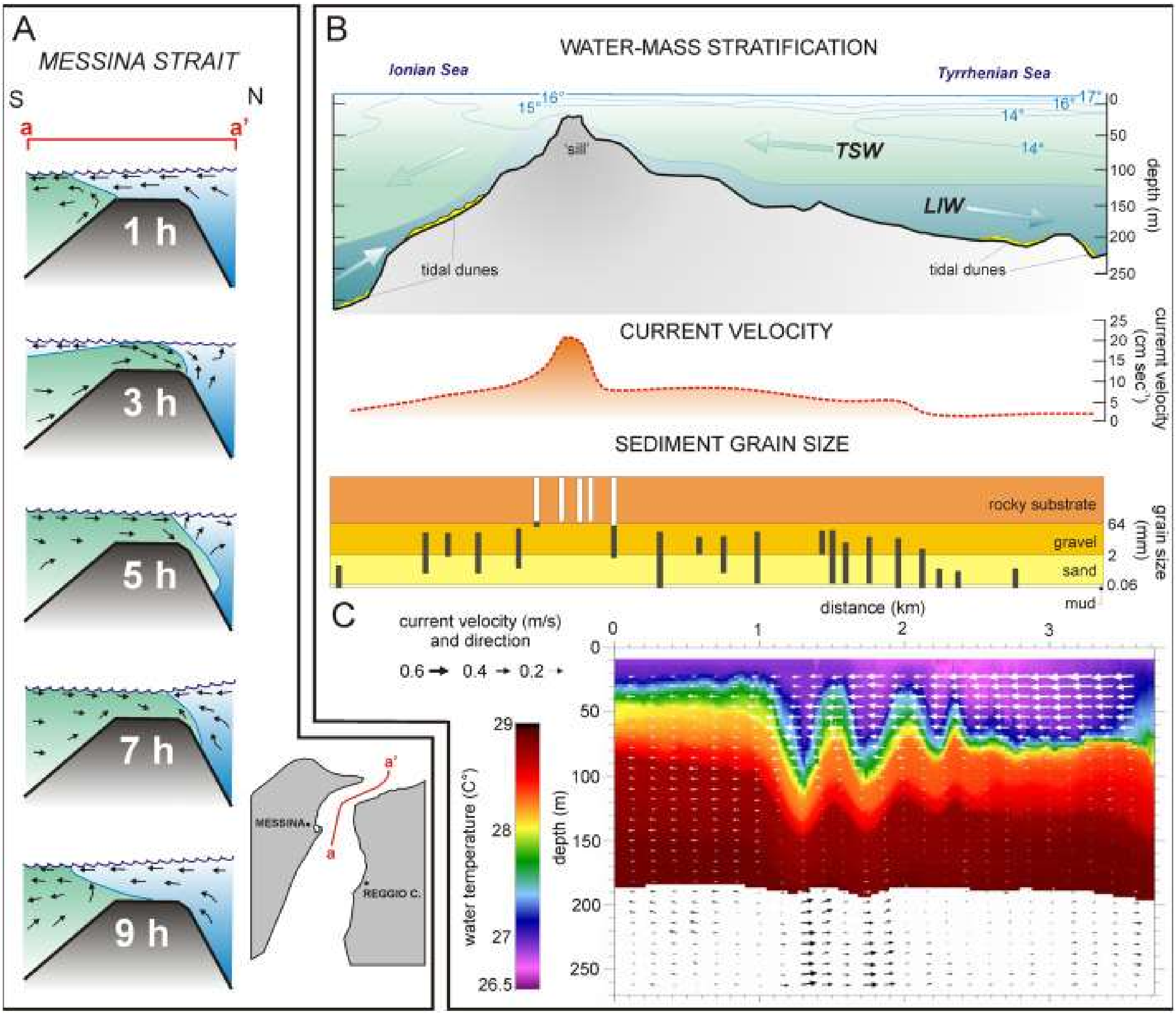

Figure 21:(A) Conceptual model of overlapping and inversion of water masses between the Tyrrhenian Surface Waters (TSW) and the Levantine Intermediate Waters (LIW), over a period of approx. 9 h and reconstructed along section a-a'. (B) Longitudinal distribution of seawater temperatures (in degrees Celsius) across the Messina Strait, sediment grain size and current velocity. (C) Temperature and direction fields across the internal wave propagating through the Strait of Messina at a depth between −0 and −250 m. Note the opposite direction of the two overlapping water masses separated by the internal waves. All profiles roughly coincide with the trace shown in (A). (image from Sergio G. Longhitano "Between Scylla and Charybdis (part 1): the sedimentary dynamics of the modern Messina Strait (central Mediterranean) as analogue to interpret the past").

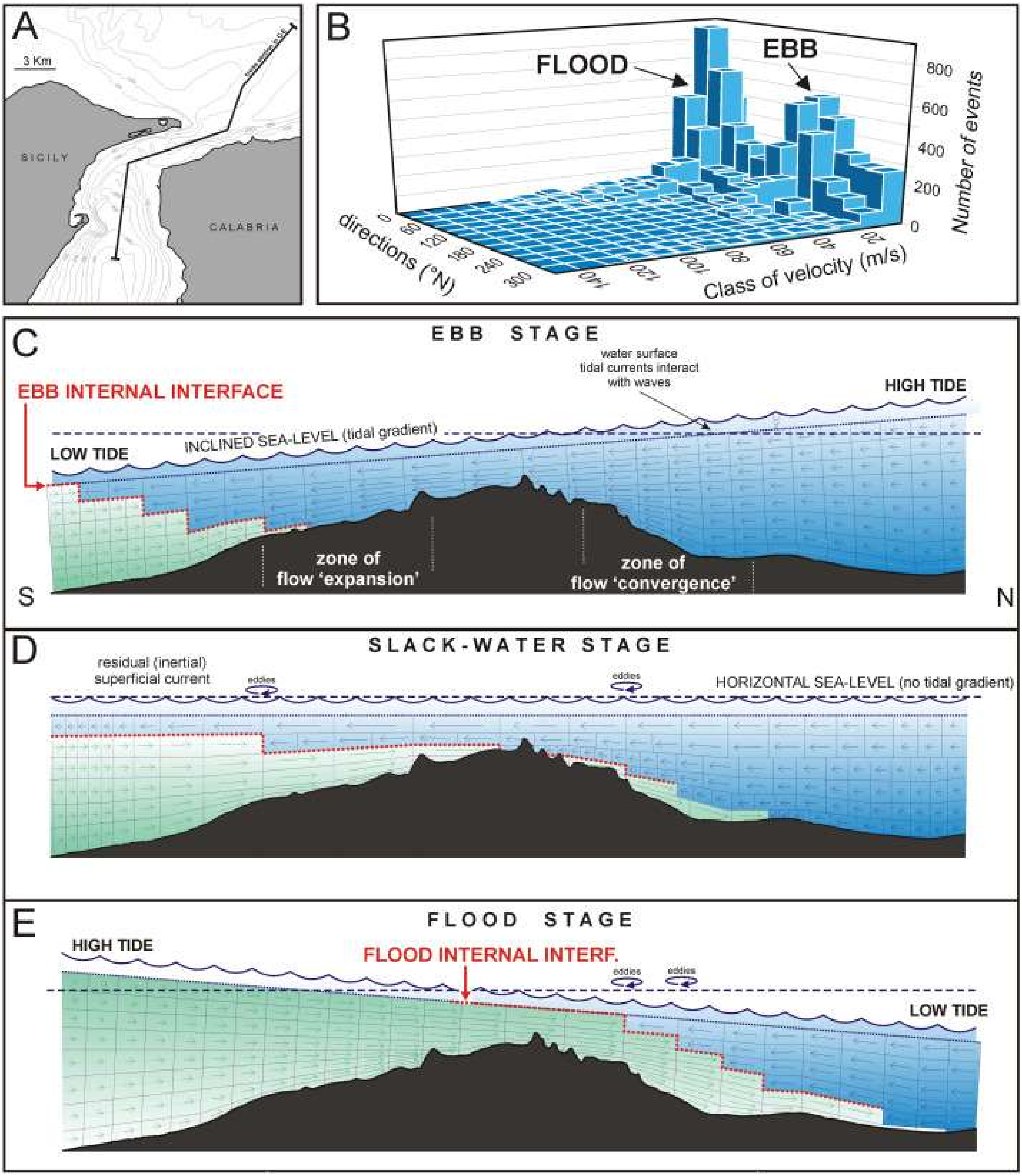

Figura 22: Schematic model (south to north) of this occurring on a stretch running the full length of the strait in the centre. In the reflux phase, the Tyrrhenian waters flow over the Ionian ones and cover the whole channel (A); after this phase the water levels of the two adjacent seas tend to reach a common level, some of the lighter waters of the Tyrrhenian still flow in a north-south direction (B); in the flood phase, the denser waters of the Ionian flow under the lighter ones, flooding the entire canal and running along the seabed into the Tyrrhenian Sea (C). (image from Sergio G. Longhitano "Between Scylla and Charybdis (part 1): the sedimentary dynamics of the modern Messina Strait (central Mediterranean) as analogue to interpret the past").

Morpho-bathymetric characteristics of the Strait of Messina

Recent multibeam-based investigations on the modern Messina Strait bottom reveal subaqueous morphobathymetric features, which allow a number of areas with specific morphologic characters and sedimentary processes to be identified:

- The 'strait-centre zone' is the narrowest and shallowest by-pass sector, where the tidal currents reach their maximum strength eroding and scouring the substrate.
- Towards NE and S, two larger 'dune-bedded zones' occur. Here, clastic sediments transported as bed load and in suspension are accumulated and continuously reworked forming characteristic bedform fields, whose features reflect complex current patterns due to a strong tidal asymmetry.
- The 'strait-end zones' represent distal depositional areas, where decelerating currents rework fine-grained smaller moribund dunes.
- The 'strait-margin zones' are diffusely characterised by mass-wasting processes along the steepest sublittoral sectors, where sediment instability are caused by earthquakes or sea storms.

The Messina Strait subaqueous sill (the strait-centre zone)

The submarine sector connecting the Ionian and the Tyrrhenian basins coincides with the narrowest segment of the Messina Strait. This 3-km-wide area is also the shallowest part of the strait centre, consists of a −70 to −110m deep sill and hosts the zone of 'tidal maxima', the zone where the tidal currents reach their maximum velocity (Figure 23A). This saddle exhibits distinct morphological features, defined as 'pinnacles' by Selli et al. (1979). They consist of a series of 50-m-wide and 100–200-m-long narrow ridges, separated by 50-m-deep parallel incisions, with a general NWSW direction of elongation (Figure 23A). Local submersible observations, integrated with recent surveys using a remotely operated vehicle, reveal a rocky substrate (Figure 23B) and remnants of lowstand, fluvio-deltaic deposits, presently subjected to erosion due to the strong currents (Figure 23C). This sector is not totally deprived of sediments, as coarse-grained deposits, here kept in suspension by the strongest tidal currents, can be entrapped within these elongate depressions or in sectors partially protected from the dominant currents (Figure 23D and E). These sediments form elongate, laterally-discontinuous residual accumulations, which mirror the form of the hosting depressions. Away from the sill, moving down current towards the two connected Tyrrhenian and Ionian basins, sediment volumes increase rapidly assuming the form of gravel dunes, lineation, furrows and ribbons (Figure 23A), as consequence of the decreased bed shear stress exerted by tidal currents, which are still able to transport in suspension sand- and mud-size particles.

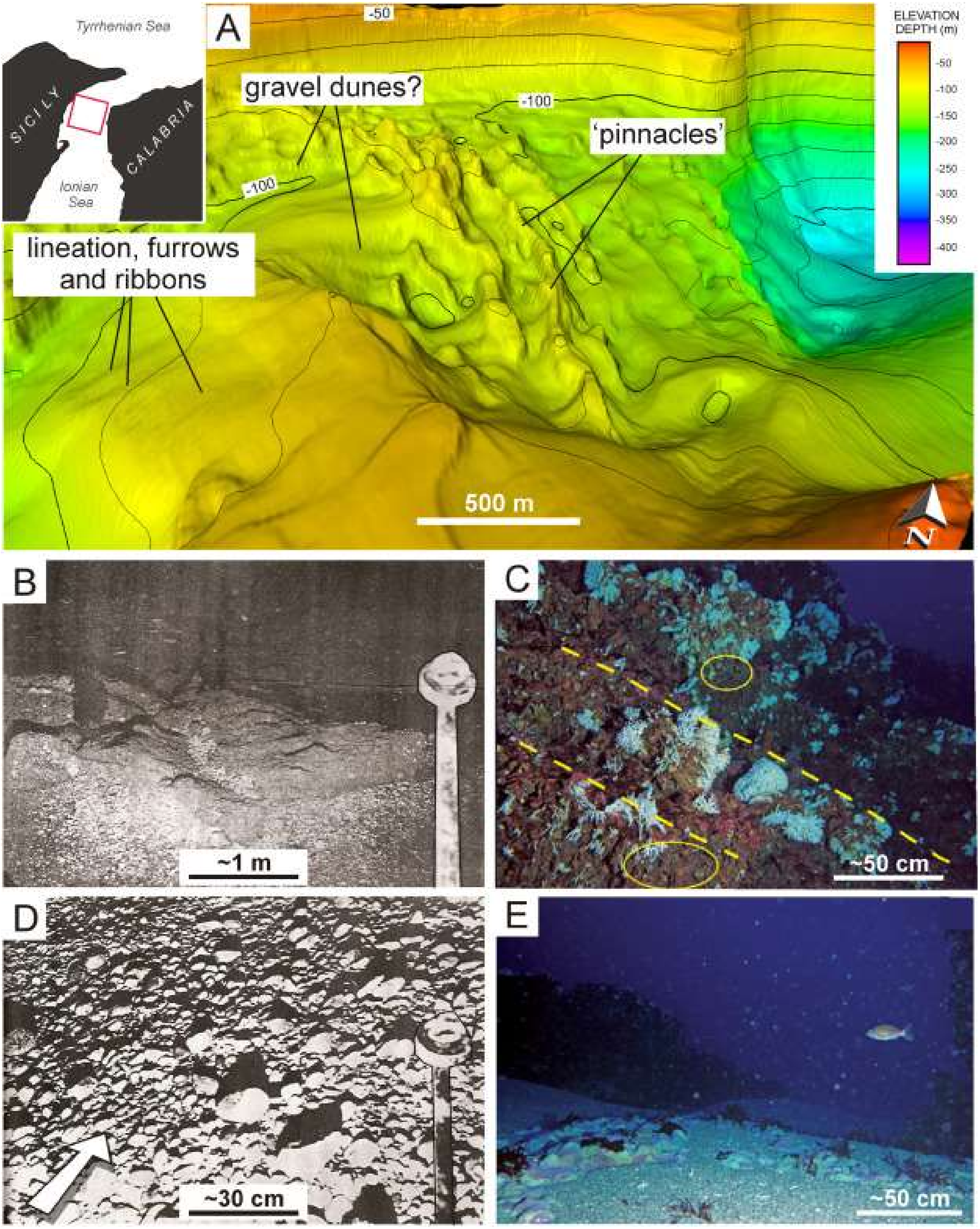

Figure 23:(A) Three-dimensional view of the central-area Messina Strait seen from the south (see box). (B) Underwater rock outcrop photographed during a survey. (C) Conglomerates interpreted as low deltaic deposits (dashed lines indicate sloping bottom). (D) Coarse-grained sediments, while downstream in (E) finer deposits (black and white photos in B and D, are from Colantoni, 1987; color photos in C and E, are by Antonioli et al., 2014).

In many modern current-dominated continental shelf, the area hosting the tidal maxima is commonly a smooth or scoured zone, where currents perpetually sweep the sea floor. Tidal currents erode the sea bottom generating features typically elongated in the same direction of the local current pattern. In the Messina strait centre zone, where the tidal currents reach velocities of 2–3ms−1, the morpho-bathymetry of the bottom exhibits erosional features stretching perpendicularly to the strait margins. This orientation of the erosional features observed in the sill of the Messina Strait is not consistent with the direction expected from the currents, but more likely reflects the pattern of a river incision. The rivers flowing down from the steep edges of this area were then oriented somewhat perpendicular to the axis of the strait, eroding the area and forming the basic pattern recognizable today.

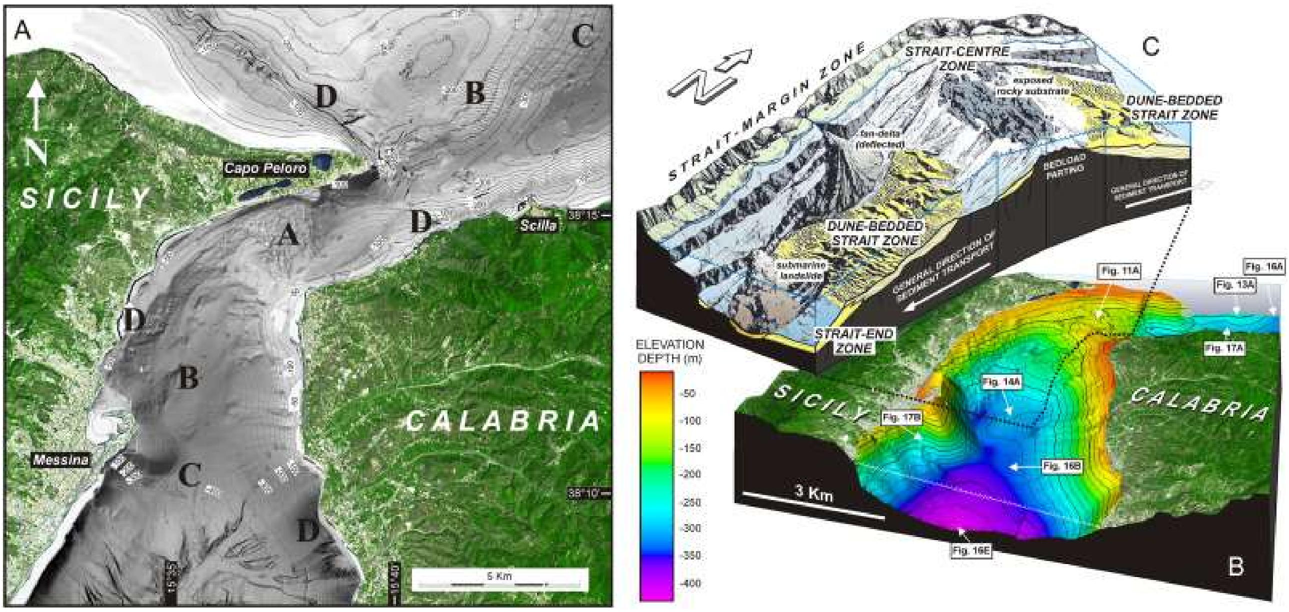

Figure 24:(A) Strait of Messina of (B) Block model showing the main bathymetric characteristics of the central bottom of the Strait of Messina, location details presented in the following fig. (C) Hand-drawn image of the central strait, showing the relationships between the by-pass zone of the central strait and the two adjacent highly depositional dune zones, located downstream of each direction opposite to the main currents.

3.2 Area

In order to decide which is the best location for the placement of the TEC GEMSTAR, preliminary analysis is necessary. Through the investigation of the bathymetry, the stratigraphy and the velocity field of the area, obtained from different surveys realized in recent years, it was possible to get an overview of the main characteristics of the site of interest.

Many aspects need to be considered to find the most suitable position to facilitate the anchoring of the device at the strait's bottom: in particular efficiency aspects, related to the velocity distribution along the depth, legislative aspects, since the presence of several laws and restrictions reducing the available area inside the strait, mostly due to the heavy naval traffic that characterizes the strait, and granulometry aspects are also quite important, helping choosing the proper anchoring system.

In addition, as the depth increases it's worthy to remember that the process of placement of the mooring system and the device becomes extremely challenging for both technical reasons and the costs related to the procedure.

For the analysis, let's focus on the different surveys which have been provided by the company SEAPOWER scrl, consortium with University of Naples Federico II.

Two different field surveys are available:

- **"Relazione Ambitech"** (2018), reporting the results of the bathymetric and the stratigraphic surveys of the right side of the strait, near the shores of Punta Pezzo, in the municipality of Villa San Giovanni;
- **"Report rilievi Idrosfera"** (2019), reporting the bathymetric and stratigraphic surveys of the left side of the strait, in the nearshore area between the harbour of Messina and the province of Torre Faro, in the northern left side of the strait. In this second survey are present also some informations about the stratigraphy in the area near Punta Pezzo.

In the following chapters everything will be explained more in detail, privileging the data concerning the area near Punta Pezzo, being closer to the area of possible positioning of the device.

Privileging the data concerning the area near Punta Pezzo, being closer to the area of possible positioning of the device.

3.2.1 Ambitech survey

The report describes the investigations carried out in the stretch of water requested in concession by the SEAPOWER company, in front of the coast of Punta Pezzo, in the municipality of Villa S. Giovanni (RC), in the period December 2017 - February 2018.

Specifically, two different investigations were carried out:

- execution of the bathymetric survey with Multibeam EchoSounder (MBES) echo sounder;
- execution of the stratigraphic survey with Sub Bottom Profiler.

Before proceeding in detail, we see in Figure 25 the survey area, which is located near the north entrance of the Strait of Messina, close to the Calabrian coast, where the Strait channel bends from the northeast-southwest direction to the north-south direction.

The panel on the right shows a detail shot of the investigated area, or the stretch of water overlooking the Santo Spirito harbor. The yellow polygon indicates the area under investigation, while the circular areas numbered from 1 to 8 indicate the areas requested in concession.

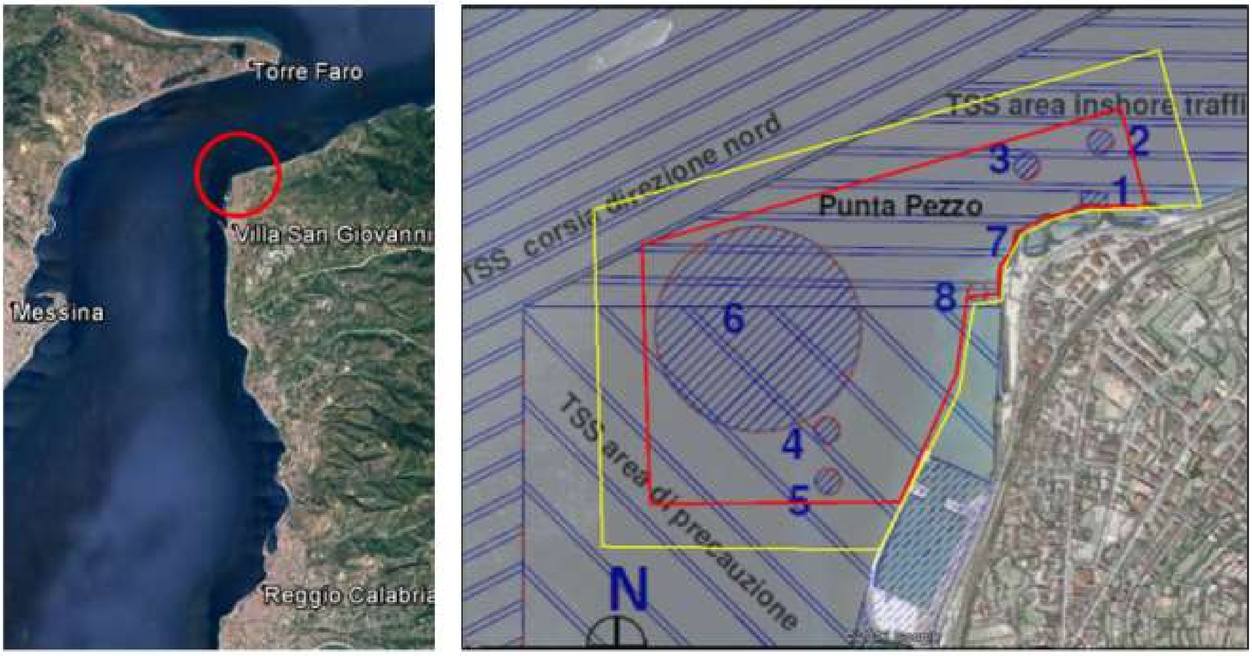

Figure 25:Localization of the survey area in the Strait of Messina (figure on the left) and zoom of the specific area for the survey (polygon in yellow, figure on the right) (from Ambitech Report).

Bathymetric survey

The first survey sees the execution of the bathymetric survey using an MBES echo sounder, which calculates the depth of the seabed through the selection of different sound impulses. In particular, the MBES transducer was installed along the side of a small boat, thus calculating the depth of the seabed considering the time it takes for an acoustic signal to travel from the ship to the bottom and back.

The bathymetric data were corrected to take into account the tidal range, the trend of which was obtained from the records from the Mareographic Station present in the port of Reggio Calabria. After the procedure of processing the collected data, it was possible to draw a detailed bathymetric map of the area of interest, highlighting the various isobaric lines with a depth of 1 m (Figure 26).

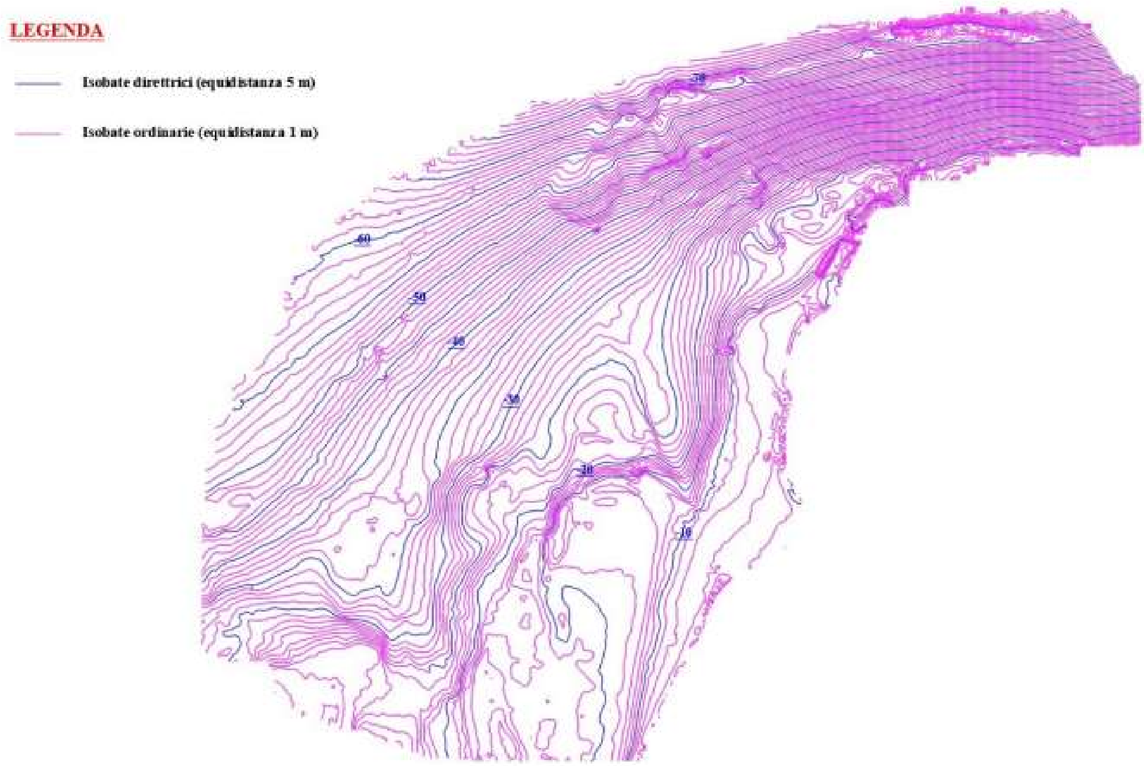

Figure 26:Bathymetric map of the area of interest for the survey. The various contour lines are displayed in purple, each separated from the adjacent ones by 1 [m]. For every 5 [m] of depth the isobaric lines are highlighted in blue. Every 10 [m] the depth of the isobaric line is indicated by the blue number (from the Ambitech report).

Stratigraphic survey

The second part consists of the execution of the stratigraphic survey through Sub Bottom Profiler, which allows the detection of the seabed and subfloor through the generation of acoustic waves that are reflected at each variation in density and therefore in the speed of the subfloor layers, providing thus indirect indications on the nature of the sediments. The reflected waves are detected by the transducer and sent to the processor in the boat which performs the digital analysis of the signal.

The results of the analysis highlighted a stratigraphic structure that reflects the particular conditions of the southern shores of the Strait of Messina, where strong currents and considerable slopes do not favour the sedimentation of the terrigenous material, which easily slides towards greater depths. In detail it was possible to identify a thin superficial layer of terrigenous sediments, mainly sands and gravels with a thickness of the order of magnitude of tens of centimetres maximum, resting on a deep substrate of hard material.

Overall, 9 stratigraphic profiles were performed along the routes indicated in Figure…., Such as LINE 1, LINE 2, etc.

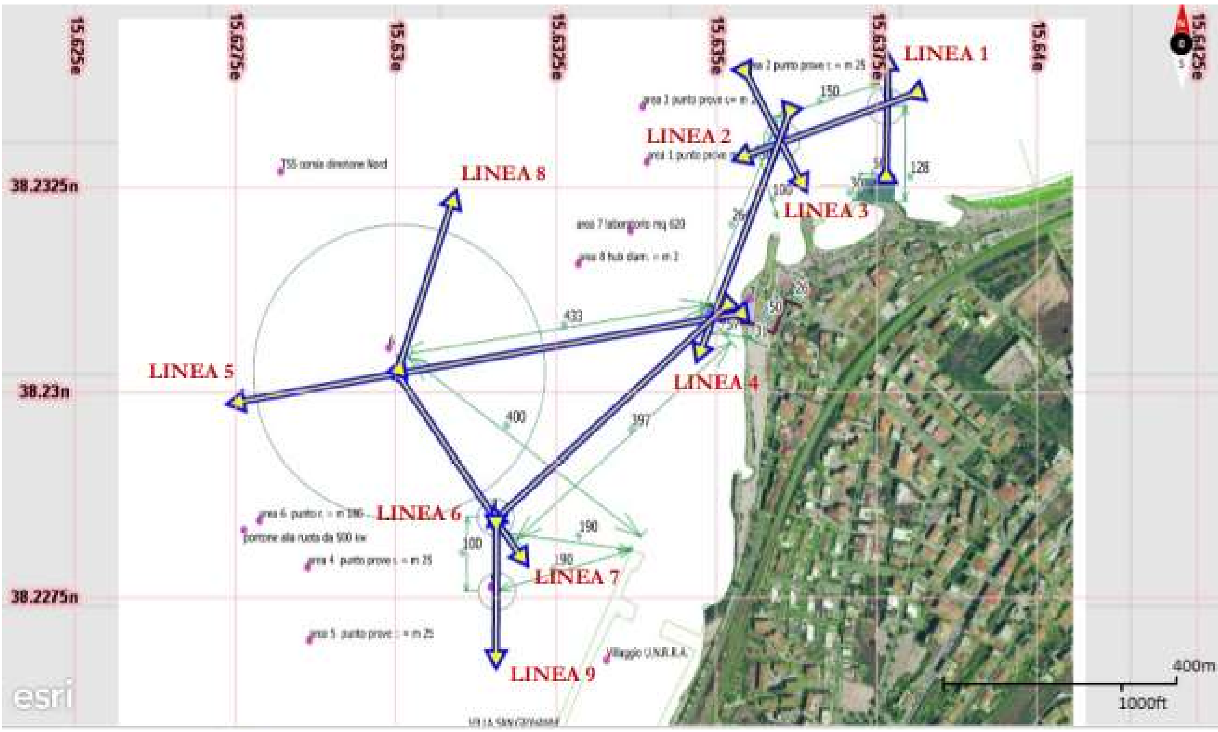

Figure 27:Map of recorded stratigraphic profiles (from Ambitech Report).

The lines of greatest interest for the project, i.e. the placement of the mooring system for the TEC GEMSTAR, are LINE 5, LINE 7 and LINE 8.

The three paths show similar characteristics: the profile is characterized of a transparent seismic facies with areas without reflected signal and which can correspond to non-stratified homogeneous rocky bodies or stratified units but with very inclined layers (igneous masses, saline diapirs, thick bodies sandy or clayey seismically homogeneous).

Furthermore, in the stratigraphic profile associated with LINE 7, as seen in the figure 29, near the coast line, there are some dunes interspersed with fairly pronounced depressions about 3 m depth. Proceeding towards the open sea, some accumulations of stratified material can be seen.

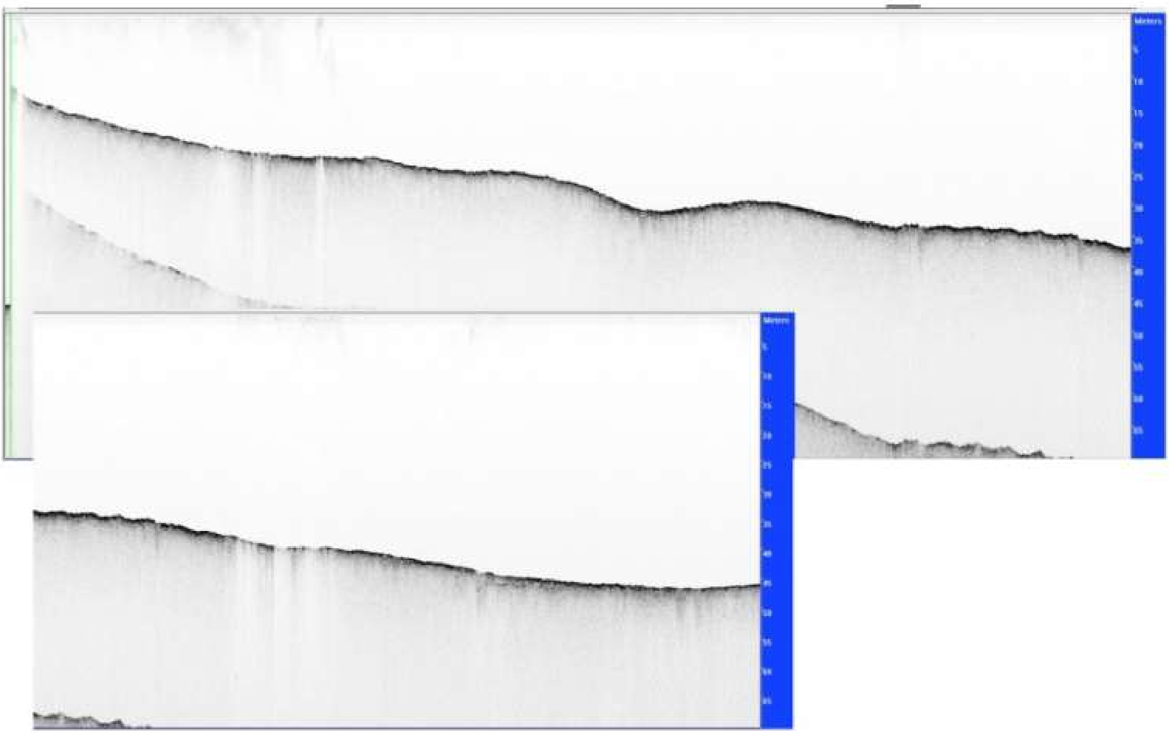

Figure 28:Profile along LINE 5 (from Ambitech Report)

Figure 29:Profile along LINE 7 (from Ambitech Report)

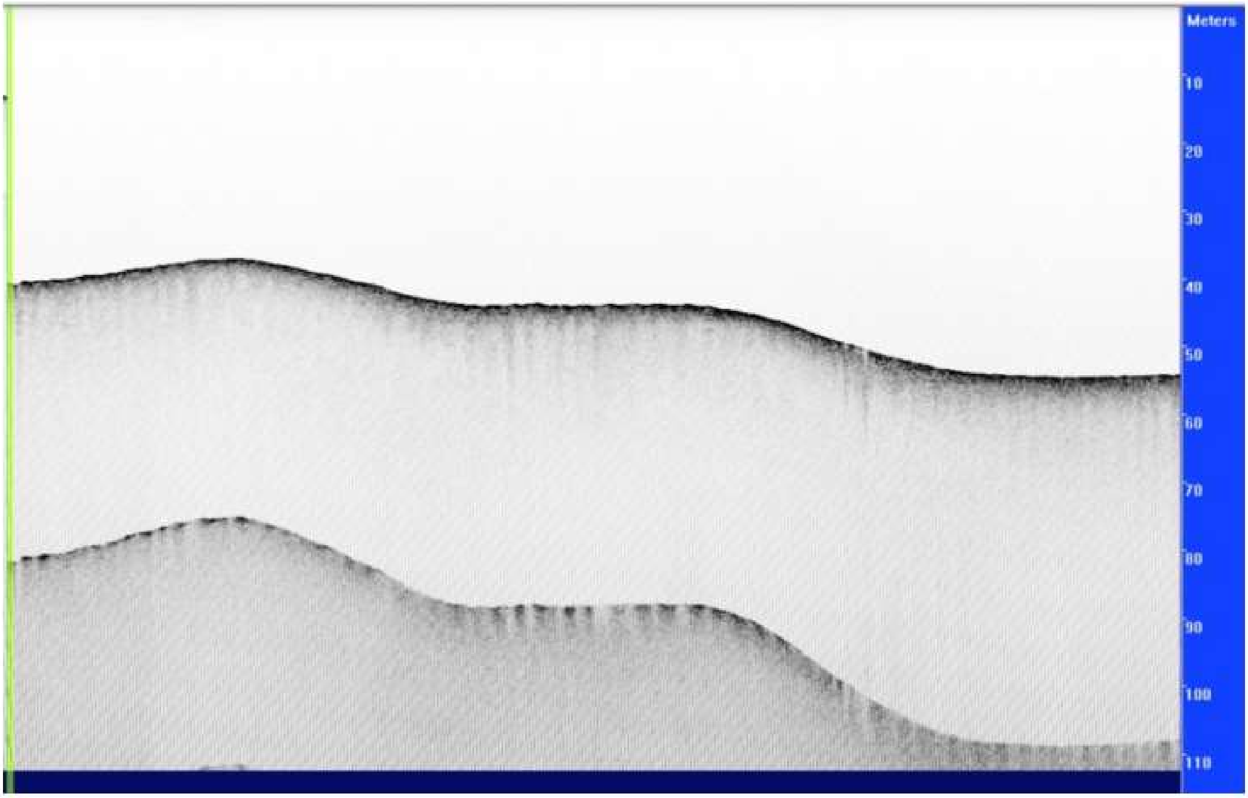

Figure 30:Profile along LINE 8 (from Ambitech Report)

3.2.2 Report Idrosfera

This second report was realized by the IDROSFERA company in 2019, precisely in the period between February-March, and provides further stratigraphic information concerning the area near Punta Pezzo, and new stratigraphic and bathymetric surveys of the area of the Sicilian side of the strait, including between the port of Messina and the town of Torre Faro.

In the case of interest, the area near Punta Pezzo is studied as a possible site for the installation of the GEMSTAR, therefore only the additional stratigraphic information of the survey is taken into consideration.

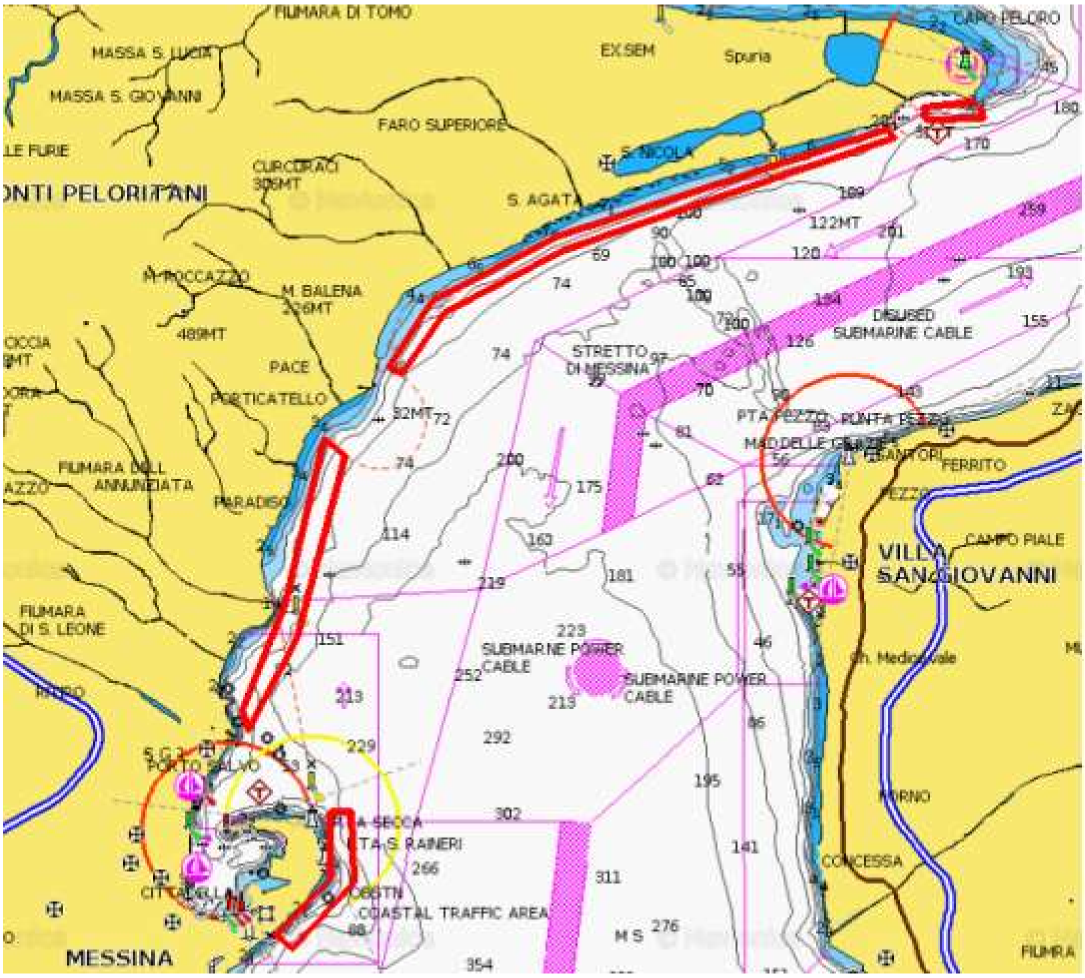

Figure 31:The areas of the Sicilian side of the strait analyzed in this survey are highlighted in the map by red polygons (from the Idrosfera Report).

Stratigraphic survey

Similarly, to the previous survey, a high-resolution seismic system was used to carry out the stratigraphic study, mounted on a boat, which travelled all the lines acquired at a speed of about 2 knots (1 meter per second).

The firing interval of the acoustic signal at the seabed has been set at 250 milliseconds, to ensure the best description of the superficial portion of the seabed, being the most useful for the purposes of the project.

The images below show the routes travelled and the resulting stratigraphic profiles for the site near Punta Pezzo. For the project, only the first three, from below, of the four routes travelled were taken into consideration, as they are the closest to the area where the device can be placed.

Figure 32:Paths for the stratigraphy at Punta Pezzo (from Idrosfera Report).

In the stratigraphies considered it was possible to distinguish a superficial layer of Holocene material, mainly fine to coarse sands and gravels, with extremely variable thickness from 30-40 cm up to even a few tens of meters moving away from the coast line and in correspondence of paleo river beds, where sedimentation is greater due to the currents.

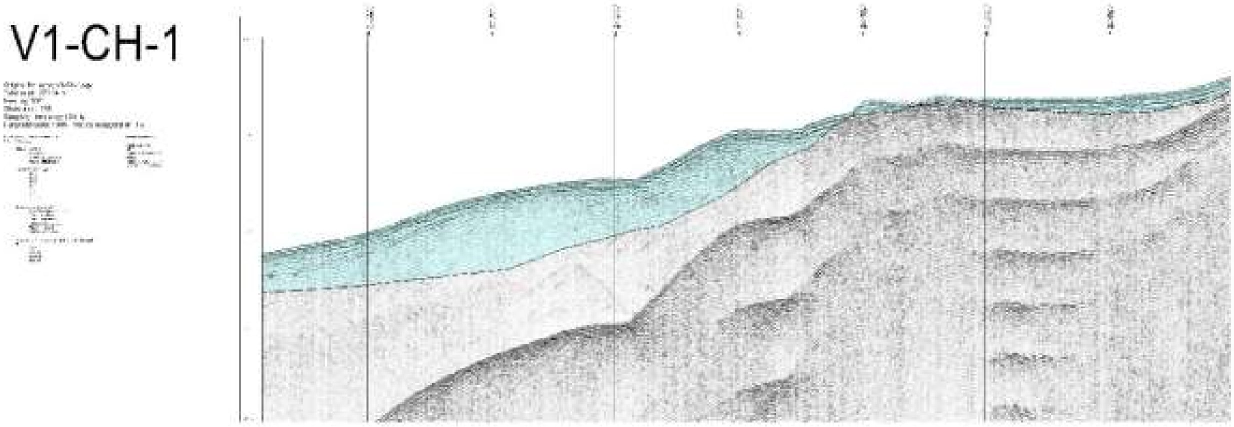

Figure 33:Result of the first stratigraphic survey path (from the Idrosfera Report).

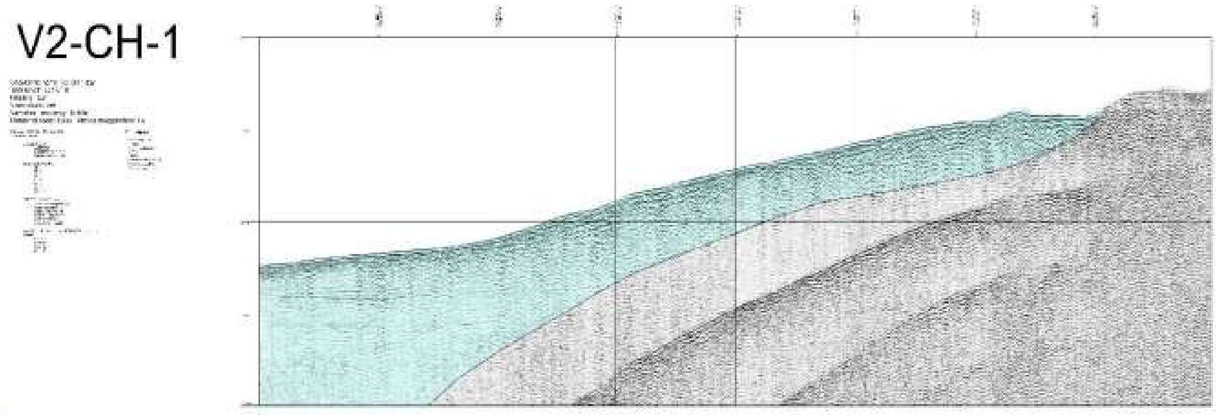

Figure 34:Result of the second stratigraphic survey path (from the Idrosfera Report)

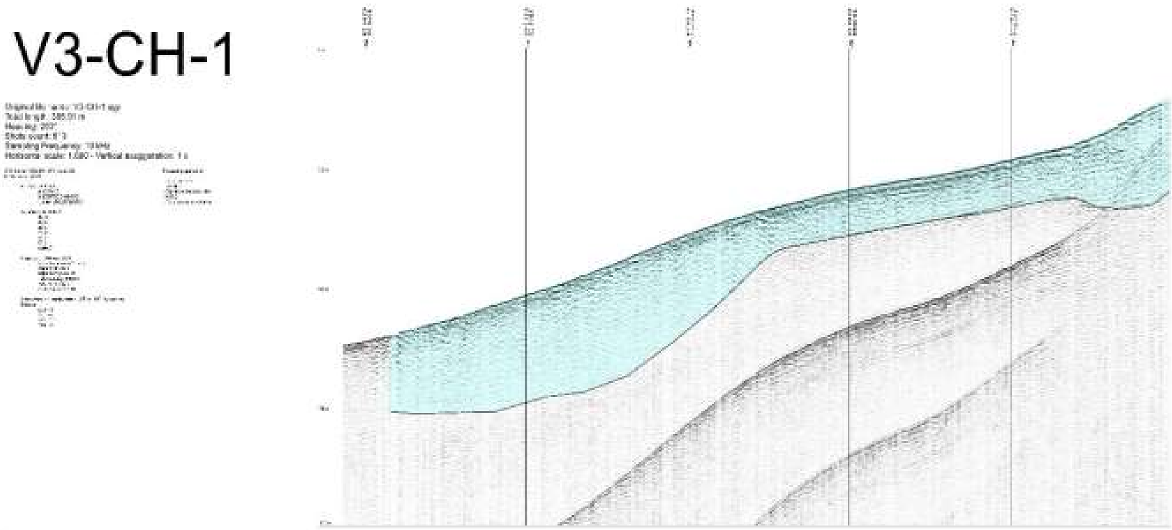

Figure 35:Result of the third stratigraphic survey path (from the Idrosfera Report)

3.3 Geological aspects

In order to support the results obtained from the stratigraphic survey of the reports, the results obtained from other surveys and publications were also taken into consideration. These data are fundamental for understanding geotechnical problems, in particular for dealing with the choice of the most suitable type of anchor for the device.

Of particular relevance are the data from a geological campaign conducted by **Munich et al**. in 1996, whose geological study is based on the interpretation of geological and geophysical data collected along a regional transept that extends along the southern arc of Calabria to the Ionian coast. The results of four deep drillings carried out in the Strait of Messina (S16, S4, S2, S5) were also considered.

An image of the data provided by these surveys is shown in Figure 36.

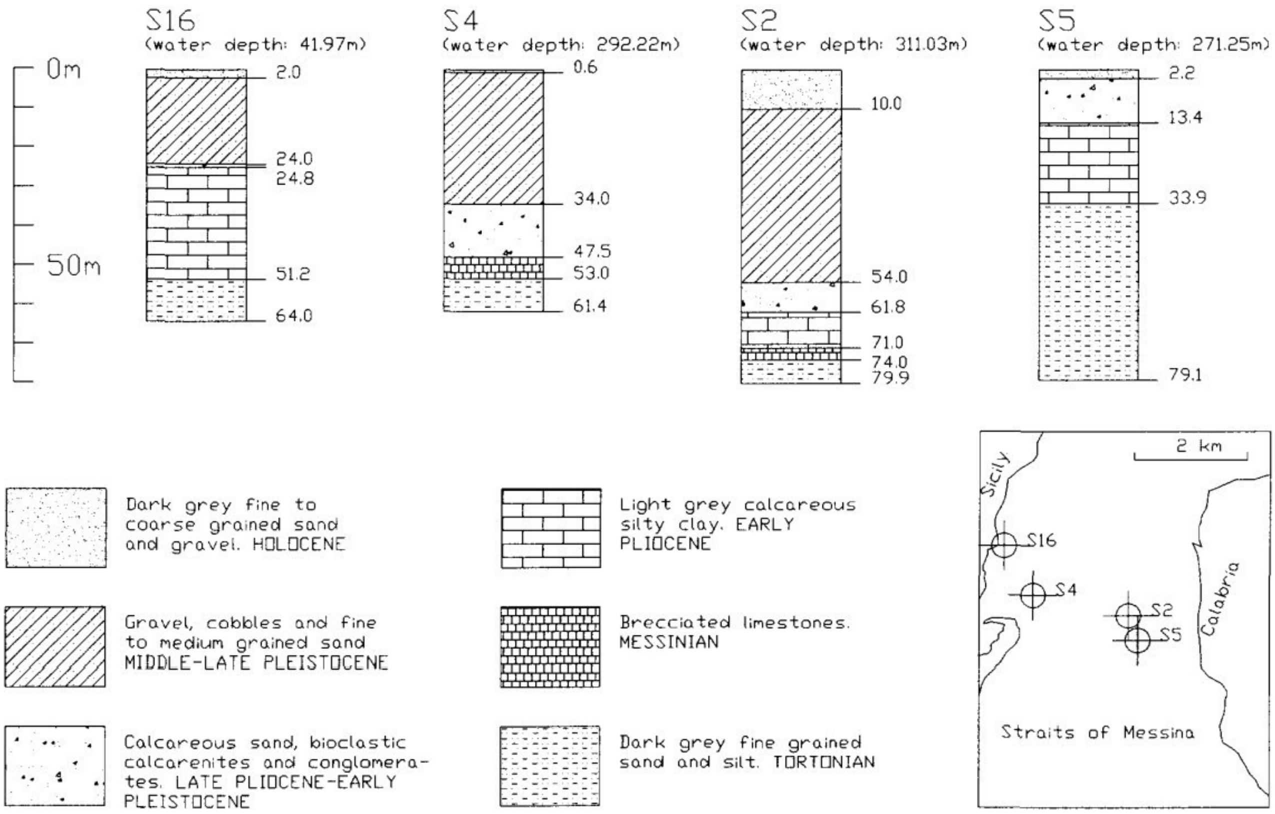

Figure 36:Drilling logs in the Strait of Messina. The box below shows the locations of each drill site (from Monaco et al. 1996).

The most representative points (S2, S4, S5 and S16) have been studied with drillings of about 80m in length made on the seabed at an altitude between -41.97 m (S16) and -311.03 m (S2).

Hole S16, whose position in the strait is visible in the window in the lower right corner of the Figure, belongs to a shallower portion of the Sicilian side of the strait at a depth of about 42 meters, while the other three samples belong to deeper portions of the channel, about 300 meters deep.

A sedimentary succession of 60-80 m thick is obtained, composed of alternations of lithotypes belonging to six main units which can be schematically represented by:

a) fine to medium-grained sands and gravels. This unit shows a thickness between 0.60 m (S4) and 10 m (S2) and represents the Holocene deposits of the Strait of Messina.

b) Gravels and coarse-grained sands consisting of well-rounded pebbles of crystalline rocks. These sediments show thicknesses ranging from 22 m (S16) to 44 m (S 2).

c) Calcareous sands and well-cemented calcarenites and organogenic calcarenites. This unit is approximately 1m (S16) to 13m (S4) thick.

d) Pliocene shale. These sediments, which correspond to Unit E of the Upper Miocene - Pliocene deposits, were drilled in correspondence with wells S1, S5 and S16 where they show thicknesses between about 7 and 26 m;

e) Intensely fractured limestones. This unit, corresponding to the Messinian limestone of Unit D of the Upper Miocene - Pliocene deposits, was only drilled by wells S2 and S4 where it shows a thickness between 3 and 5.5 m, respectively.

f) Fine-grained micaceous sands and silt corresponding to Unit B of Upper Miocene - Upper Pliocene deposits.

This succession was also observed on the occasion of the construction of the AGIP Messina well which, built on the Sicilian side of the strait (north of the city of Messina), crossed 226 m of coarse-grained sediments of the Pleistocene, 27 m of marls of the lower Pliocene, 321 m of the upper Miocene and 30 m of metamorphic rocks.

Other data on the granulometry of the seabed come from a 2016 document, **"Holocene sediments of the Messina Strait (southern Italy): relationships between source area and depositional basin", by F. Perri et al.** In this study the chemical and mineralogical distribution of the sediments collected along the Strait of Messina was analysed to reconstruct the sedimentary evolution and geological processes. Among the various points of investigation only two of them are in some way relevant to the work carried out in this project: STR3 and CAL13.

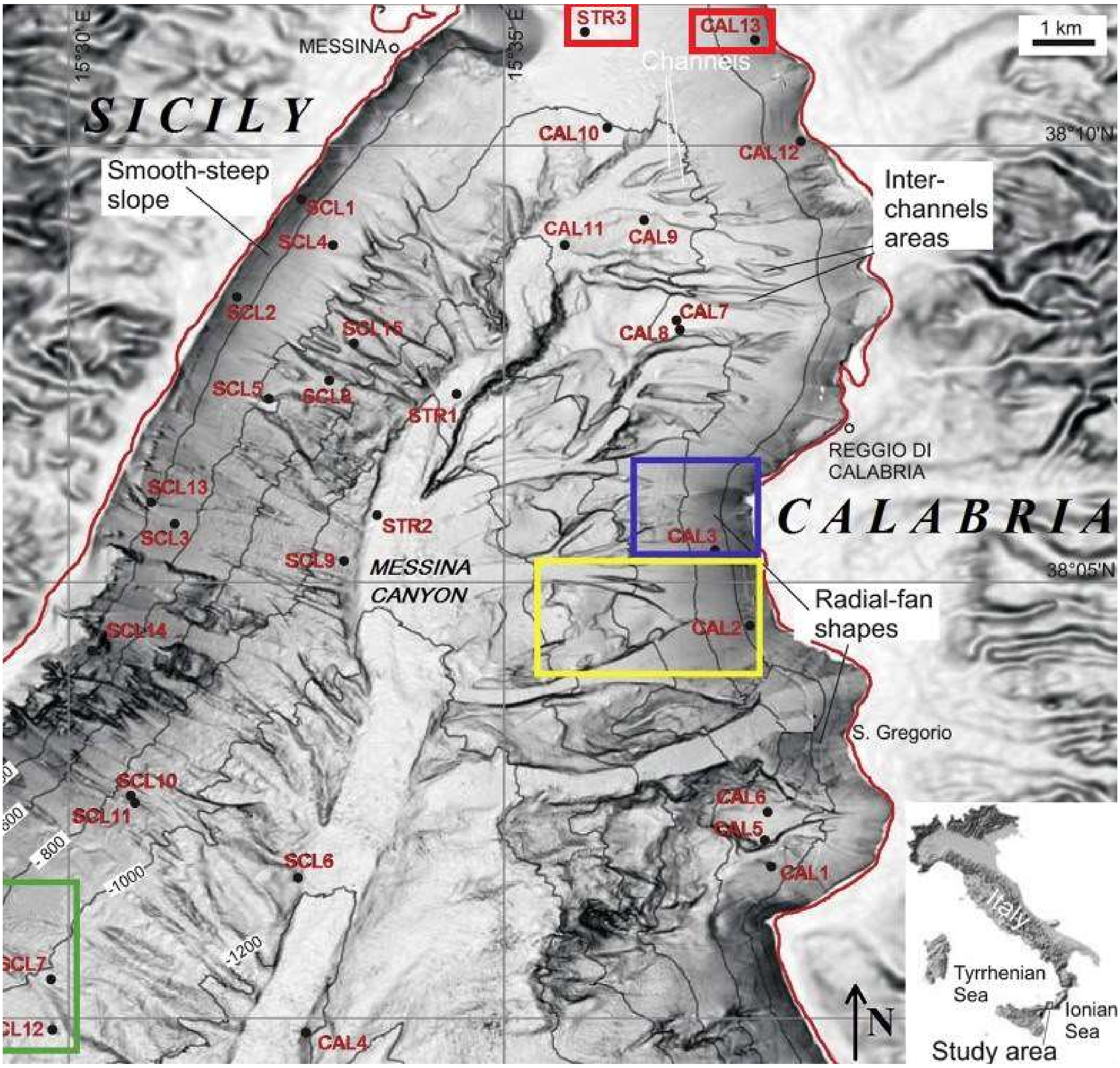

Figure 37: Detail of the detailed bathymetric map of the surveyed area. The two relevant points for this project are the one highlighted by the red squares, STR3 and CAL13, more or less at the same longitude as the city of Messina (from F. Perri, "Holocene sediments of the Messina Strait (southern Italy): relationships between source area and depositional basin", 2016).

For the two points highlighted with red rectangles in the Figure 37, the mineralogy (in percentage by weight) is shown in the following table:

Samples	Qtz	K-field	Plg	ΣPhyll	Calc	Fe-ox	ΣFeld
STR3	50	6	15	29	tr	0	21
CAL13	50	6	14	30	tr	0	20

In addition to these data, the particle size found at the respective sampling points is also reported: the STR3 site is characterized by sand with traces of silt, clay and gravel, while the composition of the bottom of the CAL13 site could be described as a mixture of gravel and sand.

Further confirmation on the composition of the seabed in the strait is provided by **the geological map of the onshore and offshore areas of the Strait of Messina** (Figure 38) modified by: Ghisetti et al., 1983, Gargano, 1994, and Lentini et al., 2000 for onshore geology; Selli et al., 1979 for the distribution of the narrow bottom sediments, where the bottom portion of interest of the strait is mainly made of smooth gravel bottom and rough rocky bottom.

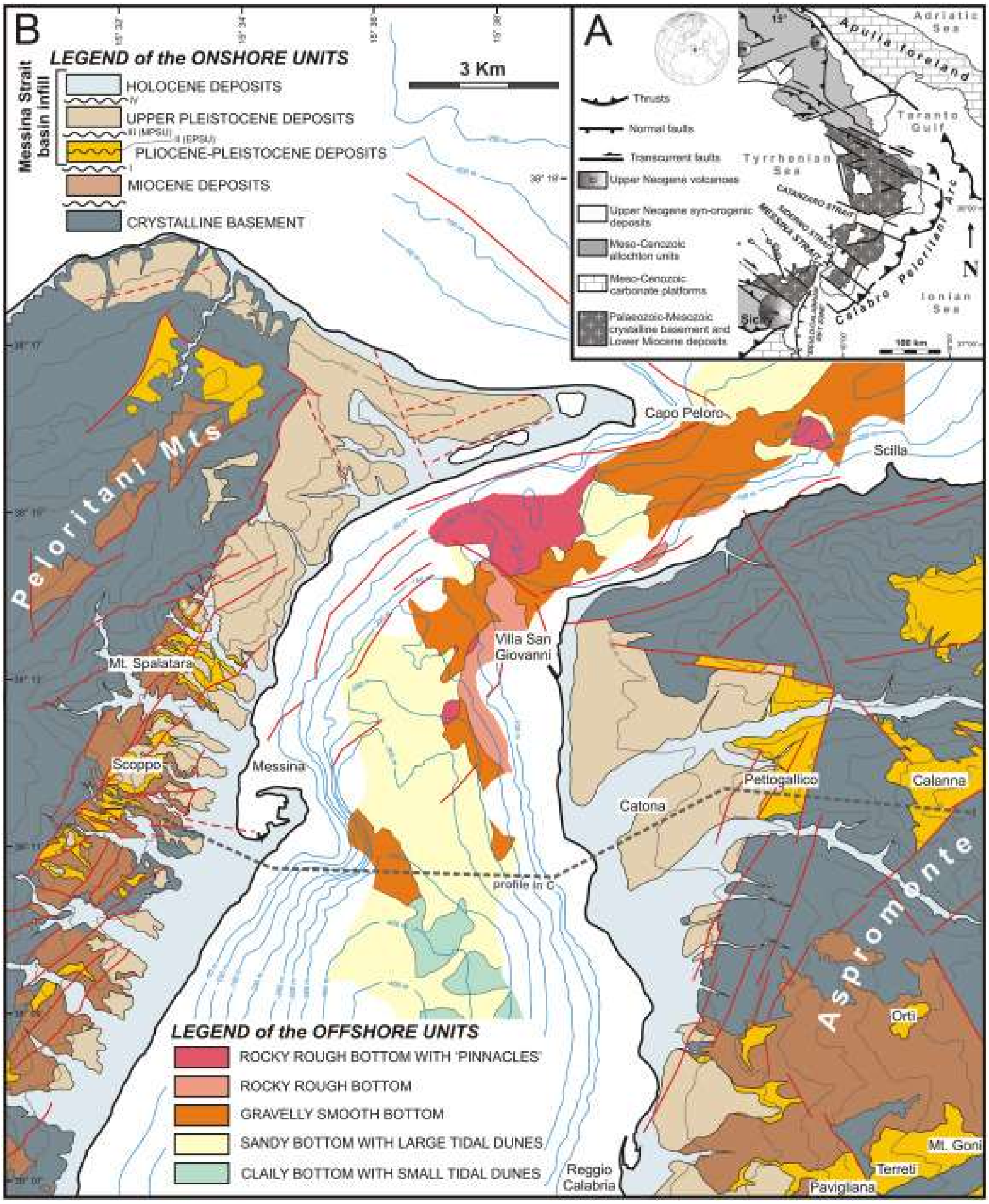

Figura 38:Geological map of the onshore and offshore areas of the Strait of Messina

Additional considerations

Additional aspects, which must necessarily be satisfied in choosing the area where to place the device, are:

- Few meters of water on top of the GEMSTAR must be left free from any obstruction to allow the passage of boats and crafts, at least 10-12 meters;
- It is important to ensure a correct spacing between the bottom of the GEMSTAR and the bottom, to avoid any possible collision or interference between the ground and the rotor blades.

3.4 Velocity range

The identification of the velocity range of the currents passing through the strait of Messina is an important procedure for the decision of the placement position of the energy converter. Sites with a favourable depth and seabed composition but a velocity range with peaks at low velocity (<1 [m/s]) are considered not suitable, since the energy output derived from the TEC would be too low. Fortunately, the strait of Messina is one of the few places in the Italian coastline where the production of energy due to tidal range is a realistic possibility, mainly due to the narrow profile of the channel and the fact that the strait is a point of juncture between two seas, the Tyrrhenian and the Ionian. For a rough estimation of the velocity range in the zone of interest for this project, near Punta Pezzo, a paper from 2012 has been taken as guideline, by the title of “Stima della produzione elettrica da correnti marine nello stretto di Messina” (Estimation of the energy production from sea currents in the strait of Messina), from Domenico Coiro and Giancarlo Troise. In this paper, the velocity field for different points in the strait is calculated, starting from the array of data about current velocity provided by the tide tables for the strait of Messina of the year 2004, from the Naval Hydrographic Institution. In this tide tables, the data for the peaks of current velocity for each day of the year are provided. Here, the values of current velocities flowing from the Tyrrhenian Sea to the Ionian Sea are considered of negative sign, while the velocities of the currents flowing in the opposite direction are considered positive. The array of data provided is valid for a specific point in the strait, of coordinates 38° 14’ 00’’ N of latitude and 15° 38’ 00’ E of longitude, which is in Punta Pezzo, the site of interest for this project. In the following table, the values for the month of January 2004 are shown as example of the data provided by the tidal tables. For each day of the month, the times of slack water and peak velocity are shown, with the relative velocities of each peak, expressed in knots.

Day	Slack water	Time	Velocity [kn]	Slack water	Time	Velocity [kn]	Slack water	Time	Velocity [kn]	Slack water	Time	Velocity [kn]
1	2.5	0.14	1.64	9.08	5.4	-2.6	14	11	0.93	21.5	17.6	-3.9
2	3.54	1.09	2.04	10.4	6.5	-2.7	14.4	12	0.63	22.2	18.5	-3.9
3	4.51	1.55	2.45	11.6	7.4	-3	15.2	13	0.46	22.6	19.3	-4
4	5.4	2.36	2.85	12.6	8.4	-3.3	16	14	0.39	23.4	20.2	-4.1
5	---	3.11	3.22	6.23	9.2	-3.6	13.4	15	0.42	16.4	21	-4.2
6	0.13	3.45	3.53	7.05	10	-3.9	14.2	16	0.52	17.3	21.4	-4.3
7	0.5	4.16	3.78	7.43	10	-4.2	14.5	16	0.68	18.1	22.3	-4.4
8	1.29	4.48	3.94	8.19	11	-4.5	15.2	17	0.9	19	23.1	-4.4
9	2.09	5.23	4	8.55	12	-4.6	15.5	17	1.13	19.5	23.5	-4.3
10	2.52	5.59	3.93	9.3	13	-4.8	16.3	18	1.35	20.5	---	---
11	3.38	0.4	-4.2	10.1	6.4	3.7	17.1	13	-4.8	21.4	19.1	1.55

12	4.26	1.29	-4	10.4	7.2	3.4	17.5	14	-4.8	22.5	20	1.72
13	5.2	2.25	-3.7	11.2	8.1	2.9	18.4	15	-4.7	23.6	21	1.88
14	---	3.24	-3.4	6.2	8.6	2.4	12	16	-4.6	19.3	22.1	2.07
15	1.13	4.27	-3.2	7.3	9.6	1.8	12.5	17	-4.6	20.2	23.2	2.36
16	2.31	5.36	-3.2	8.49	11	1.4	13.4	17	-4.5	21.1	---	---
17	3.43	0.31	2.79	10.1	6.4	-3.4	14.4	12	1.09	22.1	18.5	-4.6
18	4.48	1.36	3.3	11.3	7.5	-3.8	15.5	13	1.05	23	19.4	-4.7
19	5.44	2.31	3.81	12.4	8.4	-4.2	16.5	15	1.18	23.5	20.3	-4.9
20	---	3.22	4.24	6.34	9.4	-4.7	13.3	15	1.38	17.5	21.3	-5
21	0.37	4.08	4.52	7.22	10	-5	14.2	16	1.56	18.4	22.1	-5.1
22	1.22	4.51	4.63	8.05	11	-5.3	15	17	1.71	19.3	23	-5
23	2.06	5.3	4.53	8.46	12	-5.3	15.4	18	1.78	20.2	23.5	-4.8
24	2.5	6.08	4.23	9.25	12	-5.2	16.2	18	1.79	21	---	---
25	3.34	0.32	-4.5	10	6.5	3.8	17	13	-5.1	21.5	19.2	1.74
26	4.19	1.19	-4.1	10.4	7.2	3.2	17.4	14	-4.7	22.4	20.1	1.64
27	5.08	2.08	-3.6	11.1	7.6	2.5	18.2	14	-4.4	23.4	20.5	1.54
28	---	3	-3.1	6.01	8.3	1.8	11.4	15	-4	19.1	21.5	1.46
29	0.47	3.59	-2.6	7.05	9.1	1	12	16	-3.6	19.5	22.6	1.47
30	2.02	5.02	-2.4	8.33	10	0.4	12.1	17	-3.4	20.5	---	---
31	---	0.17	1.67	3.16	6.1	-2.3	---	11	-0.1	21.4	18	-3.3

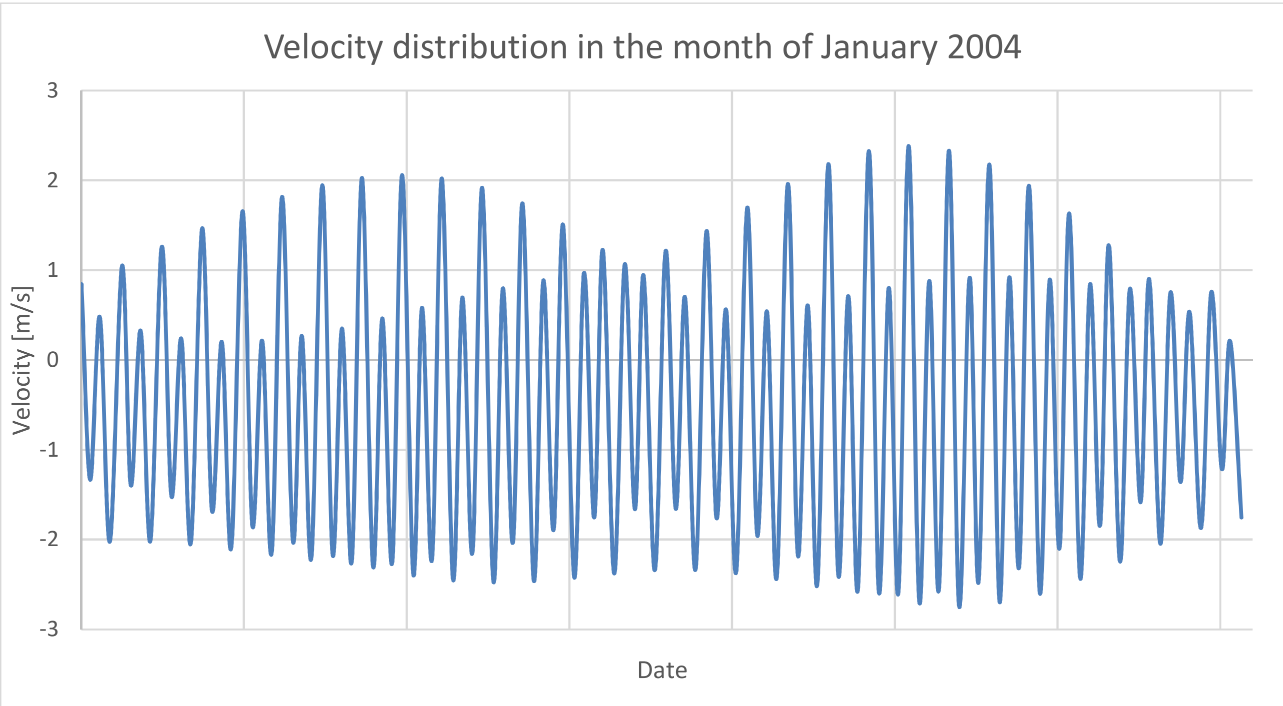

Figure 39:Speed distribution at Punta Pezzo for the month of January 2004, drawn from the data in the Table.

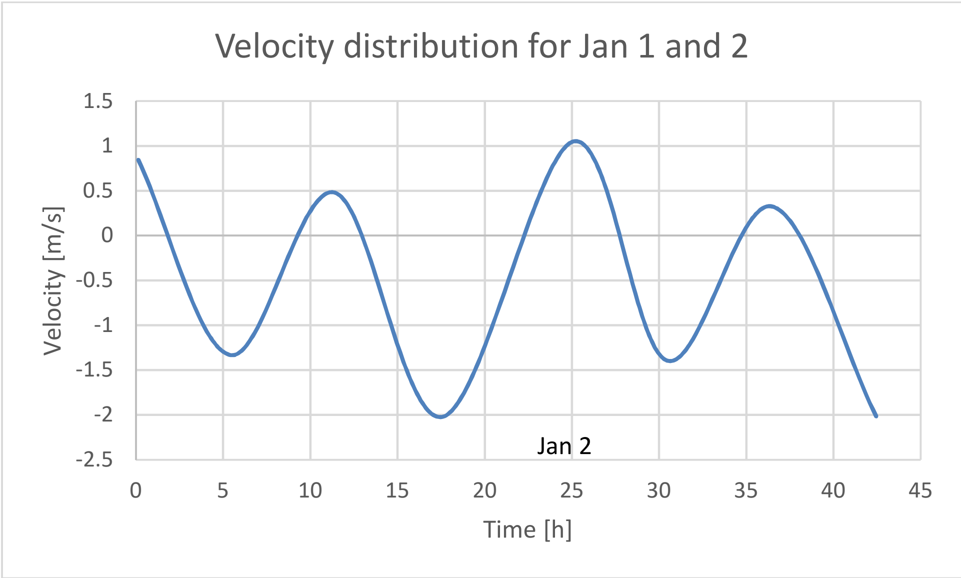

Figure 40:Speed distribution at Punta Pezzo in the first two days of January 2004.

From the tables it is also possible to plot the values of slack water and max velocity for an entire year, as shown in figure 41 as example for the year 2004 for the location in Punta Pezzo.

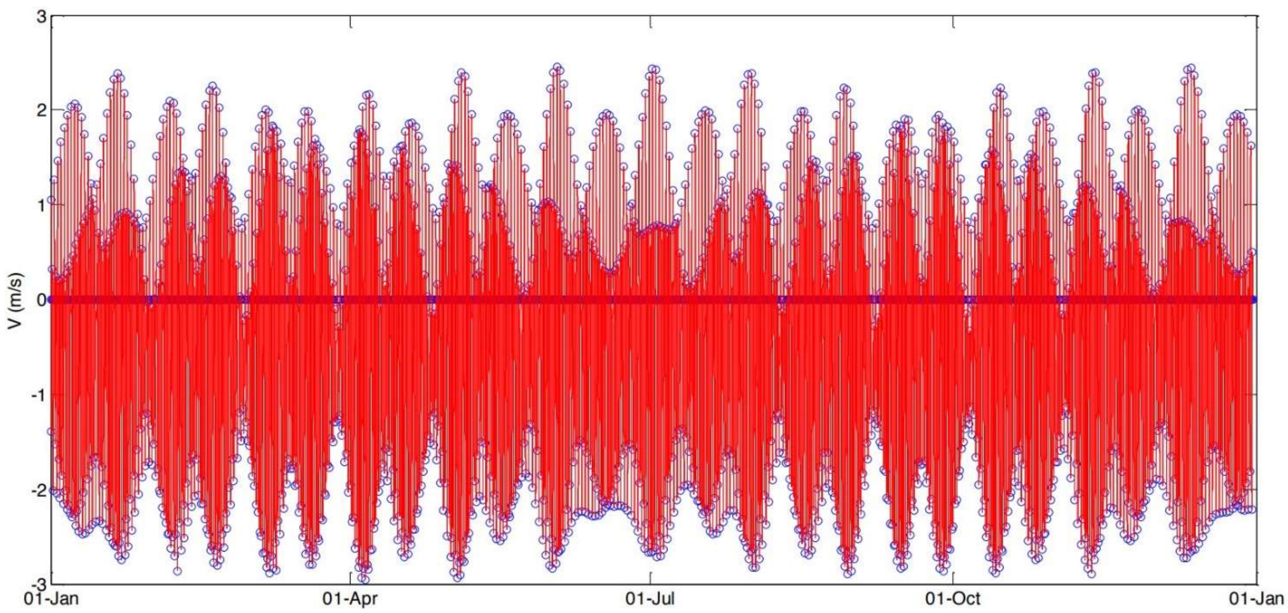

Figure 41:Speed profile for the year 2004 at Punta Pezzo. The speeds of the currents flowing from the Tyrrhenian Sea to the Ionian Sea are considered to have a negative sign, positive in the opposite direction.

From the plots, a typical semi-diurnal distribution of the cycles of the tide is distinguishable, while, at larger scale, a variation of the peaks on a monthly level can be seen. For each day, there are four different peaks of velocity, two for each direction of the current, therefore there are 2 changes in current direction per day. From the plots are also visible slightly higher values of peak velocities in the current direction flowing from the Tyrrhenian Sea to the Ionian Sea. Overall, the values are contained, in both directions of the flow, below the 3 [m/s] threshold, which is the value that has therefore been set as the max value of velocity for the proper working condition of the TEC. For higher values of velocity, even though those are to be considered as exceptional events, the GEMSTAR will enter in a "safe mode", stopping the energy production for the window of time in which the current velocity is considered too high. It is also true that, to maximise energy production, the ideal working condition for the device is just slightly below its limit condition.

3.5 Conclusions

Considering the data collected, some areas near the shore of Punta Pezzo have been selected for this project. The following image (Figure 42) shows five possible areas for positioning the TEC on the bathymetric map of the area of interest. The angle of inclination of the seabed is also reported, which must be considered in the projecting phase.

The data, relating to the different areas, are shown in the table:

ID	Lat	Lon	Profondità (m)	Distanza dalla costa (m)	Pendenza (%)	Raggio dell'area (m)	Superficie (m^2)
Sito _Ic_x1	38° 13.863'	15° 37.893'	35	313	12.2%	35.0	3848
Sito _Ic_x2	38° 13.867'	15° 37.838'	44	394	16.1%	45.0	6362
Sito _Ic_x3	38° 13.871'	15° 37.766'	55	499	13.6%	50.0	7854
Sito _Ic_x4	38° 13.875'	15° 37.689'	60	610	4.1%	55.0	9503
Sito _Ic_x5	38° 13.927'	15° 37.818'	62	455	14.9%	60.0	11310

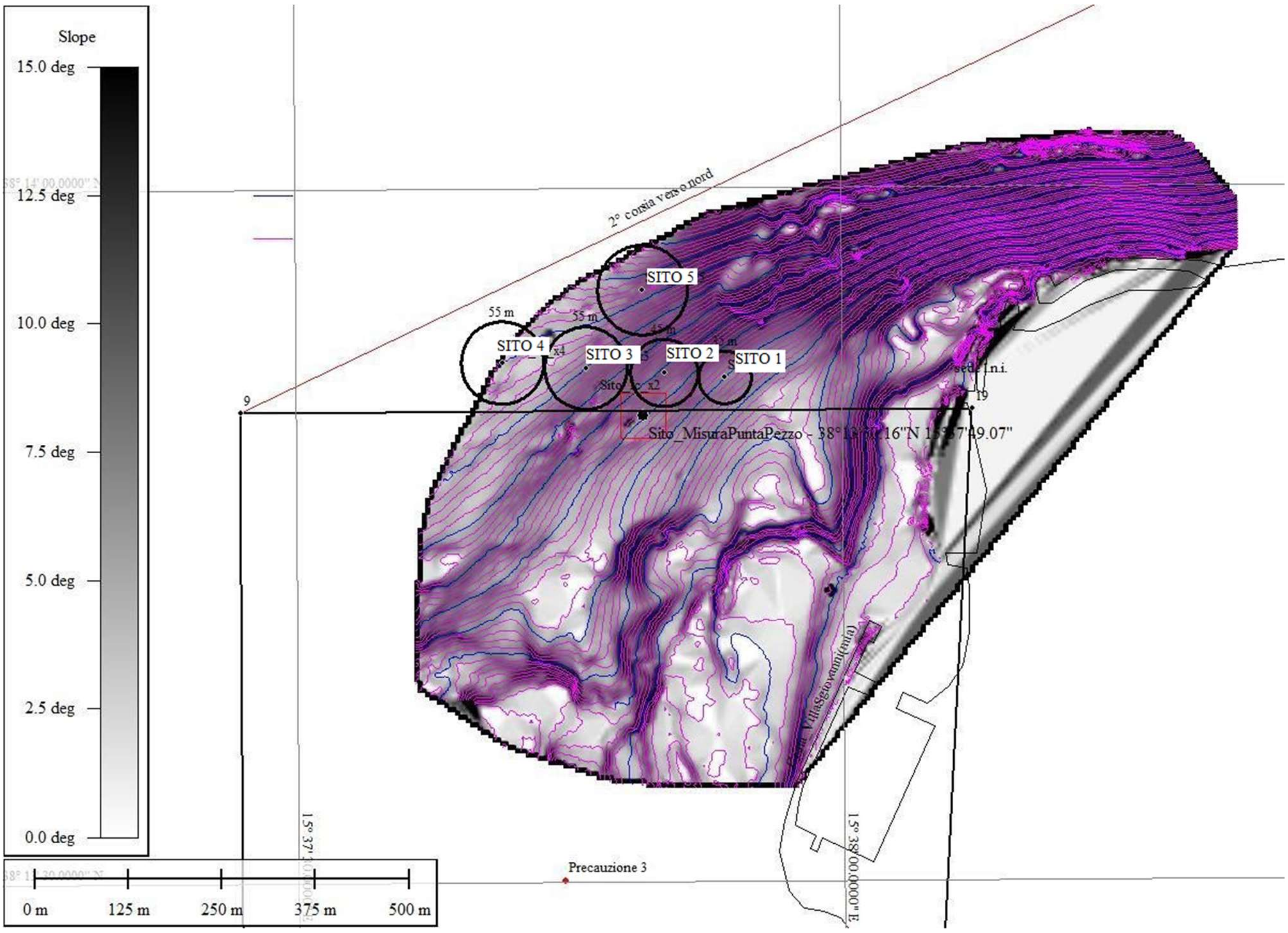

Figure 42:Map of possible areas for positioning the TEC near Punta Pezzo. Together with the bathymetry of the area, the angle of inclination of the seabed is also highlighted.

Known the bathymetric and stratigraphic characteristics of the possible areas and taking into account the needs of the case, it was possible to make a reasoned choice of what could represent the most suitable area in which to place the device.

For this reason, site 1 with a depth of 35 m was chosen.

Subsequently, the bathymetric and stratigraphic characteristics of the area will be fundamental in choosing the type of anchor.

Chapter IV

MOORING SYSTEMS

This chapter provides a brief overview on the main components of a mooring system: configuration, anchor and lines. In particular, the mooring system chosen for the device GEMSTAR will be described.

4.Mooring systems

There exists a multitude of possible mooring configurations for WEC and TEC floating or submerged devices and the selection of the most suitable mooring system is vital for the station keeping and survival of a device.

There are several criteria which influence the selection of a mooring system, including the forces which the system will have to withstand from currents, waves and wind, the weight of the structure itself and the depth in which the structure is to be moored.

In general, the requirements for WEC and TEC mooring systems can be summarised as follows:

- Accommodate tides.
- All components must have adequate strength, fatigue life and durability for the operational lifetime. Corrosion must be considered and controlled in the design, and abrasion due to bottom contact or contact with other lines must be minimised or avoided if possible.
- Be easy to monitor and maintain.
- Be economical.
- Minimize environmental impacts on the seabed or native flora and fauna.
- Not adversely affect the performance of the device by interfering with the device motion used for energy capture.
- Occupy as little space as possible on the seabed, in order to allow the devices to be installed close to each other in arrays.
- A degree of redundancy is highly desirable for individual devices.

Components of a mooring system

There are three main components of the system which must be selected to compose a good mooring system:

1. Configuration: single point or spread mooring;
2. Anchorage: deadweight, drag, pile or plate;
3. Line type: chain, wire or rope.

1.Configurations

The two key divisions of mooring configurations are single point moorings and spread moorings, according to whether there is one or multiple lines connected to the device.

A **single point mooring** consists of a single anchor and single mooring line, so this arrangement has no redundancy: if the single line fails then the entire system will fail. Therefore, in the design phase, particular care should be taken when dimensioning each single component of the mooring system. This set up is required if the device is to be allowed to weathervane around the point of mooring, allowing the alignment with the current flux. This will require a large operational footprint, and, likely, preclude the use of this type of system when multiple TEC devices are employed in an energy farm, unless they are properly distanced from each other, increasing significantly the area required for the correct placement of the devices. There are many configurations of single point mooring systems which all perform this function.

A **spread mooring** consists of multiple lines, arranged in a symmetrical pattern, which generally meet the device at multiple points. This configuration essentially fixes the heading angle so that the device retains a fixed heading or orientation. The alignment of the device should be decided according to the most frequently occurring direction of the environment, for example in line with the typical wind direction or current. To sum up, this mooring configuration provides position, directional and rotational control. As result of the multiple lines system, the redundancy of the structure increases significantly, redistributing the applied loads on more lines and consequently allowing for a reduction of the dimensions of each cable and anchor.

There are two main line configurations which can be applied to both the single point and spread mooring configurations: taut mooring lines (Figure 43a, b) and catenary/slack (Figure 43c, d), depending on whether the line is stretched tight under pretension, or hangs loose.

Respectively in a **catenary mooring**, the line(s) approach the seabed horizontally before they reach the connection with the anchor; this ensures that the forces on the anchor are horizontal and the weight of the line provides the majority of the restoring force for station keeping. The system can allow some freedom of movement.

While a **taut-line** system is composed of wire or synthetic ropes and is normally highly pre-tensioned. The mooring lines arrive at the seabed at an angle, and do not make contact with the seabed. The loadings on the anchor are therefore both horizontal and vertical. Since taut-line systems are usually quite stiff, both in horizontal and vertical directions, they can significantly reduce vertical motions of the device and so be used to minimise the excursion of the device. The avoidance of contact with the seabed of the taut mooring system has further benefits: the mooring line does not damage the seabed, and the seabed does not damage the line. This benefits both environmental concerns and maintenance requirements of the line. Compared to a catenary configuration, a taut mooring system usually occupies a smaller footprint area on the seabed and the excursion of the device is reduced.

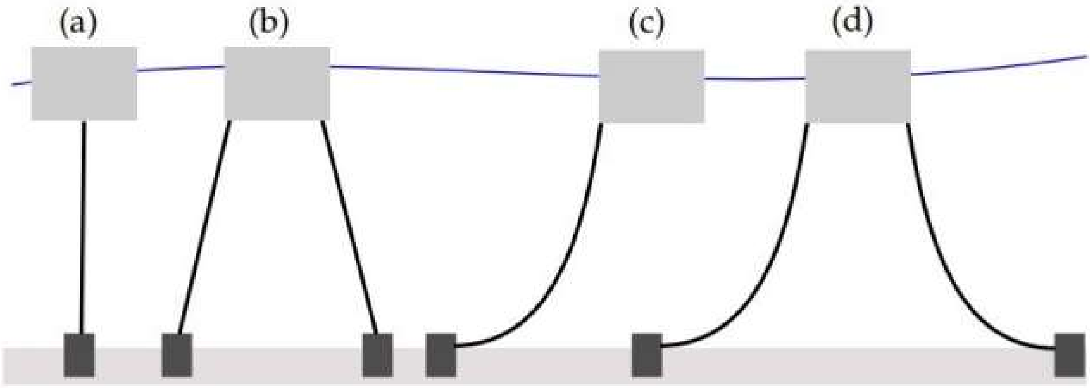

Figure 43:Some possible configurations: (a) Taut; (b) Taut spread; (c) Catenary (d) Multi-catenary (from J. Davidson and J. Ringwood "Mathematical modelling of mooring systems for Wave Energy Converters-A review", 2017).

The selection between of taut and catenary mooring line depends mainly on the requirements of the floating structure. Taut moorings are more suited to highly accurate position keeping and allow only as much compliance as is allowed by the elongation of the mooring lines. While in locations where rough environmental loadings are an occurrence, catenary mooring configurations allow compliance to reduce damage to the floating structure.

Many other mooring configurations are possible for example the possibility to form S or Wave type configurations including intermediate buoys and sinkers in the mooring lines (Figure 44e, f, g).

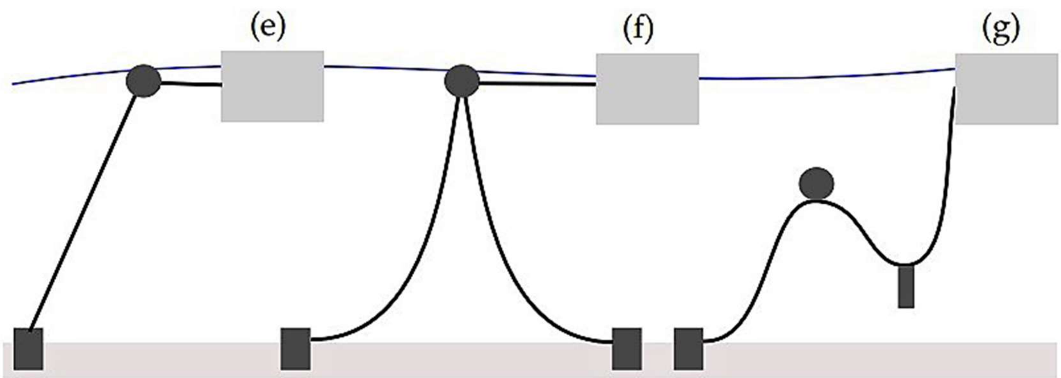

Figure 44:Other possible configurations: (e) SALM; (f) CALM; (g) Lazy-S (from J. Davidson and J. Ringwood "Mathematical modelling of mooring systems for Wave Energy Converters-A review", 2017).

2. Anchorage

The anchors that are in floating systems of marine current turbines are fluke, pile, deadweight, and plate structures (Figure 45).

a) *Fluke (or drag embedded) anchors* are installed by pulling on the anchor line and dragging it along the sea floor. Eventually, the fluke will penetrate the sea floor and the anchor will be embedded.
b) *Pile anchors (PA)* are installed either by hammering them into the ground, or by drilling and grouting them in place, depending on the nature of the sea floor.
c) *Deadweight anchors (DWAs)* are simply placed on the sea floor and hold the turbine in place by their sheer weight and friction with the sea floor.
d) *Plate anchors* can be installed using various methods, all requiring a metal rod or tube to push the anchor to the desired depth below the seabed and then rotate them to their final orientation.

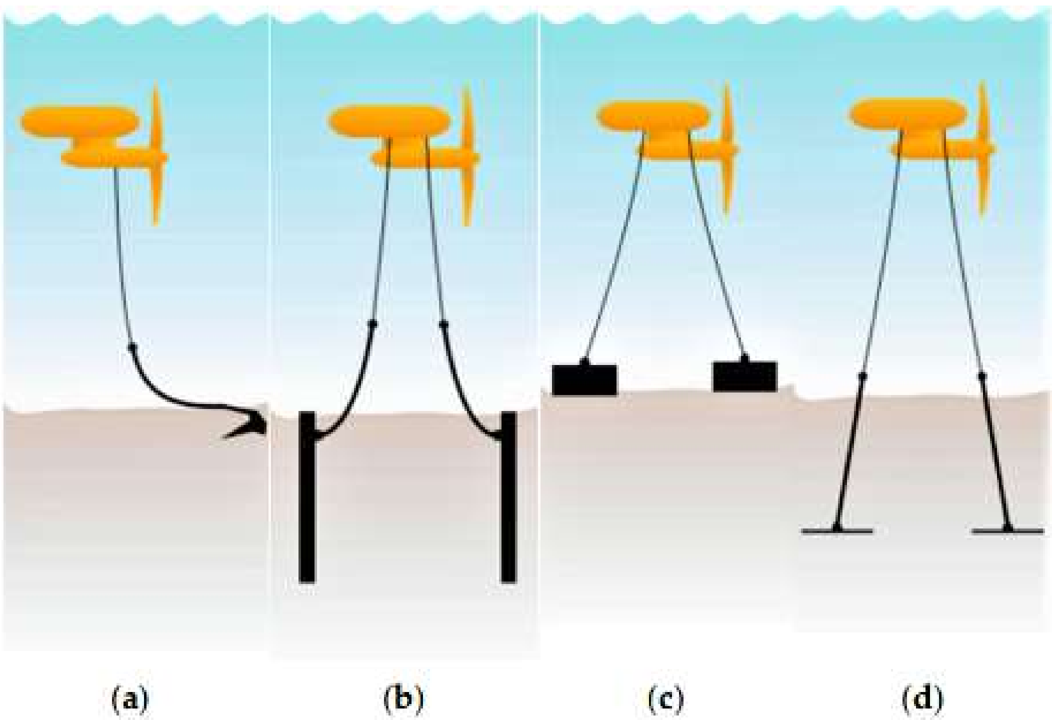

Figure 45:Types of foundations for anchoring ocean current turbines:(a)Fluke, (b)Pile, (c)Deadweight, (d)Plate

The most relevant aspects to be considered in selecting an anchor type are:

- Local water depth;
- Type of seabed;
- Installation complexity;

- Characteristics of the turbine;
- Transportation of the system components.

The soil properties are the most important element to consider.

Fluke and plate anchors would be very complicated, even unfeasible, on a rocky seabed indeed the most suitable anchors for the type of soil in the Strait of Messina, which is weak rock, are deadweight (DWA) and pile anchors (PA).

Weak rock often has complex mechanical behaviour, mostly dis-homogeneous and anisotropic, due to the presence of defects or pre-existing discontinuities, and is considered a mid-point between soil and hard rocky spoils. This means a specific design procedure is needed, which considers its geotechnical properties. The behaviour of weak rock is related to its secondary structure, that is, the spacing and thickness of the soil-filled cracks and joints, and its compressive strength. Therefore, placing foundations on weak rock may result in greater displacements and deformations; specific calculation procedures are needed.

Let’s see more about the two suitable type of anchor for a weak rock soil.

Pile Anchors (PA)

Pile anchors are composed of hollow tubes which are drilled or hammered into the seabed and can be grouted into position. Compared to other types of foundations, pile foundations have an important axial and lateral load capacity, indeed they are able to transmit high axial loads through soft superficial sediments down to competent bearing soils or rock.

Pile foundations require highly specialized installation equipment, however they are usually deployed in clay and sandy soils, due to the difficulty of drilling rock.

Pile foundations can still be installed in hard seafloors (rock and coral) by drill-and-grout technique, but drilled-and-grouted piles require more specialized skills and installation equipment and incur high installation costs. Costs are high and increase even more rapidly in deeper water or exposed locations where more specialized installation vessels and driving equipment are required.

In addition, more extensive and better-quality site data are required than the data required for other anchor types, especially accurate soil properties.

Figure 46:Offshore pile driving operation

Dead weight anchor (DWA)

The deadweight anchor is the simplest anchor. A dead weight anchor (DWA) is made of concrete, without/ with steel reinforcement, and must have the necessary weight to bear the environmental demands and the action of the turbine: it consists of a heavy object placed on the seafloor to resist vertical and/or horizontal loads. The holding capacity comes mainly from the weight of the anchor and partially from the friction between the anchor and the soil.

The advantages of this type of anchoring are that they do not require drilling, indeed on a very hard seabed they might provide the only reasonable anchoring option, since they are the only type of anchoring system that does not necessarily require much soil penetration to work properly. Plus, in comparison with embedded anchors, they can be built from materials commonly used for onshore structures and can be easily recovered from the installation site. Deadweight anchors are often used because they are inexpensive.

On the other hand, they may require heavy lift capabilities for installation and they are considered a poor choice in the case of sloping seafloors, since downslope movements along the seafloor can be expected. That is why the design procedure for DWAs considers the addition of so-called shear keys, which increase the lateral anchor holding capacity by inducing failure in the soil and not at the anchor soil interface, increasing the performances of the anchor. In addition, the usable water depth is reduced so deadweight can be an undesirable obstruction.

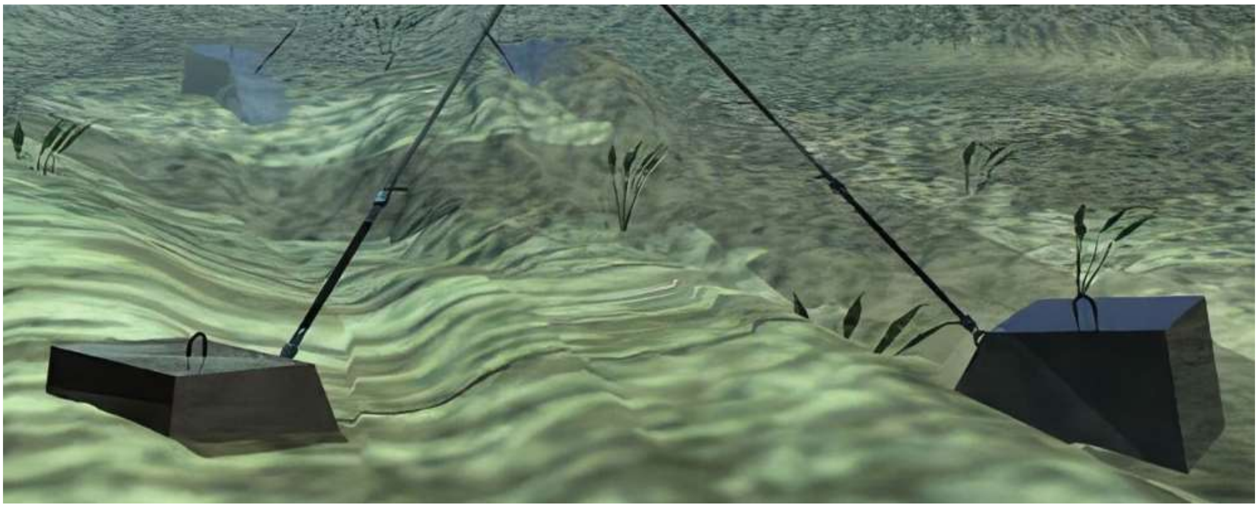

Figure 47:Deadweight anchor example

3.Line type

Mooring line selection is dependent on many factors. The type of line will determine how the system functions, as the elasticity of the line varies greatly with material selection. Let's see the different options: chain, wire or rope.

Chains

There is a long history of the use of chains as mooring lines. This wealth of experience can help to reduce capital costs by reducing safety factors required for materials with less experience.

Chains are most commonly made from steel of varying grades including and are relatively heavy. There are two types of chain links namely studless and studded chain links (Figure 48).

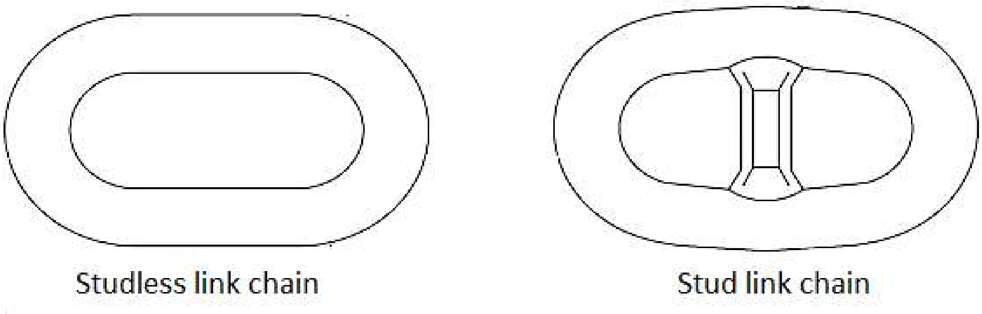

Figure 48:Studless link chain and stud link chain

Studless links chains avoid issues relating to loose or missing studs which can reduce maintenance and inspection costs, and can also reduce the line weight by up about 10%. However, the fatigue life can be comparable to half that of a studded chain.

Studded link chains are preferable in terms of ease of handling and are considered to have a higher reliability than studless link chains; however, the fatigue life can decrease significantly with loose or broken links. The links require additional inspection of stud connection or welding.

Technical requirements and guidance for the design, materials, manufacture and testing of mooring chains are given by DNV-OS-E302, (Det Norske Veritas, 2008). The strong catenary stiffness effect, the low elasticity and the high breaking strength make this mooring line suitable for long-term mooring.

A steel chain in an ocean environment will be subjected to corrosion, so adequate preventative measures should be taken, either by active or passive anti corrosion methods and periodic inspections and maintenance will be required too in order to keep it clean from biofouling, that can increase the weight per unit and damage the chain due to excessive abrasion. In addition, the use of chain in a catenary mooring construction will involve a large amount of scour and abrasion, particularly in the thrash zone.

The selection of the length of chain is an important decision to ensure that it serves its function. The chain length and size will depend on the size of the load which it is mooring, this includes tidal and wave forces and the weight of the floating structure to be moored and the nature of the seabed. The length of chain will also depend on the depth of water and the tidal range in the location, the length will typically vary between 3 and 7 times the water depth to ensure that the required compliance is provided by the mooring system.

Wire ropes

Wire ropes come in many different compositions in order to satisfy a multitude of applications and so withstand different loading, abrasion, bending fatigue, crushing and corrosion conditions.

The wire mooring line is lighter and has a higher elasticity and a lower catenary effect than a chain mooring line. These applications make that the steel wire mooring system is used for higher water depths.

Technical requirements and guidance for the design, materials, manufacture and testing of mooring wire ropes are given by DNV-OS-E304, (Det Norske Veritas, 2008). The two factors that govern the selection of a wire rope are: required strength and bending fatigue.

Wire ropes are identified primarily by the type of construction, more specifically by the number of strands in the rope and the number of wires in each strand. The stranded rope constructions include a number of strands wound in the same rotational direction around a centre core to form the wire rope. This construction generates torque as tension increases. Here there are the torque balanced spiral rope constructions (spiral strand) that do not generate significant torque with tension changes because these constructions use layers of wires (or bundles of wires) wound in opposing directions to obtain the torque balanced characteristics.

Typical wire rope constructions are spiral strand, six strand rope and the multiple strand rope.

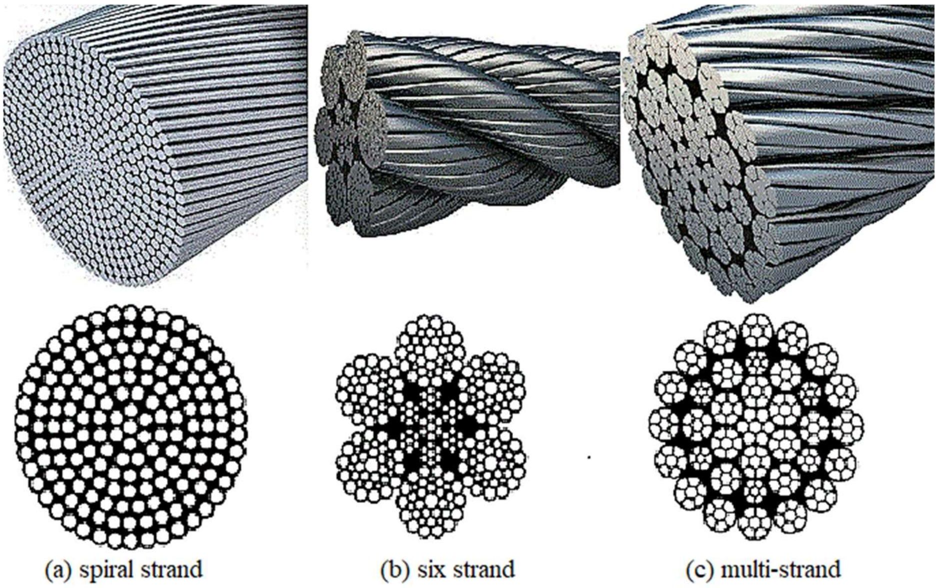

Figure 49:Different kind of wire rope:(a) spiral strand, (b) six strand and (c) multi-strand

In multiple strand wires the strands are wound around the core in the same direction, while in the spiral strand wires the strands are wound around the core in different directions. Multiple strand ropes are cheaper than spiral strand and have a greater elasticity, however are more susceptible to corrosion. Spiral strand ropes generally have a higher strength and fatigue resistance; in addition, one of the benefits of spiral strand ropes is that they do not generate torsion forces as loads increase, as is the case with multiple strand ropes, and so are preferable in permanent moorings. The ropes can be covered with a sheath, to help prevent corrosion of the strands.

Synthetic fibre ropes

The widespread use of synthetic ropes within the maritime sector is a relatively modern occurrence and this short term experience in real conditions results in a high safety factor being applied.

Synthetic fibre ropes have seen a significant increase since the expansion of deep water mooring, where conventional mooring systems using steel wire ropes and chains have become significantly more difficult and expensive to install.

Synthetic ropes are lighter weight mooring lines and they can offer superior elongation properties for compliance of the mooring system than that of chain and wire ropes: these properties make them more common for very deep water tether applications. Synthetic ropes have relatively poor abrasion characteristics when compared to chain or steel wire and, thus, must not be used in situations where they can contact the seabed, so they are suitable for taut line applications.

Fibre rope segments in mooring lines are normally protected by an outer jacket, which has an adequate resistance to hydrolysis, chemical corrosion, creep phenomena, fish bites, friction and shear, with a proper flexibility at minimum exposure temperatures in order to meet the requirement to protect the rope core.

Reasons for selecting a synthetic rope solution may include factors such as:

- high strength to weight ratios;
- near neutral buoyancy;
- high elasticity;
- corrosion resistance.

On the other hand, the cost of a synthetic fibre rope is relatively high.

There are several different materials which can be used for mooring lines; each has properties which should be considered in the selection of the most suitable rope for the mooring system. The most commonly used materials include: polyester, aramid, HMPE (high modulus polyethylene), Nylon.

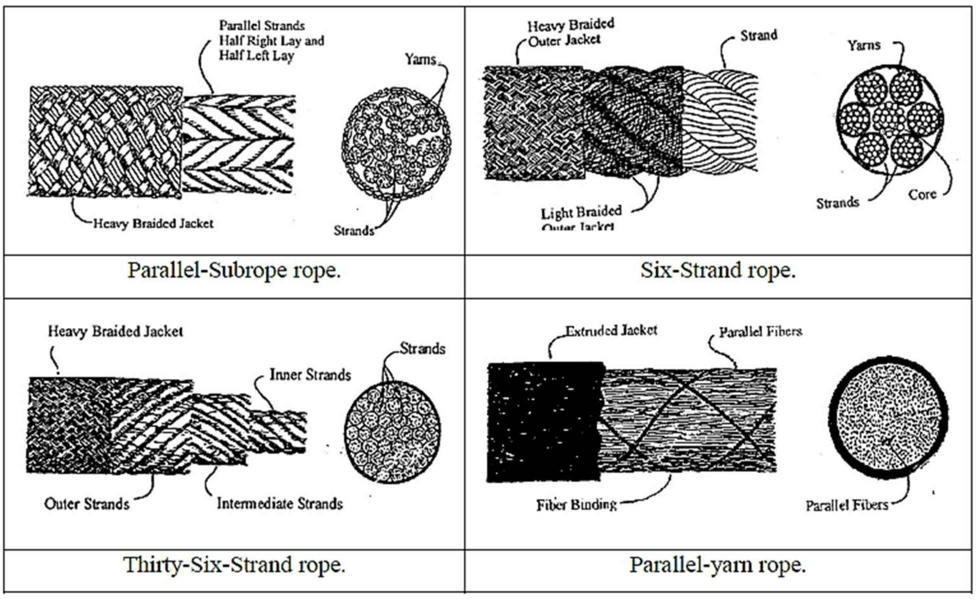

Figure 50:Different kind of synthetic rope

4.1 GEMSTAR's mooring system

Let's see the different components selected in order to create a good mooring system for the device GEMSTAR.

1.Configuration

The configuration single point mooring, that is a single tense anchor line, would represent the simplest solution, but at the same time it has some drawbacks: a large operational footprint and the absence of redundancy. So that is why a spread mooring configuration, consisting of two taut lines, was taken into consideration: it allows to reduce the operational footprint and have a certain degree of redundancy and therefore safety.

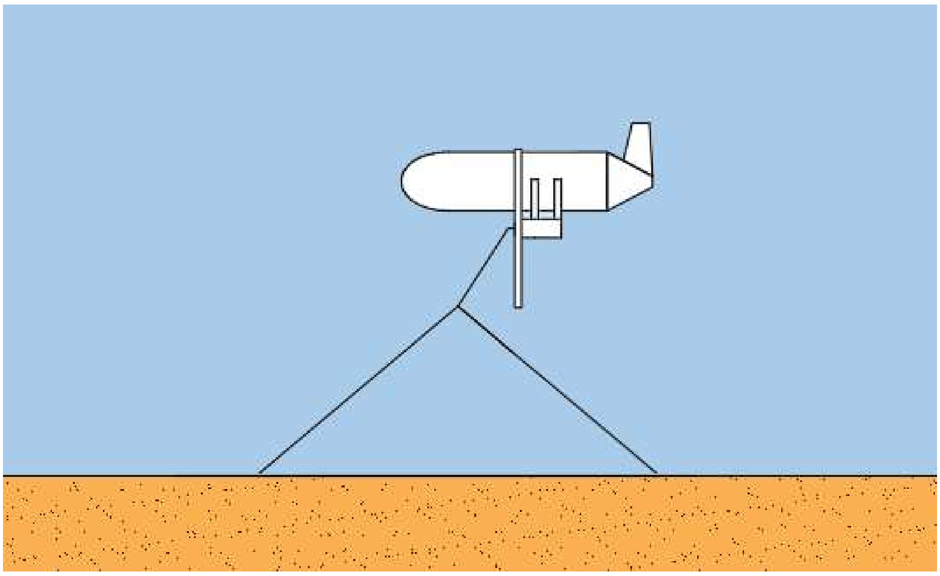

Figure 51:GEMSTAR two lines configuration

The solution involves two lower mooring lines connected to the respective anchoring points on the seabed (B1 and B2) and converging in a single connection point (C). An upper cable then joins the connection point (C) to the device at the attachment point (A). The angle of inclination of the lower cables with respect to the horizontal plane was chosen equal to δi = 40 °, while the angle of inclination of the upper cable with respect to the horizontal plane is variable and called δs.

The two possible situations that can occur based on the conditions in which the device will find itself working are:

- if δs> δi = 40 ° then both cables are under tension and the angle δi remains constant equal to 40 °.
- if δs <δi = 40 ° then only one of the two cables is under tension and the angle δi is no longer fixed equal to 40 °, but can also be smaller.

From previous analysis the acting forces on both the device and the two lines are known, such us:

- Bnet= B-W=1100 kN and it is the net vertical buoyancy force equal to the sum of the buoyancy force B and the weight force of the device W.
- FH= horizontal force, variable according the current velocity.
- S1= 1932 kN and it is the tension on the most stressed line, calculated in ULS condition.
- S2= 121.5 kN and it is the tension on the less stressed line, calculated in ULS condition.

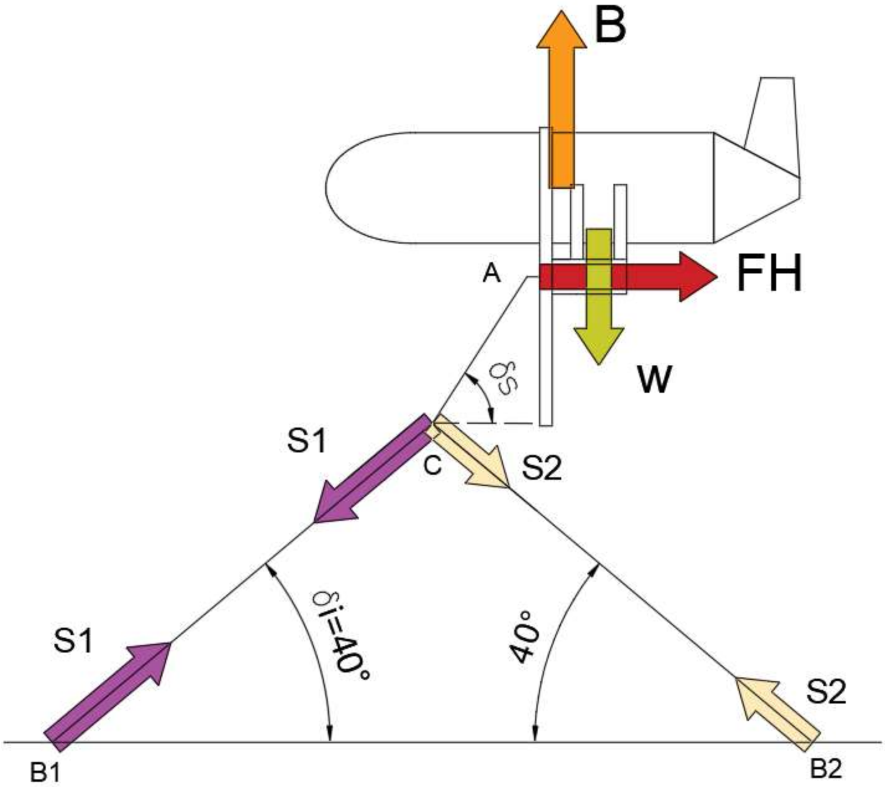

Figure 52:CAD scheme of the forces acting on both lines and device

2.Anchorage

Since a pile anchor would be excessively expensive for the installation of a single device, it was realized an innovative anchoring solution, which uses a dead weight anchor.

The dead weight anchor designed consists of a concrete caisson, which, thanks to its buoyancy capacity, allows the immediate solution to the problem related to the transport of the anchor to the installation site, simply by being pulled by a special boat.

To solve the problem of placing the anchor at a depth of 35 m, an innovative solution was developed in order to make the anchor much lighter during the suspension phase. This solution exploits the introduction of an upward push, obtained by storing a volume of air inside PVC pipes placed in the cells of the caisson itself, which in fact counterbalances a large part of the weight of the caisson.

The designed anchor consists of a concrete rectangular base caisson whose main dimensions are: 3.16 m height, 19.76 m bigger side, 11.16 m smaller side with a total of 45 square cells, with a 2 m side and 2.6 m height. In addition, there two additional triangular portions along the shorter side of the body.

In each cell 100 PVC pipes with a diameter of 200 mm, in the specific PN6 pipes, are placed for a total of 11’700 m of pipes and an air volume of 332.4 m^3 so the upward push generated by the air volume is Sair pipes= 332.4 tons.

The submerged weight of the designed anchor is 345.5 tons.

During the suspension phase the submerged weight of the anchor is way smaller than 345.5 tons thanks to the air volume stored inside the pipes.

$$W_{sub\ designed\ anchor} - S_{pipes\ air} = 345.46 - 332.43 \approx 13\ ton$$

3.Lines

In the analysed mooring system, there are an upper line with a length of 7 m and two lower lines with a length of approximately 10.5 m each and for all three lines a suitable synthetic ropes were chosen in order to endure the tensions S1 and S2.

Installation phases

The anchor installation can be divided into the three main phases:

1) Transport phase: the anchor is dragged by a special boat to the installation site since it can float and the emerged portion is around 39 cm;
2) Suspension phase: the space between the PVC pipes in the caisson is filled with water and the caisson can then be lowered, supported by a dipper bar, onto the seabed since it only weights around 13 tons;
3) Laying phase: the pipes are also filled with water and the caisson is thus definitively secured to the seabed reaching the final designed submerged weight of 345.5 tons.

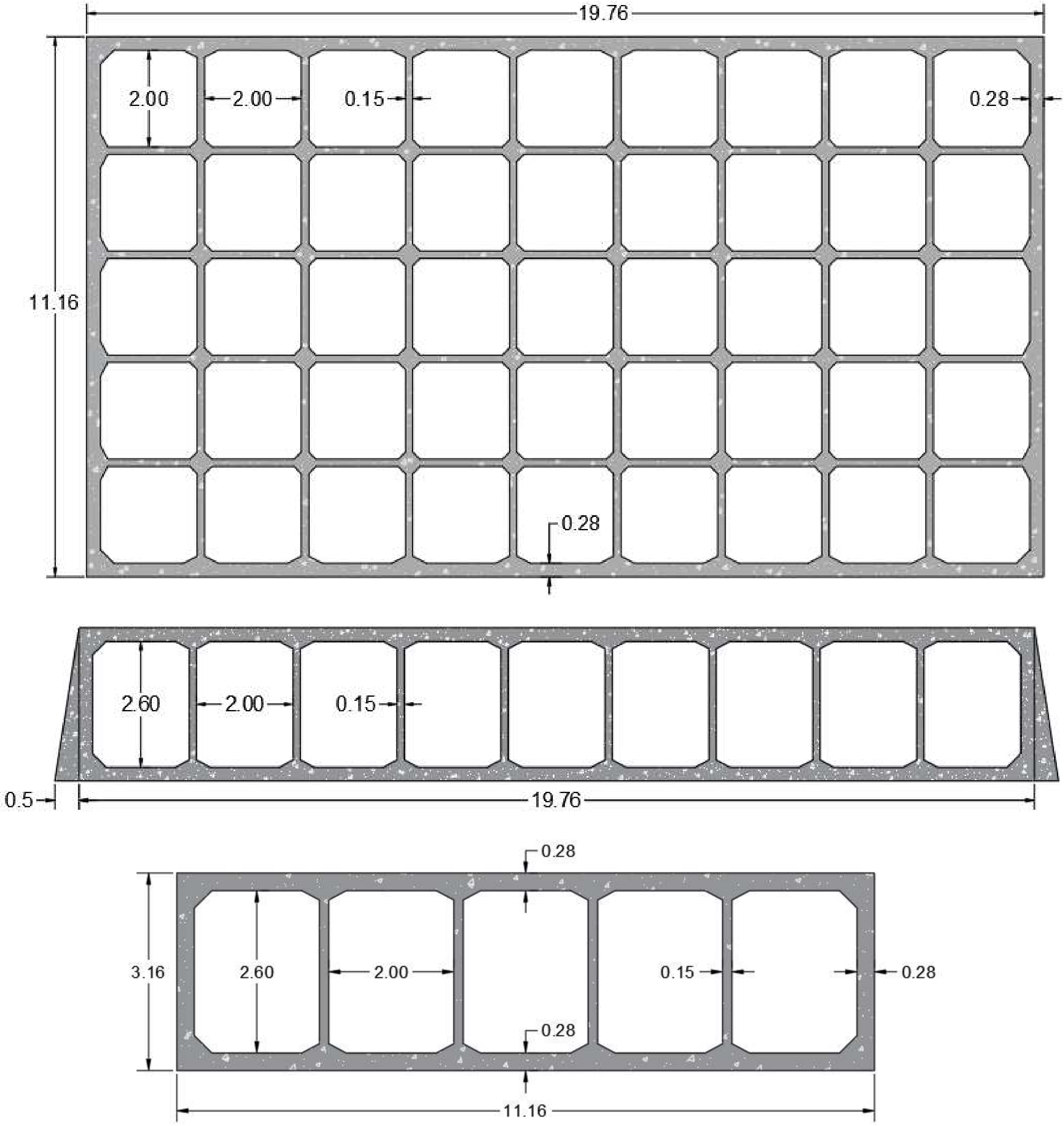

Figure 53: Plan, longitudinal section and transversal section of the designed anchor

Chapter V

OpenFOAM

This chapter provides a brief overview of the program and its tools.

5.OpenFOAM

Since for more complex problems an analytic solution is not available and tests are expensive, computer generated solutions become a valid path to follow.

Computational fluid dynamic (CFD) is a branch of fluid mechanics that uses numerical analysis and algorithms to solve and analyse problems that involves fluid flows. The fundamental bases of almost all CFD problems are the Navier-Stokes equations, and the finite volume method (FVM) is a common discretization method used in CFD codes, as it has an advantage in memory usage and solution speed, especially for large problems, high Reynolds number turbulent flows, and source term dominated flows.

OpenFOAM (Open Field Operation And Manipulation) is a free and open source finite volume CFD toolbox originally developed at the Imperial College. It is a cell-centred finite volume framework for computational fluid dynamics supporting unstructured polyhedral meshes. OpenFOAM is first and foremost a C ++ library, used primarily to create executables, known as applications, to solve complex problems such as turbulence, fluid flows, electromagnetic, chemical reactions, combustion, etc. It also features applications to pre- and post- process, including mesh generation tools (e.g. blockMesh, snappyHexMesh), setting and modifying field values, mesh decomposition and sampling data. The overall structure of OpenFOAM is shown in Figure 54.

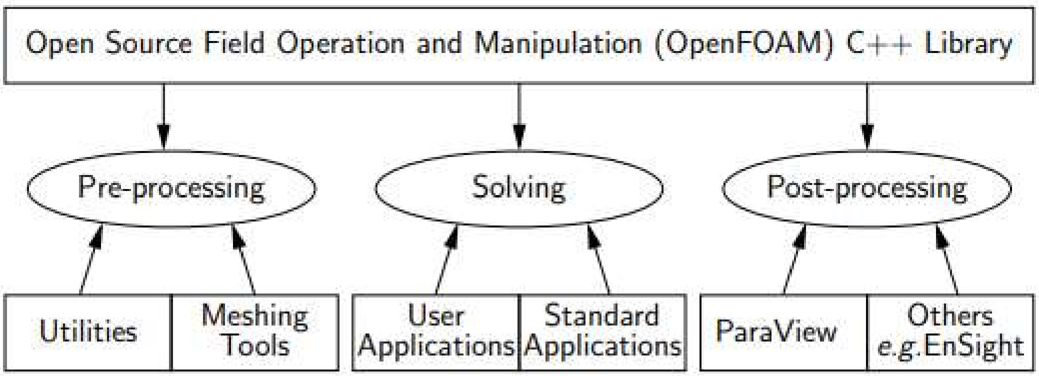

Figure 54:Structure of OpenFOAM

The basic directory structure for a OpenFOAM case, that contains the minimum set of files required to run an application, is shown in Figure 55 and described as follows:

- A ***constant directory*** that contains a full description of the case mesh in a subdirectory polyMesh and files specifying physical properties for the application concerned, like transportProperties.
- A ***system directory*** for setting parameters associated with the solution procedure itself. It contains at least the following 3 files: *controlDict* where run control parameters are set including start/end time, time step and parameters for data output; *fvSchemes* where discretisation schemes used in the solution may be selected at run-time; and, *fvSolution* where the equation solvers, tolerances and other algorithm controls are set for the run.
- The ***'time' directories*** containing individual files of data for particular fields. The data can be: either, initial values and boundary conditions that the user must specify to define the problem; or, results written to file by OpenFOAM. The OpenFOAM fields must always be initialised, even when the solution does not strictly require it, as in steady-state problems. The name of each time directory is based on the simulated time at which the data is written, and since simulations usually start at time t = 0, the initial conditions are usually stored in a directory named 0.

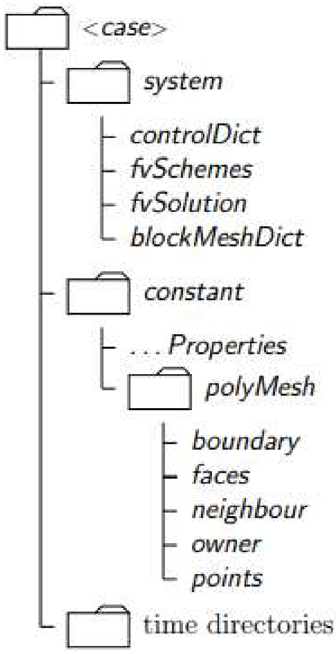

Figure 55.Directory structure

Running applications

OpenFOAM is distributed with a large set of pre-compiled applications but users also have the freedom to create their own or modify existing ones. Applications are split into two main categories:

- *solvers* that are each designed to solve a specific problem in computational continuum mechanics;
- *utilities* that perform simple pre-and post-processing tasks, mainly involving data manipulation and algebraic calculations.

Each application is designed to be executed from a terminal command line, typically reading and writing a set of data files associated with a particular case.

OpenFOAM is also able to run in parallel on distributed processors. The method of parallel computing used by OpenFOAM is known as domain decomposition, in which the geometry and associated fields are broken into pieces and allocated to separate processors for solution.

PRE-PROCESSING- Mesh generation

The mesh is an integral part of the numerical solution and must satisfy certain criteria to ensure a valid, and hence accurate, solution.

The meshing tools, included in OpenFOAM, are:

- the ***blockMesh utility*** for generating simple meshes of blocks of hexahedral cells and each block of the geometry is defined by 8 vertices, one at each corner of a hexahedron;

- the ***snappyHexMesh utility*** for generating complex meshes of hexahedral and split-hexahedral cells automatically from triangulated surface geometries.

Starting with a block structured mesh that defines the extensions of the domain, created by the means of the *blockmesh*, SnappyHexMesh then can include automatically any .stl file (stereo lithography) or .obj file, which describe the geometry of modelled objects. The solver then starts to split all cells close to the .stl surface. When the refinement is finished, all cells inside the .stl are removed. The user defines the outside with a Cartesian coordinate beforehand. Specific refinement regions (boxes, cylinders or spheres) can be assigned. Furthermore, SnappyHexMesh incorporates many parameters to ensure a good quality mesh.

SOLVING

OpenFOAM does not have a generic solver applicable to all cases. Instead, users must choose a specific solver for a class of problems to solve. The equations and algorithms differ from one solver to another, so that the selection of a solver involves the user making some initial choices on the modelling for their particular case. The choice of solver determines many of the parameters and physical properties required to define the case, but leaves the user with some modelling options that can be specified at runtime.

Some examples of solver's categories of continuum mechanics are: incompressible flow, heat transfer, multiphase, Lagrangian, combustion...

For a successful simulation, setting appropriate **boundary conditions** is vital, and ill-posed boundary conditions will lead to physically incorrect predictions, and in many cases solver failure. Users must specify the boundary conditions for each solved field.

POST-PROCESSING- ParaView

Extended capabilities are added by third party programmes. The most representative case is ParaView, which is the main programme used for post-processing purposes.

ParaView is an open-source, multi-platform data analysis and visualization application, and through it users can quickly build visualizations to analyse their data using qualitative and quantitative techniques.

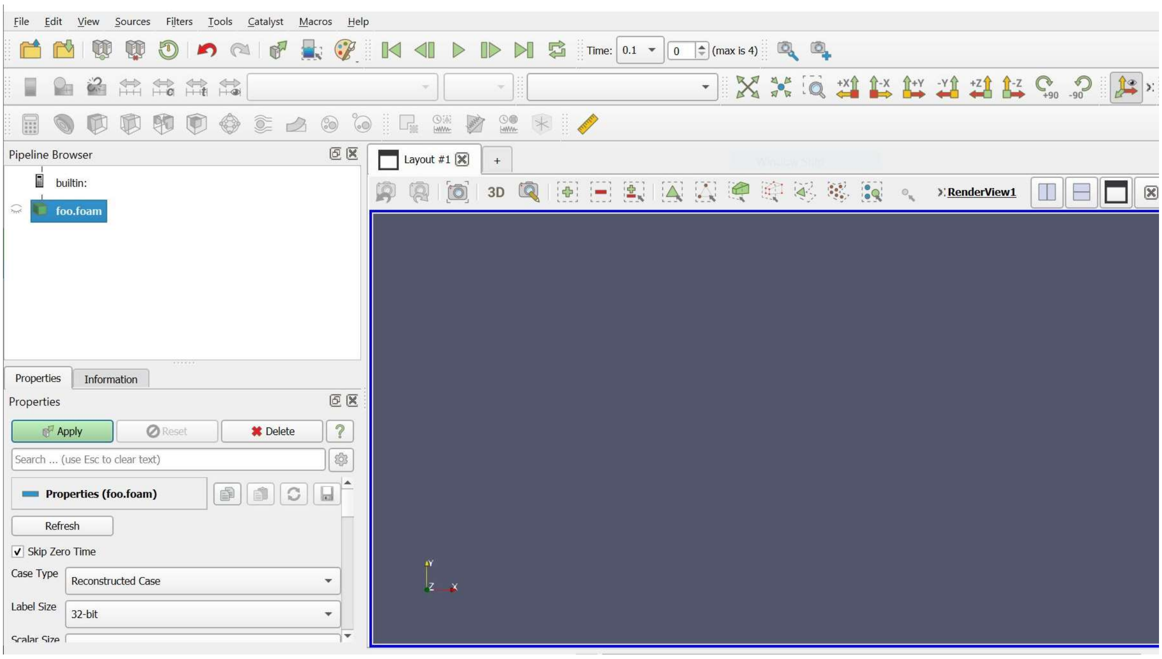

Figure 56:Paraview

Chapter VI

GOVERNING EQUATIONS

This chapter provides a brief overview of the fundamental bases of almost all CFD problems: the Navier-Stokes equations, that describe the motion of an incompressible viscous fluid, and the turbulence models.

6.Governing equations

The most general equations that describe the motion of an incompressible viscous fluid (Newtonian) are called Navier (1827) and Stokes (1845).

$$\frac{\partial u}{\partial t}+\frac{\partial u}{\partial x}u+\frac{\partial u}{\partial y}v+\frac{\partial u}{\partial z}w-2\Omega v\sin\phi+\frac{1}{\rho}\frac{\partial p}{\partial x}-\nu\left(\frac{\partial^2 u}{\partial x^2}+\frac{\partial^2 u}{\partial y^2}+\frac{\partial^2 u}{\partial z^2}\right)=0$$

$$\frac{\partial v}{\partial t}+\frac{\partial v}{\partial x}u+\frac{\partial v}{\partial y}v+\frac{\partial v}{\partial z}w+2\Omega u\sin\phi+\frac{1}{\rho}\frac{\partial p}{\partial y}-\nu\left(\frac{\partial^2 v}{\partial x^2}+\frac{\partial^2 v}{\partial y^2}+\frac{\partial^2 v}{\partial z^2}\right)=0$$

$$\frac{\partial w}{\partial t}+\frac{\partial w}{\partial x}u+\frac{\partial w}{\partial y}v+\frac{\partial w}{\partial z}w+g+\frac{1}{\rho}\frac{\partial p}{\partial z}-\nu\left(\frac{\partial^2 w}{\partial x^2}+\frac{\partial^2 w}{\partial y^2}+\frac{\partial^2 w}{\partial z^2}\right)=0$$

They provide the u, v, w velocity components of a fluid as well as the value of the pressure p, respect to a reference frame x, y, z, where the z axis is assumed vertically. In addition to these equations it must be considered the continuity equation, that expresses the mass conservation for a fluid with constant density ρ:

$$\nabla\cdot\vec{v}=\frac{\partial u}{\partial x}+\frac{\partial v}{\partial y}+\frac{\partial w}{\partial z}=0$$

The Navier-Stokes equations can be seen as a balance of forces. The first four terms represent the forces of inertia, related to the acceleration of the fluid, the fifth term concerns the mass forces due to the gravity acceleration g and the Coriolis acceleration (with Ω the rotation speed of the earth and φ latitude), the last two terms represent the surface forces due respectively to the pressure and viscosity of the fluid. Viscous (normal and tangential) stresses are represented as:

$$\frac{\tau_{ij}}{\rho}=\nu\left(\frac{\partial u_i}{\partial x_j}+\frac{\partial u_j}{\partial x_i}\right)$$

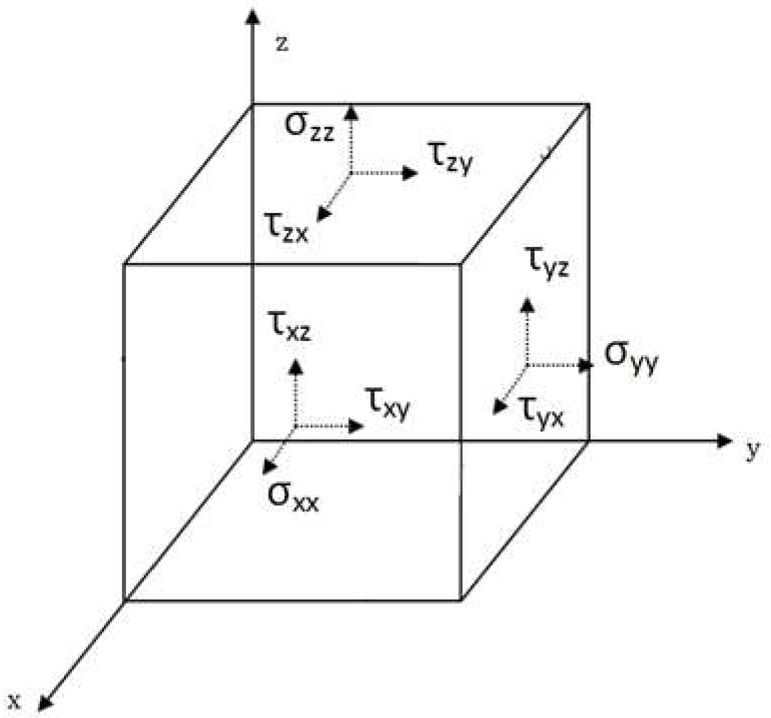

Figure 57:Normal and tangential stresses on a fluid element

Rewriting the N-S equations, an important factor for the description of the type of motion can be obtained: the Reynolds number. It is a dimensionless quantity and it is the ratio between the inertial forces and the viscous forces of a fluid. It is essentially described by the formula:

$$Re = \frac{inertial\ forces}{viscous\ forces} = \frac{\rho u L}{\mu} = \frac{uL}{\nu}$$

where:

- Re= Reynolds number
- ρ = density of fluid (kg/m³)
- u = velocity of fluid (m/s)
- μ= dynamic viscosity of fluid (kg/ms)
- L= characteristic length of solid in which fluid is flowing (m)
- ν= kinematic viscosity of fluid (m^2/s)

Depending on the Reynolds number value, the type of motion can be distinguished in: laminar (prevalence of viscous force), transitional or turbulent (prevalence of inertial forces).

The Navier-Stokes equations, associated with the continuity equation if incompressible fluid, make a system composed of 4 equations with 4 unknowns (u, v, w and p), which associated with suitable initial and boundary conditions make a well-posed problem. Basically it is a perfectly solvable system, capable of providing an instantaneous and precise description of the entire flow field in any hydrodynamic regime (laminar, transition or turbulent).

Despite this, the exact analytical solution is known only for some simple cases, such as uniform laminar motion and with simple geometries. Generally, the equations must be solved numerically describing the turbulent character of the motion, even if it is irregular in time and space, dissipative, rotational, three-dimensional, non-homogeneous, anisotropic and non-linear.

The direct numerical solution (DNS) can be obtained only for low Reynolds numbers (10^4) and computing domains that are not too large.

For high Reynolds numbers, the computational cost associated to a direct numerical solution of N-S would be too high, and so other solution strategies are necessary: the so called Turbulence Models.

6.1 Turbulence models

The modelling of turbulence constitutes one of the most important aspects of CFD modelling and correctly modelling turbulence is the key in obtaining correct and reliable CFD results.

This group of models distinguishes two main types of turbulence models:

- **Reynolds Averaged Navier-Stokes Equation (RANS):** an averaging operation can be applied to the Navier-Stokes equations to obtain the mean equations of fluid flows called Reynolds Averaged Navier-Stokes (RANS) equations. RANS modelling is the most common and widespread approach in industrial applications.
- **Large Eddy Simulation (LES):** In LES, the smallest scales of turbulence are spatially filtered out while the largest, most energy containing scales are resolved directly. In most LES models, the filtering of the equations is obtained at mesh size level, relegating the modelling to flow scales smaller than the grid size. LES modelling offers increased range of applicability and increased fidelity of the solution but all of this comes with an increased computational cost.

Let's see more in detail the RANS, being the model chosen for the current analysis.

6.1.1 RANS

The averaged Navier-Stokes equations, called RANS or Reynolds Averaged Navier-Stokes Equations, are equations with magnitudes no longer instantaneous, but averaged over a certain time interval, sufficiently small compared to the phenomena, sufficiently large compared to turbulence disturbances. For many practical applications, the knowledge of the average quantities can be enough for the solution of the problem.

The turbulent motion can be represented as the superposition of an average motion and a fluctuating motion over time.

Thus, to derive the Reynolds Averaged Navier-Stokes Equations (RANS), it is assumed that the dependent variables (velocity and pressure) consist of a mean part φ and a random fluctuating turbulent part φ', such that φ = φ + φ'. This is called *Reynolds decomposition*.

It's necessary to make an integration over time to eliminate the motion's fluctuating part due to turbulence: renouncing to a detailed description of these pulsations, it's possible to evaluate the average values of the quantities involved.

The process of Reynolds averaging is now to insert u = u + u', v = v + v', w = w + w' and p = p + p' into the N-S equations, and thereafter take the average of the whole equation term for term:

$$\bar{u}\frac{\partial \bar{u}}{\partial x} + \bar{v}\frac{\partial \bar{u}}{\partial y} + \bar{w}\frac{\partial \bar{u}}{\partial z} + \frac{\partial \bar{u}}{\partial t} - 2\Omega \sin\phi\, \bar{v} + \frac{1}{\rho}\frac{\partial \bar{p}}{\partial x} - \nu\Delta^2\bar{u} + \left(\frac{\partial}{\partial x}\overline{u'u'} + \frac{\partial}{\partial y}\overline{u'v'} + \frac{\partial}{\partial x}\overline{u'w'}\right) = 0$$

$$\bar{u}\frac{\partial \bar{v}}{\partial x} + \bar{v}\frac{\partial \bar{v}}{\partial y} + \bar{w}\frac{\partial \bar{v}}{\partial z} + \frac{\partial \bar{v}}{\partial t} + 2\Omega \sin\phi\, \bar{u} + \frac{1}{\rho}\frac{\partial \bar{p}}{\partial y} - \nu\Delta^2\bar{v} + \left(\frac{\partial}{\partial x}\overline{u'v'} + \frac{\partial}{\partial y}\overline{v'v'} + \frac{\partial}{\partial x}\overline{v'w'}\right) = 0$$

$$\bar{u}\frac{\partial \bar{w}}{\partial x} + \bar{v}\frac{\partial \bar{w}}{\partial y} + \bar{w}\frac{\partial \bar{w}}{\partial z} + \frac{\partial \bar{w}}{\partial t} + g + \frac{1}{\rho}\frac{\partial \bar{p}}{\partial z} - \nu\Delta^2\bar{w} + \left(\frac{\partial}{\partial x}\overline{w'u'} + \frac{\partial}{\partial y}\overline{w'v'} + \frac{\partial}{\partial x}\overline{w'w'}\right) = 0$$

adding the continuity equation for the fluctuating turbulent part:

$$\nabla \cdot \overrightarrow{v'} = \frac{\partial u'}{\partial x} + \frac{\partial v'}{\partial y} + \frac{\partial w'}{\partial z} = 0$$

The Reynolds equations coincide with the original ones, except for the last bracket related to the time average of the pulsating products of the velocity, called Reynolds terms or additional turbulent stresses. These terms have the same sign and the same structure of the stresses due to viscosity; therefore, it is reasonable to consider them as additional stresses to turbulence, defined as:

$$\frac{\tau'_{ij}}{\rho} = -u'_i u'_j = \nu_T \left(\frac{\partial u_i}{\partial x_j} + \frac{\partial u_j}{\partial x_i} \right)$$

The coefficient ν_T is called turbulent kinematic viscosity, unlike ν it is not a characteristic constant of the fluid, but a tensor dependent on the characteristics of the motion. There are several "turbulence closure models" with different complexity:

- 0 equation models, viscosity is modelled on the basis of empirical assumptions (e.g. mixing length);
- 1 or 2 equation models, turbulent viscosity is determined as a function of turbulent quantities (e.g. turbulent kinetic energy) for which it is necessary to solve additional transport-diffusion equations (e.g. k-epsilon, k-omega, etc.).

6.1.2 k-epsilon model

The k-epsilon model is the most popular two-equation turbulent model. The first proposal dates back to Chou (1945), but the first significant contribution is due to Jones and Launder (1972) with the model called standard k-epsilon. The turbulent kinematic viscosity is defined as:

$$\nu_T = C_\mu \frac{k^2}{\epsilon}$$

where:

- k= turbulent kinetic energy
- ε= rate of turbulent dissipation
- C_μ= coefficient equal to 0.09

The equation for turbulent kinetic energy k is:

$$\frac{\partial k}{\partial t} + \upsilon_j \frac{\partial k}{\partial x_j} = \tau_{ij} \frac{\partial \upsilon_i}{\partial x_j} - \epsilon + \frac{\partial}{\partial x_j}\left[\left(\nu + \frac{\nu_T}{\sigma_k}\right)\frac{\partial k}{\partial x_j}\right]$$

The equation for the dissipation rate of turbulent kinetic energy is:

$$\frac{\partial \epsilon}{\partial t} + \upsilon_j \frac{\partial \epsilon}{\partial x_j} = C_{\epsilon 1} \frac{\epsilon}{k} \tau_{ij} \frac{\partial \upsilon_i}{\partial x_j} - C_{\epsilon 2} \frac{\epsilon^2}{k} + \frac{\partial}{\partial x_j}\left[\left(\nu + \frac{\nu_T}{\sigma_\epsilon}\right)\frac{\partial \epsilon}{\partial x_j}\right]$$

with the coefficients equal to $C_{\varepsilon 1}$ = 1.44, $C_{\varepsilon 2}$ = 1.92, C_μ = 0.09, σ_k = 1 and σ = 1.3.

Implementation of the k - model in OpenFOAM

In the model initial conditions, the turbulent kinetic energy is estimated as:

$$k = \frac{3}{2}\left(I\left|u_{ref}\right|\right)^2$$

where:

- u_{ref} = speed of the reference flow [m/s]
- I =intensity of the turbulence [%].

Depending on the situation, *I* assumes different percentages:

- for cases with high turbulence (complex geometries, turbines, compressors, etc.), it's considered a percentage between 5% and 20%;
- for cases with medium turbulence (non-complex geometries, low speeds, low Reynolds numbers), it's considered a percentage between 1% and 5%;
- for cases with low turbulence, it's considered an index of less than 1%.

In the model, by default, *I* is equal to 10%.

The turbulent dissipation is calculated as:

$$\epsilon = \frac{C_\mu^{0.75} k^{1.5}}{L}$$

where $C_\mu = 0.09$ and L is the turbulent length scale [m].

The $k - \varepsilon$ equations are only valid for fully turbulent high Reynolds number flow, and are thus not valid near the wall. Therefore, these equations are not integrated all the way to the walls. Instead it is used a patch, a turbulent wall-law onto the solution near the walls.

Chapter VII

CASE STUDY MODEL SET UP

This chapter describes the model set up for the case study, such as mesh generation, boundary conditions, solver and case control parameters.

7. Case study model set up

As described in the previous chapters, the innovative anchorage solution proposed for the TEC device GEMSTAR in the Messina Strait is exposed to strong sea currents, which reach a velocity of 3 m/s, and furthermore positioning a such huge structure on the seabed could interfere with the marine environment: flora and fauna typical of the strait, endangering the ecosystem.

The numerical analysis simulates the water current coming from just one direction, but the situation would be the same if simulating it from the opposite direction, as the current direction changes with the tide.

Furthermore, this simulation wants to model the water motion over the anchorage, in order to investigate which design of the anchorage is more convenient for the hydrodynamic and the environmental conditions.

Before jumping into the actual analysis, it's necessary to do a series of pre-process and solving procedures in order to set up the chosen model and so being able to get more reliable results.

The OpenFOAM's solver adopted is *simpleFoam:* a Steady-state solver for incompressible, turbulent flow, using the SIMPLE algorithm, while the turbulent model adopted is a RANS, and precisely the k-epsilon model.

The pre-process and solving operations are described following the steps specified below:

1. Geometry and mesh generation
2. Governing equations and turbulence model
3. Boundary conditions and initial fields
4. Solve and case control

Let's see them more in detail.

7.1 Geometry and mesh generation

The geometry of the anchorage was realized through **FreeCAD**: an open-source parametric 3D modeller made primarily to design real-life objects of any size.

In this way it was possible to obtain a 3D triangulated surface geometry in .obj file format and so positioning it into the defined solution domain.

Just to remind, the general measurements of the proposed anchorage are:

Bottom base length	20.76 m
Top base length	19.76 m
Height	3.16 m
Width	11.16 m

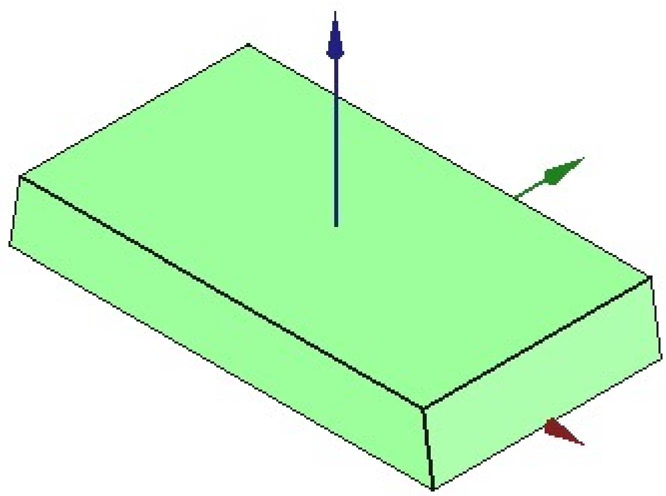

Figure 58:Geometry of the anchor in Freecad

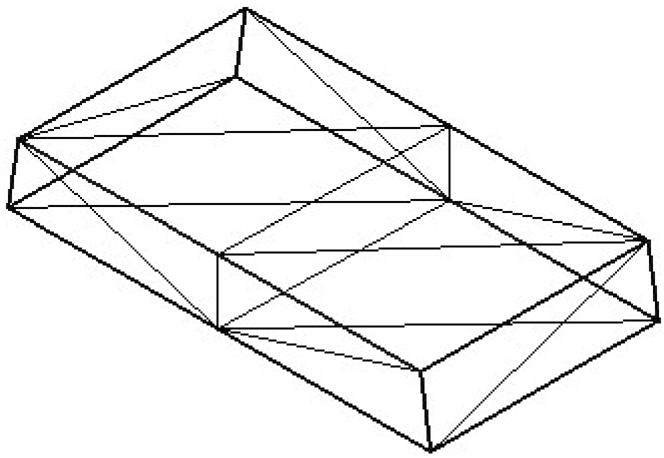

Figure 59:Mesh of the anchor in Freecad

Once the geometry was completed, it was possible to define the size of the fluid domain box and also its computational mesh (unstructured hexahedral mesh) through the utility blockMesh.

The fluid domain is a 3D box and, to be able to observe the development of turbulent motion on the anchor until it is almost exhausted in space, it is fixed 150 m long, while 35 m high because of the water depth of the zone, and it is 50 m wide. In addition, the cell size is 2 m in all directions x, y, z.

Around the body, the mesh size was refined in all directions, by the means of snappyHexMesh utility, in order to better capture the motion of water.

The blockMeshDict entries are: the file first specifies coordinates of the block vertices; it then defines the blocks from the vertex labels and the number of cells within it; and finally, it defines the boundary patches. The boundary patches defined are:

- inlet: type patch
- oulet: type patch
- ground: type wall
- frontAndBackAndTop: type symmetry

The structure of the domain and the global mesh can be seen in the Figure 60.

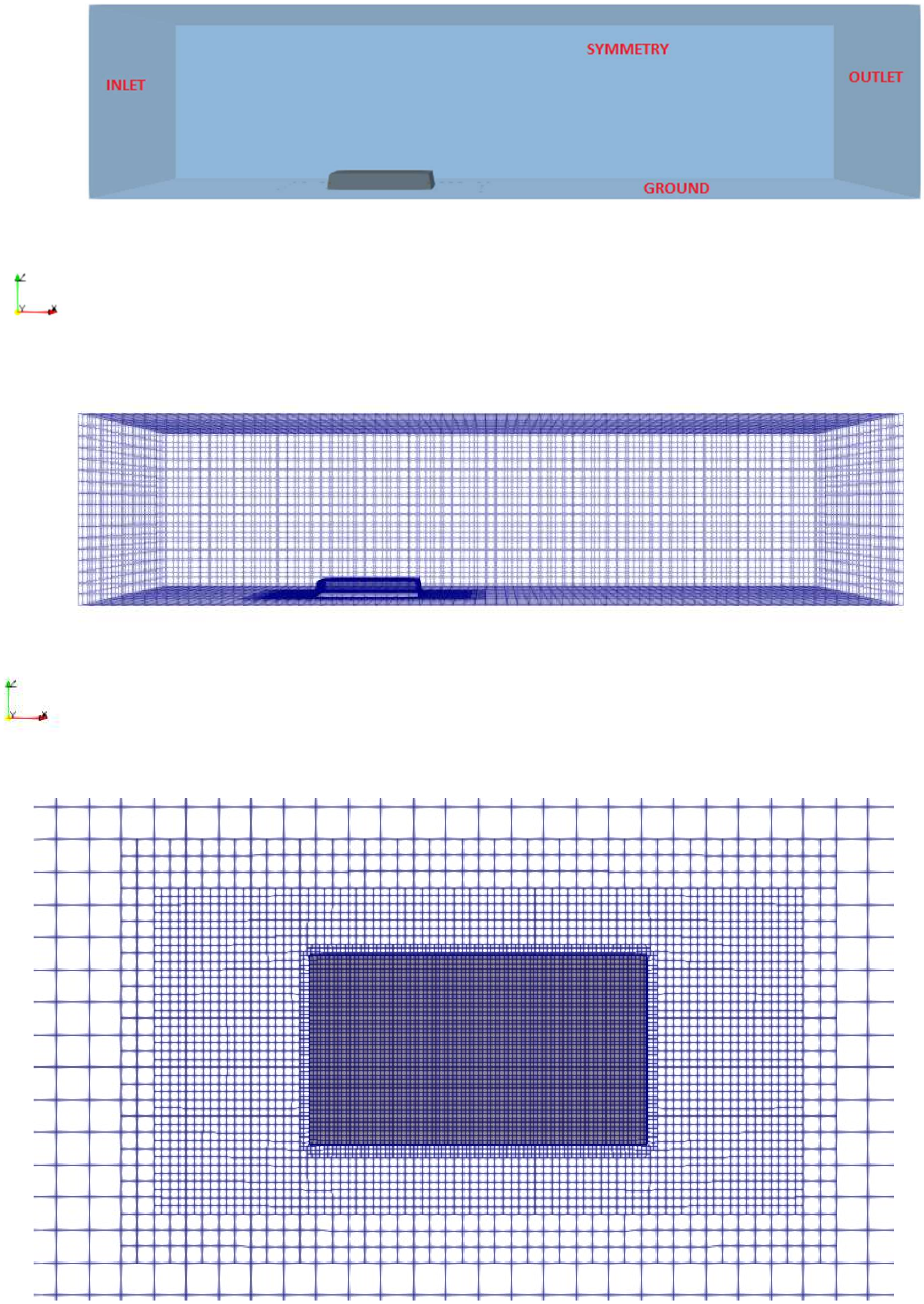

Figure 60.computational domain boundary patches(first), computational domain mesh(second), mesh refinement (third)

7.2 Governing equations and turbulence model

Being the case a steady-state and supposed the fluid viscous and incompressible, the governing equations to be solved are:

- Mass conservation for incompressible flow: $\nabla \cdot U = 0$
- Steady-flow momentum conservation: $(U \cdot \nabla)U + \left(\frac{\nabla P}{\rho}\right) = \nu \nabla^2 U$

where P, ρ and ν are, respectively pressure, density and kinematic viscosity.

The property that must be specified is the kinematic viscosity ν, and it is stored in the *transportProperties* dictionary. The keyword for the kinematic viscosity is nu, and it's expressed as the ratio between the dynamic viscosity μ (mu) and the sea water density ρ (rho).

$$\nu = \frac{\mu}{\rho} = 1.367e - 06\ m^2/s \qquad \mu = 0.0014 \frac{kg}{m*s} \qquad \rho = 1025\ kg/m^3$$

```
/*--------------------------------*- C++ -*----------------------------------*\
| =========                 |                                                 |
| \\      /  F ield         | OpenFOAM: The Open Source CFD Toolbox           |
|  \\    /   O peration     | Version:  v2206                                 |
|   \\  /    A nd           | Website:  www.openfoam.com                      |
|    \\/     M anipulation  |                                                 |
\*---------------------------------------------------------------------------*/
FoamFile
{
    version     2.0;
    format      ascii;
    class       dictionary;
    object      transportProperties;
}
// * * * * * * * * * * * * * * * * * * * * * * * * * * * * * * * * * * * * * //

transportModel  Newtonian;

nu              1.4e-06;

//rho=density                 salt water  rho=1025 kg/m3
//mu=dynamic viscosity         T=10C      mu=0.0014 kg/m s
//nu=kinematic viscosity                  nu=1.367e-06 m2/s
//nu=mu/rho                               S = 35000 mg/l = 35 ‰
// ************************************************************************* //
```

As previously said, the adopted turbulence model is the standard k−ε model with wall functions, and the additional equations and models for the turbulent flow are implemented into a OpenFOAM solver called simpleFoam.

So the two extra variables are: k, the turbulent kinetic energy, and, ε the turbulent dissipation rate. The choice of the wall function models is specified through the turbulent viscosity field ν_T, since the flow in the near wall cells is modelled, rather than resolved.

Consequentially the assigned wall boundary conditions are: a nutWallFunction boundary condition to ν_T, an epsilonWallFunction boundary condition to ε and a kqRwallFunction boundary condition to k.

The calculated initial values for k and ε are set equal to:

$$k = 0.135\, m^2/s^2 \qquad \varepsilon = 0.04\, m^2/s^3$$

7.3 Boundary conditions and initial fields

Once the mesh generation is completed, the boundary conditions can be set up for this case.

The initial field data are stored inside the 0.orig sub-directory, that contains the files: p and U, but also ε, k, nut files, already analysed in the previous point, whose values and boundary conditions must be set.

From a mathematical point of view, the boundary conditions can be divided into two types:

- Dirichlet: which prescribes the value of a dependent variable on the edge. In OpenFOAM this boundary condition is called fixedValue;
- Neumann: which prescribes the gradient value of an edge normal variable. In OpenFOAM this boundary condition is called fixedGradient. Also zeroGradient value boundary conditions are Neumann boundary conditions.

Let's see in detail the assigned conditions:

- **Velocity:** At the inlet, the velocity U is set equal to 3 m/s in the x direction through a Dirichlet boundary condition fixedValue type. At the outlet, a zeroGradient boundary condition is set, and it simply extrapolates the quantity for the patch from the nearest cell value. The noSlip boundary condition is set at the wall patch (ground) and it erases the normal and the tangential components of the velocity variable at the patch.

```
FoamFile
{
    version     2.0;
    format      ascii;
    class       volVectorField;
    object      U;
}
// * * * * * * * * * * * * * * * * * * * * * * * * * * * * * *

Uinlet          (3 0 0);

dimensions      [0 1 -1 0 0 0 0]; // m/s

internalField   uniform (3 0 0);

boundaryField
{
    inlet
    {
        type            fixedValue;
        value           uniform $Uinlet;
    }

    outlet
    {
        type            zeroGradient;
    }

    wall
    {
        type            noSlip;
    }
```

- **Pressure:** The incompressible solvers transform the pressure from static pressure, p_0 (Pa) to kinematic pressure pk (m^2/s^2). The kinematic pressure has the name p in OpenFOAM solvers, the same as the name for the static pressure p. Accordingly, to interpret the results from incompressible solvers, the kinematic pressure should be multiplied by the reference density (constant) value.

The pressure field p is set equal to 0 m^2/s^2 everywhere, and at the outlet p_0 with the totalPressure condition, that specifies:

$$p = \begin{cases} p_0 & for\ outflow \\ p_0 - \frac{1}{2}\rho|U^2| & for\ inflow\ (dynamic\ pressure, subsonic) \end{cases}$$

where:

p= total pressure

p_0= static pressure (Pa)= $p_k * \rho$

$\frac{1}{2}\rho U^2$ =dynamic pressure

In incompressible flows, the pressure is a diagnostic variable, and it has no physical meaning, but only a mathematical one.

```
FoamFile
{
    version     2.0;
    format      ascii;
    class       volScalarField;
    object      p;
}
// * * * * * * * * * * * * * * * * * * * * * * * * * *

dimensions      [0 2 -2 0 0 0 0];

internalField   uniform 0;

boundaryField
{
    inlet
    {
        type            zeroGradient;
    }

    outlet
    {
        type            totalPressure;
        p0              uniform 0;
    }

    wall
    {
        type            zeroGradient;
    }
```

- **Turbulent kinetic energy k:** At the inlet, the initial turbulent kinetic energy is set equal to $k = 0.135\ m^2/s^2$ with the boundary condition fixedValue type.

```
FoamFile
{
    version     2.0;
    format      ascii;
    class       volScalarField;
    object      k;
}
// * * * * * * * * * * * * * * * * * * * * * * * * * * * * * * * * * * * *

kInlet          0.135;   // approx k = 1.5*(I*U)^2 ; I = 0.1 ; U = 3 m/s

dimensions      [0 2 -2 0 0 0 0];

internalField   uniform $kInlet;

boundaryField
{
    inlet
    {
        type            fixedValue;
        value           uniform $kInlet;
    }

    outlet
    {
        type            zeroGradient;
    }

    wall
    {
        type            kqRWallFunction;
        value           uniform $kInlet;
    }
```

- **Dissipation energy rate ε:** At the inlet, the initial dissipation energy rate is set equal to ε = 0.04 m^2/s^3 with the boundary condition fixedValue type.

```
FoamFile
{
    version     2.0;
    format      ascii;
    class       volScalarField;
    object      epsilon;
}
// * * * * * * * * * * * * * * * * * * * * * * * * * * * * * * * * *

epsilonInlet  0.04; // Cmu^0.75 * k^1.5 / L ; L =0.07*3.16=0.22

dimensions      [0 2 -3 0 0 0 0];

internalField   uniform $epsilonInlet;

boundaryField
{
    inlet
    {
        type            fixedValue;
        value           uniform $epsilonInlet;
    }

    outlet
    {
        type            zeroGradient;
    }

    wall
    {
        type            epsilonWallFunction;
        value           uniform $epsilonInlet;
    }
```

7.4 Solve and case control

The simpleFoam solver, implemented for steady incompressible flow, is used. The numerical schemes for terms such as derivatives, interpolation procedures etc. are set in the system/fvSchemes file. In this file, it is specified that the case is steady-state by giving the SteadyState value to the keyword timeScheme. The terms ∇ and $\nabla 2$, controlled respectively by the keywords gradSchemes and laplacianSchemes, have been set to the value Gauss because it is adopted the standard finite volume discretization of Gaussian integration, which requires the interpolation of values from cell centres to face centres. The divergence term $\nabla\cdot$ is controlled by the keyword divSchemes.

The Semi-Implicit Method for Pressure-Linked Equations (SIMPLE) algorithm was used to couple the p-U equation system. This algorithm is an iterative procedure for solving equations of velocity and pressure and it is based on evaluating some initial solutions and then correcting them to reach a target residual, in this case 10e-03. The residual is an error measure in the solution so that the smaller it is, the more accurate the solution.

In the c*ontrolDict* dictionary, the time step deltaT should be set to 1, since in steady state cases it actually stands for an iteration counter. The solution requires 450 iterations to reach a reasonable convergence, hence endTime is set to 450.

Chapter VIII

POST PROCESSING ANALYSIS

This chapter shows the simulation results (velocity and pressure fields), focusing on the pressure forces calculation and drag coefficient definition.

8.Post processing analysis

After the simulation, the post-processing phase is realized through Paraview, and it allows to convert the resulting large amount of data into an understandable format for further considerations.

The following analyses will be carried out in order to optimize the design of the proposed anchorage, in order to make the more appropriate changes.

8.1 Model convergence

Before focusing on the simulation results, it's useful to check if the model shows a trend of convergence. The residual is one of the most fundamental measures of an iterative solution's convergence, as it is an error measure in the solution. In an iterative numerical solution, the residual will never be exactly zero. However, the lower the residual value is, the more numerically accurate the solution will be.

To observe so, let's plot the residuals vs iterations.

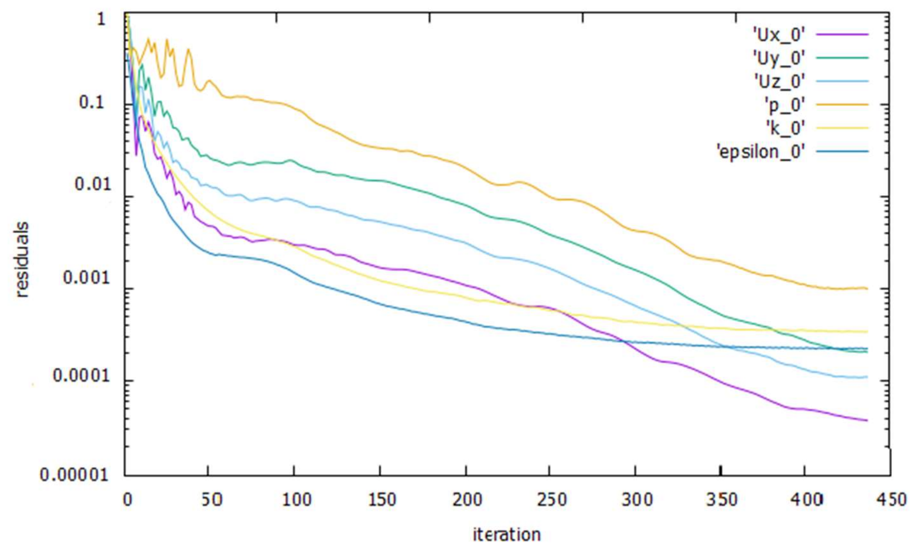

Figure 61:Residual vs iteration plot

In this case the target residual is 10e-03 and it's noticeable that the residuals are decreasing, increasing iterations, and reaching the convergence at the last iteration (450).

8.2 Simulation results

Cutting the computational domain along the central symmetry plane, it was possible to visualize how the different variables vary in space and around the anchorage. Once the model reached a certain stability and convergence, different frames of the different variables were taken.

<u>Pressure:</u> the visualized pressure is the dynamic one, so it is exercised by the water current considered. From the figures below, it can be seen that at the front face, where the water current hits the anchorage, the pressure is the highest (red) because of the stagnation zone prevails. While at the top face of the anchorage, the low pressure zone prevails (blue) because of the Bernoulli equation, which states that the pressure goes down if the fluid speed increases.

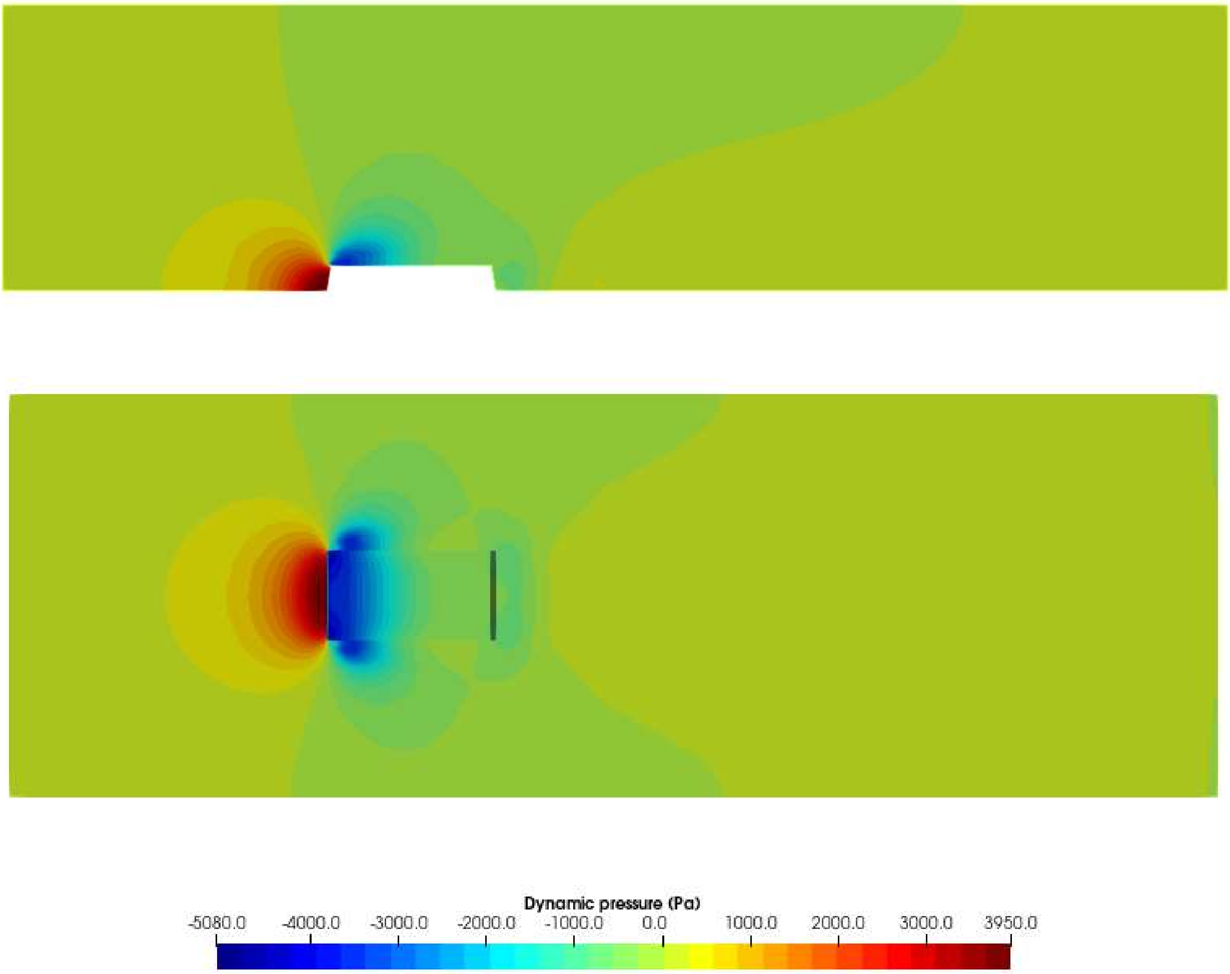

Figure 62:Dynamic pressure field result from simulation

<u>Velocity:</u> from the figures below, it can be seen the velocity field.

Some details are showed in Figure 64, where the streamlines of the fluid's motion are visible and it helps evidencing that the flow develops three recirculation zones around the body and so vortexes: the upstream, the top and the downstream recirculation zones. In particular, in the Figure 65 it is shown the vortex creation in the side faces and the creation of symmetrical vortexes in the rear face. In Figure 66, the velocity vectors are showed.

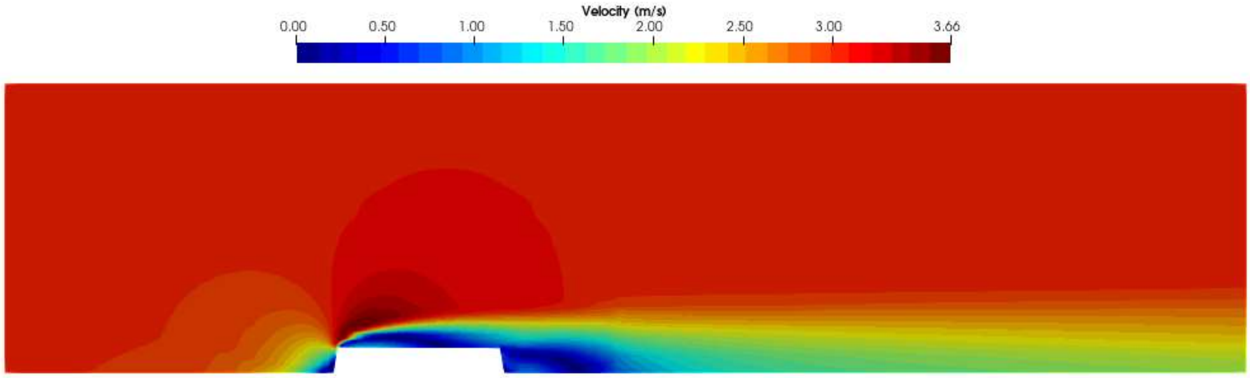

Figure 63: Velocity field result from simulation

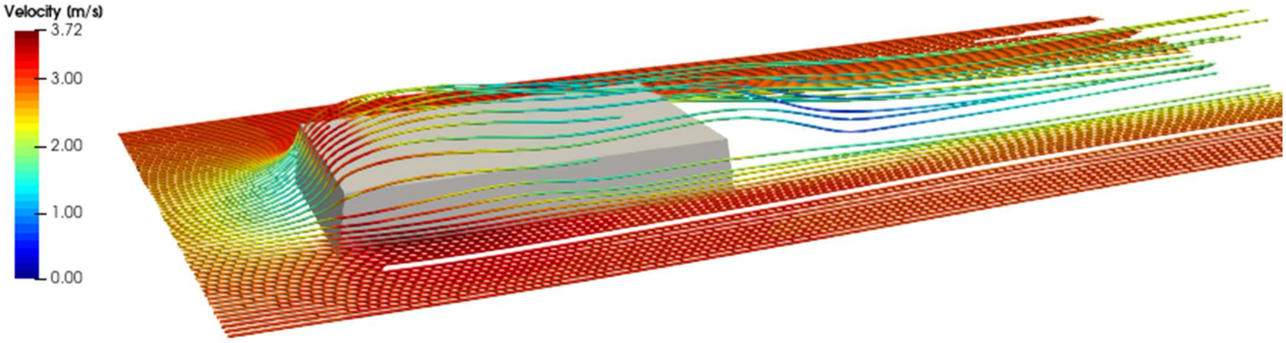

Figure 64:Velocity streamline around the anchor

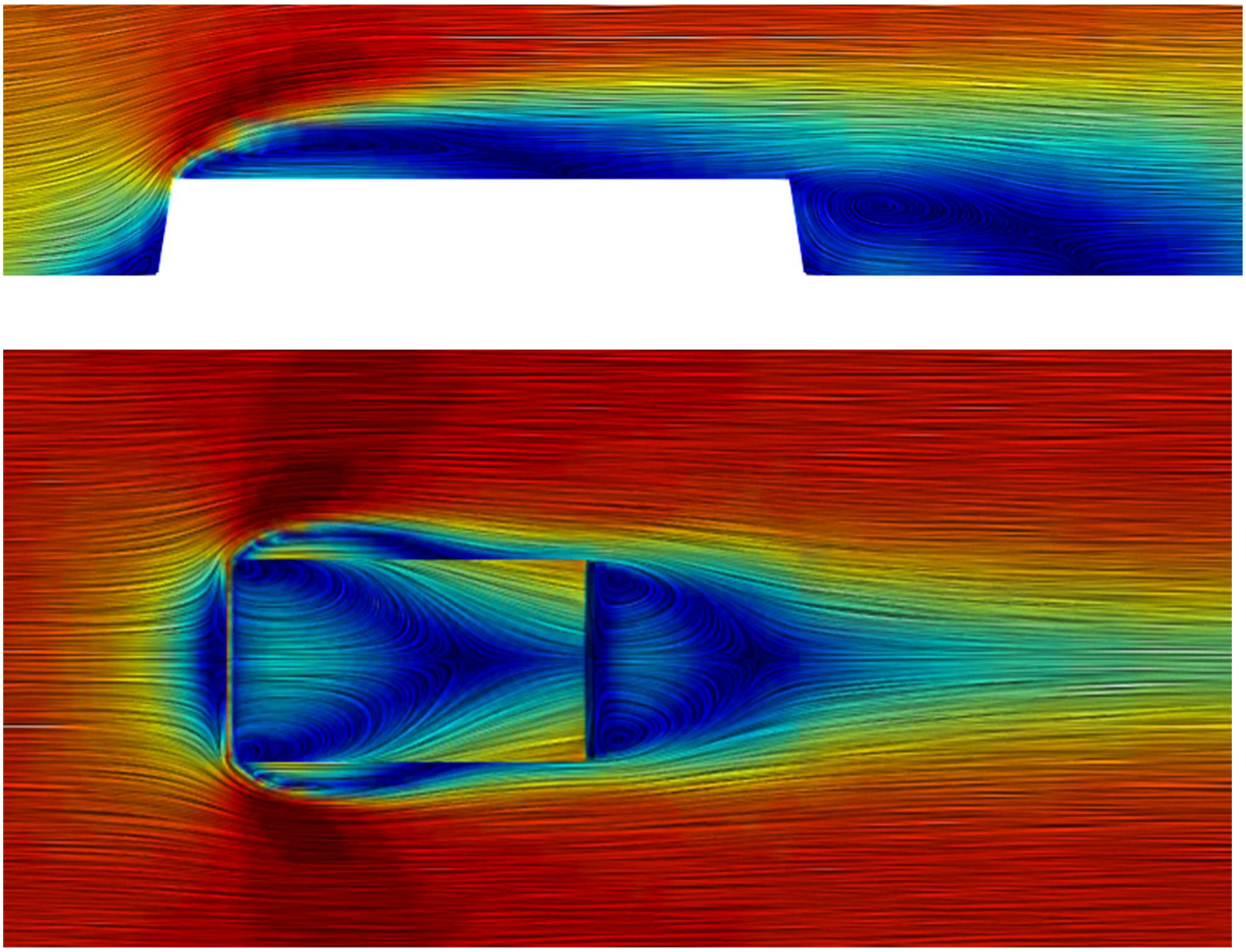

Figure 65:Velocity field with vortexes visualization in both section and plan

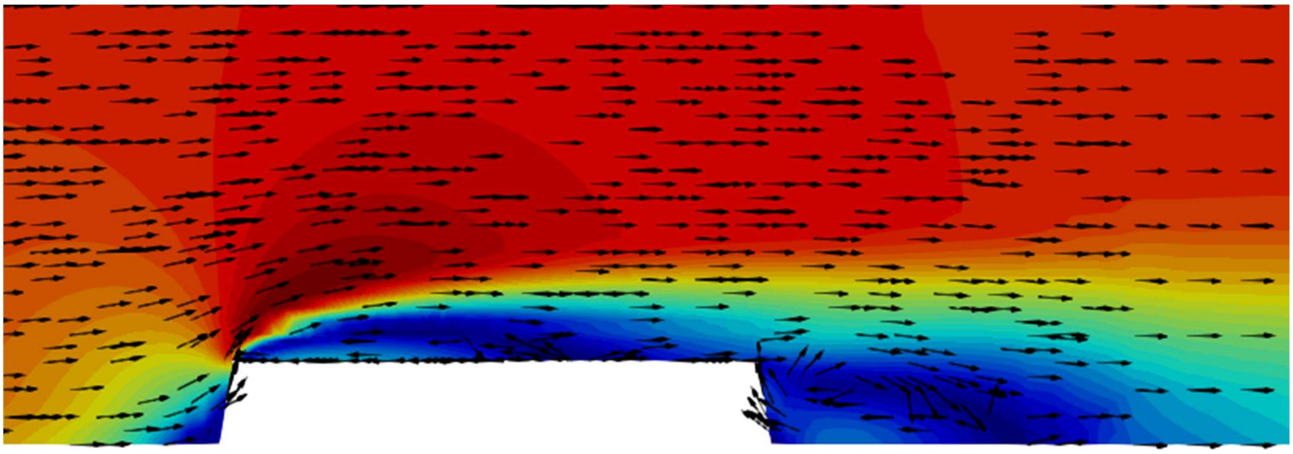

Figure 66: Velocity vectors visualization

8.3 Pressure forces

An underwater body is subjected to high pressure conditions due to the high depth at which it is localized. This pressure has two components: the hydrostatic pressure, that is the pressure exerted by, or existing within, a liquid at rest with respect to adjacent bodies, and the hydrodynamic pressure, that is the pressure generated by the motion of a liquid relative to adjacent bodies.

$$P = hydrostatic\ pressure + hydrodynamic\ pressure = \rho g h + \frac{1}{2}\rho u^2$$

The analysed anchorage is a caisson made of internal cells, that will be filled by seawater as it sinks to the seabed. This technology allows to immediately compensate the hydrostatic pressure exerted by the surrounding water, because the water inside the cells exerts a hydrostatic pressure equal and opposite to it.

After this consideration, it’s clear that the hydrodynamic pressure still remains a problem, that needs to be investigated to get a more complete picture of the situation to which the structure is subjected, and this was possible through the following procedure.

Reminding that the pressure is a force on an area, let’s see the forces that are originated from the acting hydrodynamic pressure on the anchorage.

The force generated on the object by the water current has three components:

- **Fx** – Drag force: along the direction of the current
- **Fy** – Lateral force: perpendicular to the direction of the current (horizontal)
- **Fz** – Lift force: perpendicular to the direction of the current (vertical).

Water generates force in two ways:

- Pressure force: arises from the pressure difference between two opposite sides of an object. It’s the sum of all the local forces pushing or pulling perpendicular to the surface.
- Friction force: arises from the water sliding across the surface of the object. It’s the sum of all the local friction forces parallel to the surface.

The pressure force is the main component in hydrodynamic so the friction force is neglected in the calculations.

The coordinate system chosen is the one showed in the figure below and negative values indicate a force acting in the direction opposite to the arrows shown.

	Fx	Fy	Fz
Pressure force	127.735 kN (13 tons)	-0.055 kN (-0.0056 tons)	313.977 kN (32 tons)

These forces have been calculated for each cell of the object, along the selected normal, with the following formulas:

F_x= p*Normals_X*1025 F_y= p*Normals_Y*1025 F_z= p*Normals_Z*1025

Then they have been integrated on the whole surface of the object itself, which is equal to 420 m^2. To obtain the full force, it was necessary to multiply by the water density because, as said in the previous chapter, the pressure p is a normalized data so dived by the density.

Knowing these results, it's possible to schematize the action of the pressure forces and so see their contribution on the proposed design. More precisely there are: a drag force Fx of 13 tons, which is acting on the front face of the anchorage and pushing against it, a lift force Fz of 32 tons, which is acting on the top face of the anchorage and it tends to lift up the structure and so not contributing to its stability on the seabed, and a lateral force Fy, which it's negligible.

These considerations are clearer in the figures below, where the distribution of pressures, the drag and lift pressure forces on the anchorage are shown.

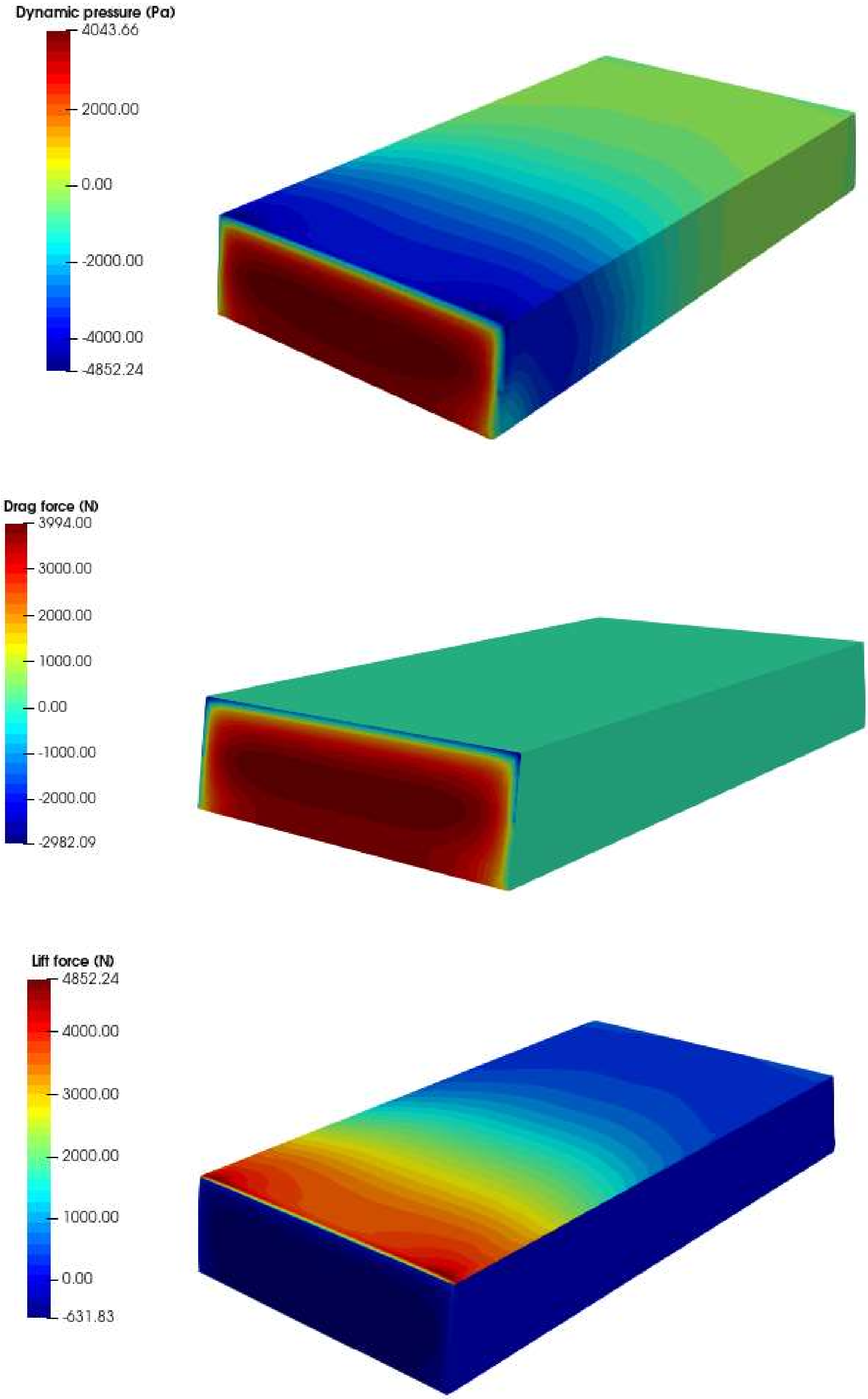

Figure 67:Dynamic pressure (first), Drag force (second) and Lift force (third) acting on the anchor

8.3.1 Drag coefficient

In fluid dynamic, the drag force is described by the following formula:

$$F_D = C_D \frac{1}{2} \rho A U^2$$

Where:

- F_D= drag force (N)
- ρ = density of fluid (kg/m³)
- u = velocity of fluid (m/s)
- C_D= drag coefficient
- A = frontal area of the solid (m²)

Knowing the drag force, and being all the other variables (u, A, ρ) known, it can be obtained the drag coefficient with the reverse formula:

$$C_D = \frac{F_D}{\frac{1}{2} \rho A U^2}$$

The Drag Coefficient (C_D) is a dimensionless quantity that is used to quantify the drag or the resistance of an object in a fluid environment, such as air or water, and it allows to account for the influence of shape, inclination and flow conditions when calculating the drag force.

Essentially, the more streamlined an object is, the lower its drag coefficient. Whereas, bulky objects will have a high drag coefficient.

However, it’s important to remember that drag coefficient varies with Reynolds number (Re): for all bodies studied the drag coefficient was inversely proportional to the Reynolds number.

The Drag coefficients allow to analyse the aero/hydrodynamic efficiency of an object, regardless of its size or velocity. This means that it’s possible to compare the aero/hydrodynamics of a cyclist with a building. Although they are extremely different, they both have a normalised drag coefficient.

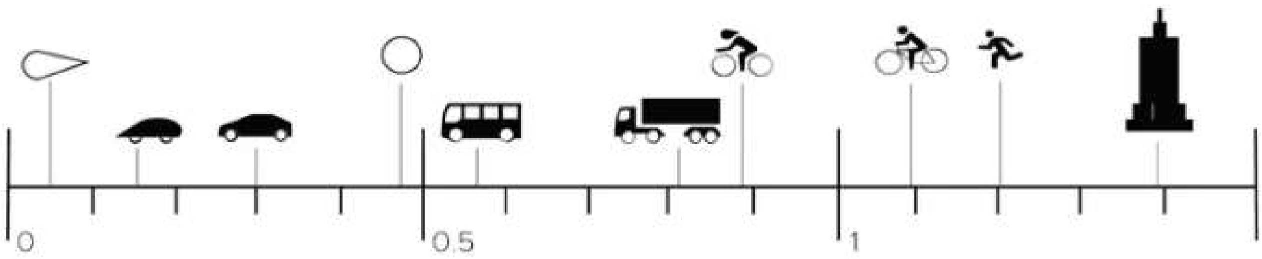

Figure 68:Scale of drag coefficient values

Drag coefficients are also an essential consideration throughout the design process. When determining which design has the highest performance, they can be ranked in order of drag coefficient.

Calculating the drag coefficient and the Reynolds number for the specific case, the results are equal to:

$$Re = 7 * 10^6 \qquad C_D = 0.79$$

The high Reynolds number confirms the turbulent flow occurring, while the drag coefficient, that is pretty high, means that the proposed design has not a very hydrodynamic shape and so it doesn't allow to avoid or mitigate the drag force that is pushing against the anchorage.

8.4 Model validation and verification

After seeing a first analysis of the results obtained from the simulation, it’s important to validate the model before getting in furthermore analysis and considerations.

The simulation model is valid only if the model is an accurate representation of the actual system, else it is invalid.

Validation and verification are the two steps in any simulation project to validate a model.

- Validation is the process of comparing two results. In this process, it's compared the representation of a conceptual model to the real system. If the comparison is true, then it is valid, else invalid.
- Verification is the process of comparing two or more results to ensure its accuracy. In this process, the model’s implementation and its associated data have to be compared with the developer's conceptual description and specifications.

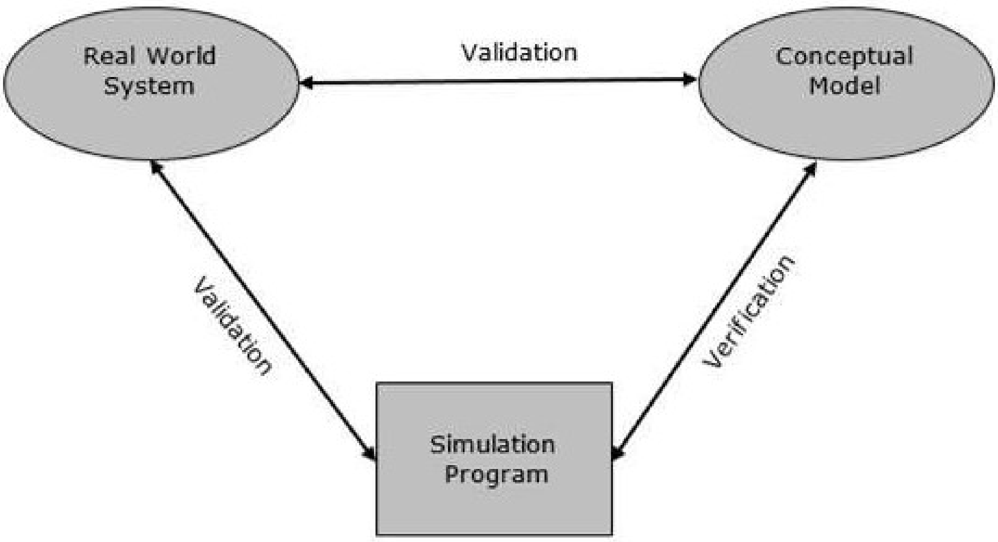

There are various techniques used to perform verification and validation of simulation model. From the moment it's not possible to carry on the validation of the model, not having any existing real system to rely on, let's focus on the verification of the model by comparing final simulation result with analytic results.

In order to do so, it's possible to compare the drag force Fx, obtained from the simulation, with the calculated one:

- <u>Simulated drag force:</u> F_x= p*Normals_X*1025= 127.735 kN

  The relative drag coefficient obtained from the reverse formula is C_D=0.79.

- <u>Calculated drag force:</u> F_D=130.109 kN

$$F_D = C_D \frac{1}{2} \rho A U^2$$

where: u= 3 m/s, ρ= 1025 kg/m^3, $A_{frontal}$= 35.27 m^2 and C_D= 0.8 from literature.

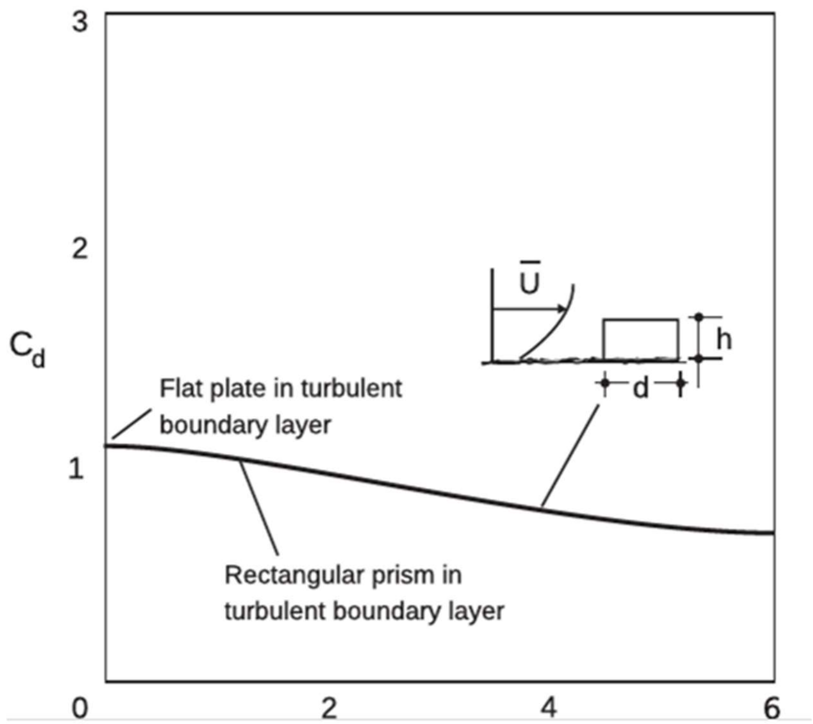

Figure 69: Mean drag coefficients for rectangular prisms in turbulent boundary-layer flow.

The simulated and calculated drag force values are pretty close to each other, validating the used simulation model and it means that the model can be considered an accurate representation of the actual system

.

Chapter IX

DESIGN SHAPE ASSESSMENT

This chapter provides a design shape analysis in order to understand which shape is more suitable for both structural and hydrodynamic purposes.

9. Design shape assessment

The simulation results evidence the forces that the anchorage could face during its life time when exposed to a high current velocity of 3 m/s. For a more correct and cautionary project they should be taken into account in the design process, in order to do not risk damages or the failure of the structure.

From the hydrodynamic point of view, it's pretty clear that the anchorage shape, being edgy and having C_D=0,79, is not the best adoptable shape.

These features don't allow to reach a good hydrodynamic on the structure, and a bad hydrodynamic means vortexes and high destabilizing forces on it.

So a shape analysis could be interesting in order to try to improve the shape of the anchorage, always taking into account design limitations, and so finding an adequate compromise between the hydrodynamic and the geometry shape.

Before starting investigating how different shapes are effected by the water current to which they are exposed to, it can be helpful to remember that a lower drag coefficient stands for a more hydrodynamic shape. The most aero/hydrodynamic shape in nature is a teardrop, which has a drag coefficient C_D of 0.04. This is the reason why so many aerodynamically efficient cars or structure often try to resembling that shape through the use of more smooth geometries.

Let's compare different shapes in order to understand which design modifications could be more suitable, and to do so it's helpful starting the analysis from the simplest anchorage shape (rectangular section).

Calculating the forces acting on the whole structure and also the ones acting only on the frontal face (red face), the one more exposed to the drag force, the results showed below were obtained. The coordinate system chosen is also indicated in the figures, so negative values represents a force acting in the direction opposite to the arrows shown.

Rectangular longitudinal section:

	Fx	Fy	Fz
Whole structure	132.79 kN	-0.019 kN	332. 90 kN
Frontal face	118.38 kN	0 kN	0 kN

C_D= 0.82

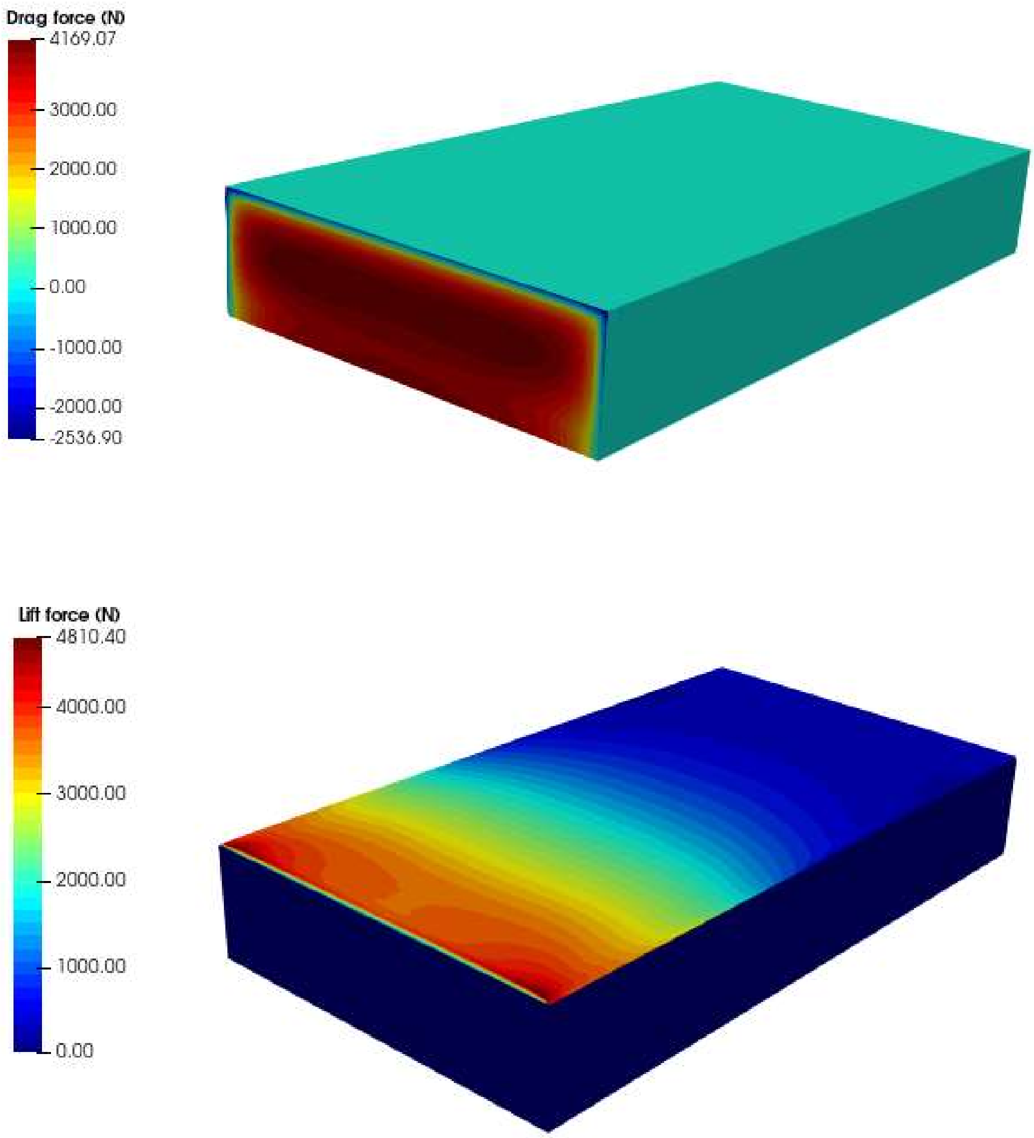

Figure 70:Drag force (first) and Lift force (second) action on the rectangular shape anchor(d=0 m)

Trapezoidal longitudinal section with d=0.5 m: It's the original design proposed and analysed in the previous simulation.

	Fx	Fy	Fz
Whole structure	127.74 kN	-0.055 kN	313. 98 kN
Frontal face	112.59 kN	0 kN	-17.81 kN (-1.8 tons)

C_D=0.79

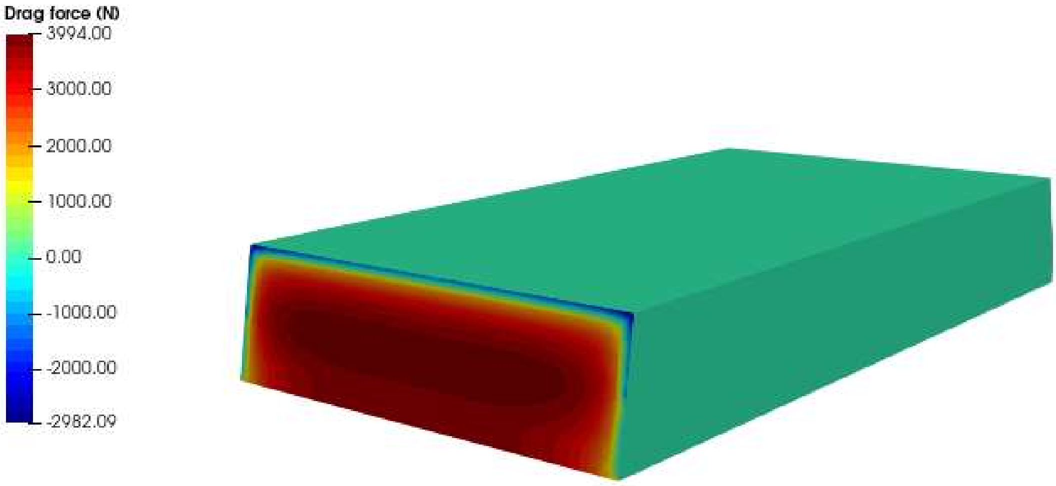

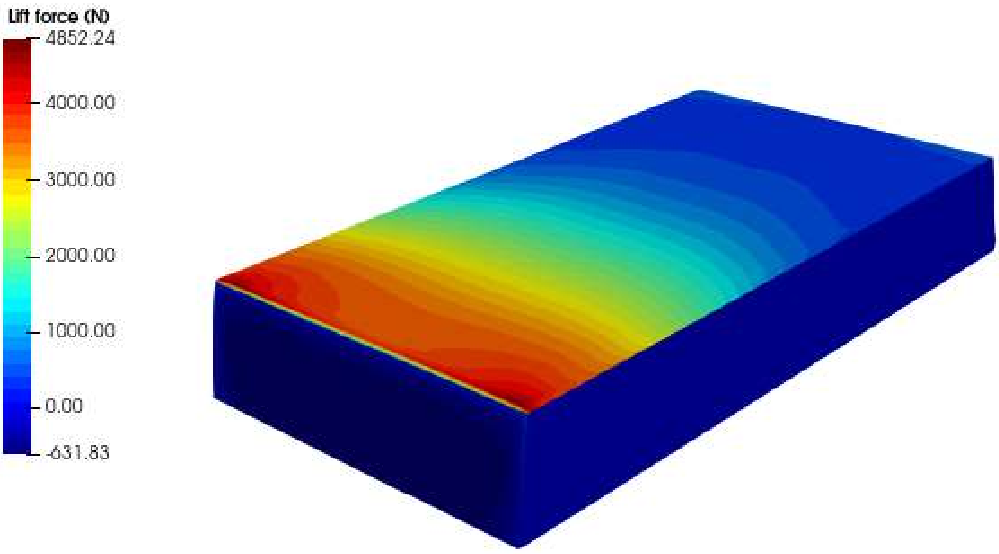

Figure 71:Drag force (first) and Lift force (second) action on the anchor with d=0.5 m

<u>Trapezoidal longitudinal section with d=1 m:</u>

	Fx	Fy	Fz
Whole structure	118.93 kN	0.016 kN	292.35 kN
Frontal face	102.00 kN	0 kN	-32.29 kN (-3.3 tons)

C_D=0.69

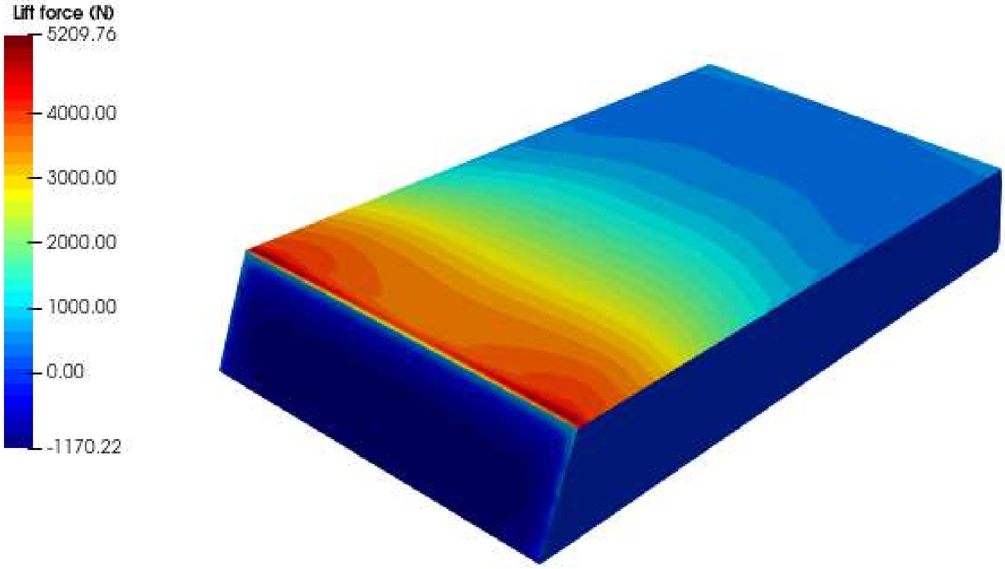

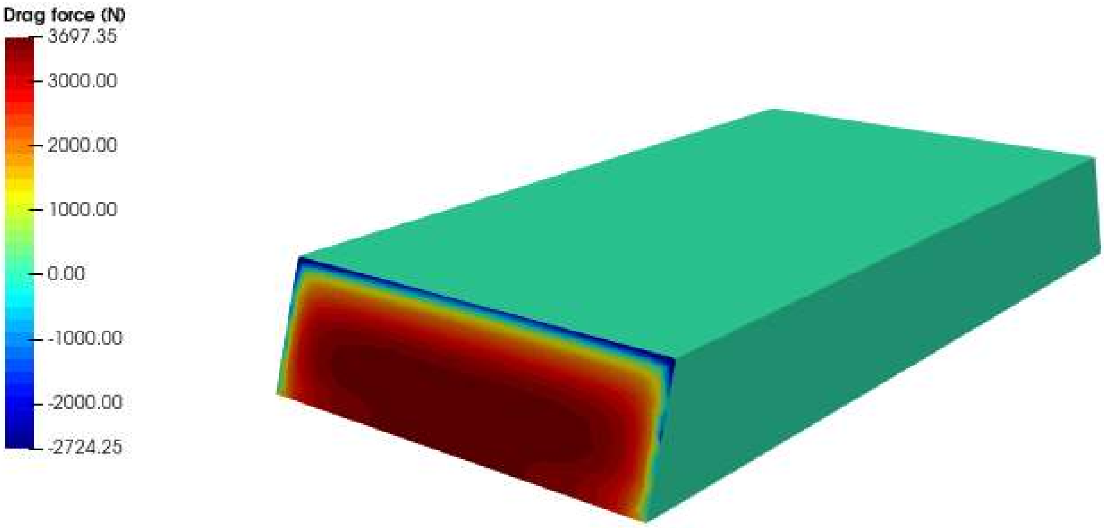

Figure 72:Drag force (first) and Lift force (second) action on the anchor with d=1 m

From these first three slightly different shapes, it’s noticeable how adding a small inclination to the geometry allows to obtain a more hydrodynamic shape, and so a smaller C_D as the inclination becomes less steep.

Thanks to these changes in shape, a decrease in the lift and drag forces, calculated on the whole structure, can be noticed.

Furthermore, through the calculation of the pressure forces on the frontal face, it can be observed the creation of a new contribution Fz acting downward thanks to the inclined face. So the inclination is able to take advantage of the water current, generating this stabilizing down force, and at the same time reducing the acting drag force Fx. Even if the down force is not particularly high: it is equal to 1.8 tons in the second geometry and 3.3 tons in the third one, it represents a first sign of shape’s improvement.

Keeping an edgy shape, it was not possible to obtain a significative optimization of the vortexes situation, but just a small reduction of them in particular on the frontal part, as it’s visible in the Figure 74 below.

Let’s see what happens with smoothed edges shapes.

Blunt trapezoidal longitudinal section:

	Fx	Fy	Fz
Whole structure	68.45 kN	-1 kN	315.27 kN
Frontal face	56.48 kN	0 kN	-10 kN (-1 ton)

C_D=0.41

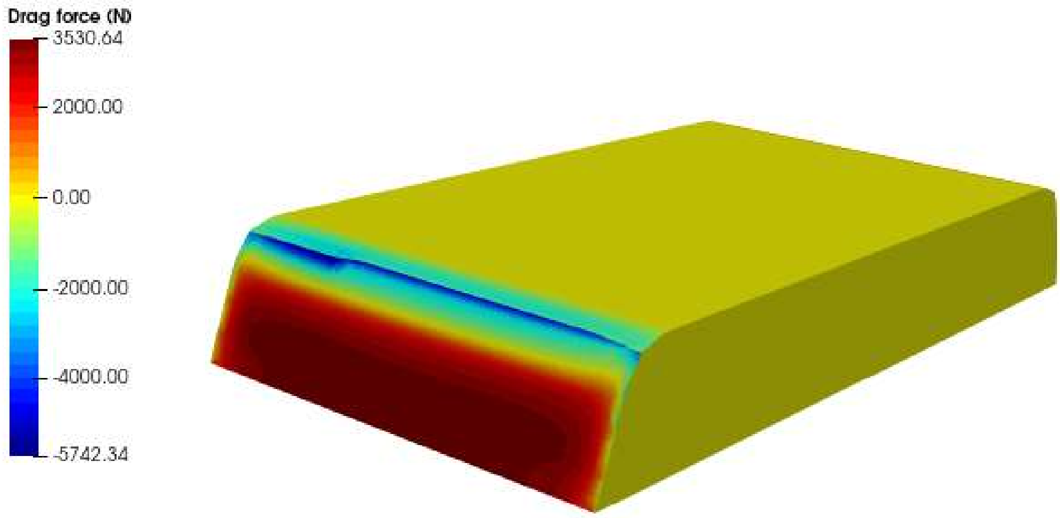

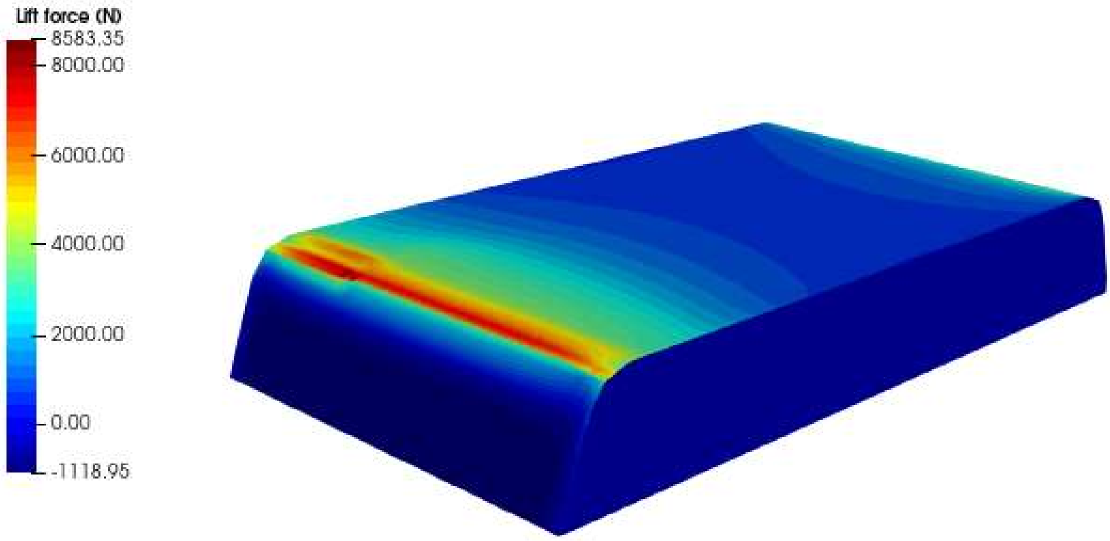

Figure 73: Drag force (first) and Lift force (second) action on the anchor with a blunter shape

The results of this last analysis show that, adopting a blunter edges shape, it's possible to obtain a significative reduction of the drag force acting on the whole structure and so a smaller C_D equal to 0.41, while the lift force remains almost the same.

In addition, keeping an inclination of the frontal faces, as already did in the previous shapes, it's present a down force contribution even if very small: it is equal to 1 ton.

What differentiate this shape from the other ones is the hydrodynamic improvement reached: in particular, a remarkable reduction of the vortexes on the top, but also on the frontal and rear part of the structure, as it can be seen in the Figure 74.

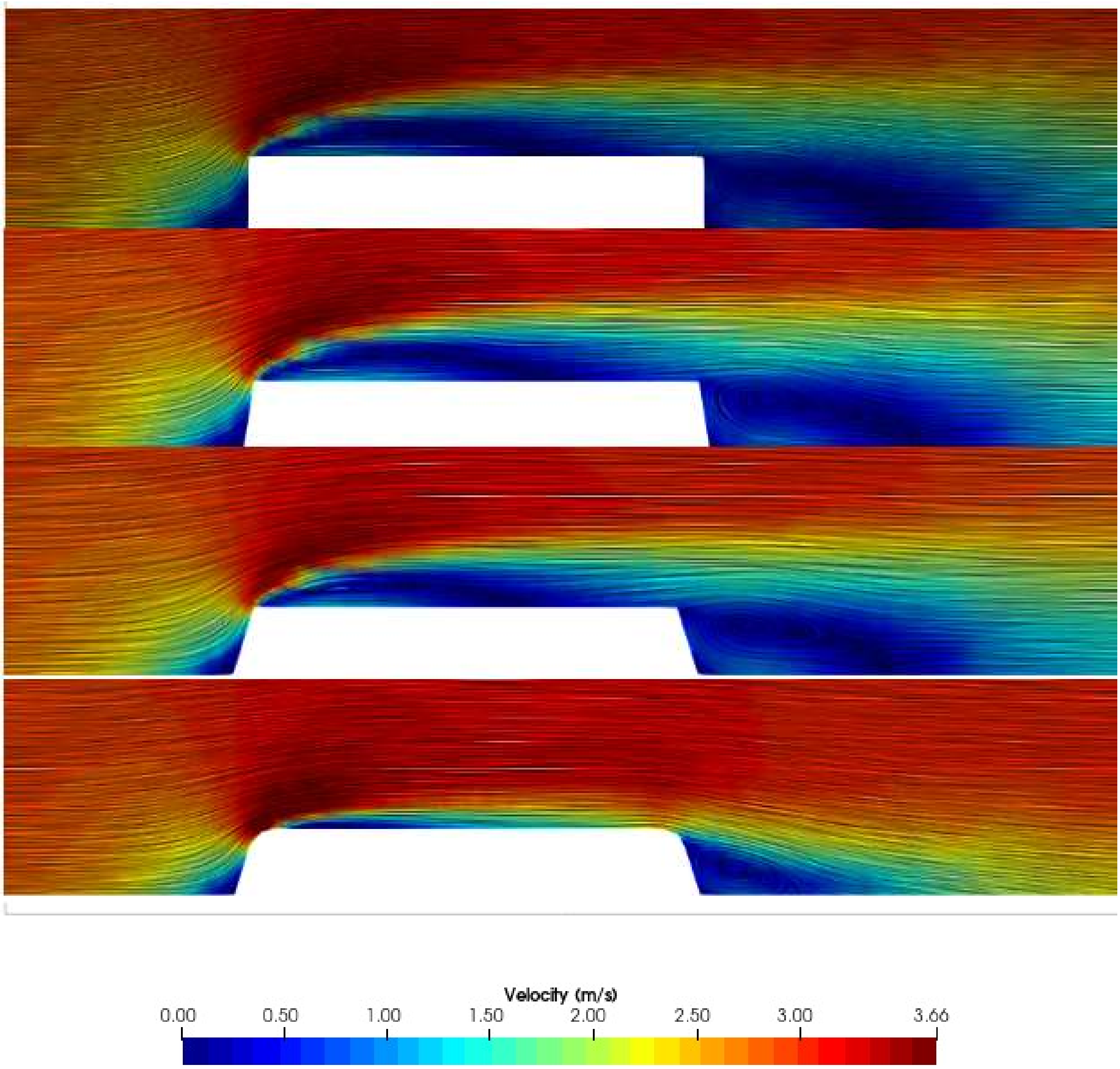

Figure 74:Comparison of the velocity field and recirculation zones between the four analysed anchor's shapes

Chapter X

ALTERNATIVE ANCHORAGE SOLUTION

This chapter provides a brief overview of what could be an alternative anchorage solution for GEMSTAR: pile anchors installed thanks to an innovating system made of a bell with inside the excavator.

10.Alternative anchorage solution

An alternative solution to a dead weight anchorage could be a pile anchor. Pile anchors are composed of hollow tubes which are drilled or hammered into the seabed and can be grouted into position. Compared to other types of foundations, pile foundations have an important axial and lateral load capacity, indeed they are able to transmit high axial loads through soft superficial sediments down to competent bearing soils or rock.

To realize this solution an innovative installation system has been designed: a steel cylindrical bell with inside all the necessary to install a pile anchor, so a remote controlled excavator able to drill the seabed and positioning a pile anchor. At the base is placed a steel plate closing the bottom of the bell itself.

Once on the seabed, the bell would be exposed to high pressure, due to the high depth location, and so it could be damaged. To avoid this and also to block the water from enter inside the system, air is pumped into the compartment so that the pressure throughout the bell body is now equal the external pressure, that is compensated.

Air and electricity supplies are provided to the bell thanks to a big cable, resembling a sort of umbilical cord, that links the bell to the controlling station in the boat at the surface. Its functioning is similar to a diving chamber.

After this brief presentation of this system, let’s see how it could be designed.

The designed bell could be easily approximate as a cylinder with a 4 m diameter and 6 m tall.

Taking into account the water pressure acting on the bell and the bell dimensions is possible to estimate the minimum thickness of the steel bell. It is sufficient to consider a control volume that cuts the cylinder section and replace the cut portion with the appropriate acting forces, such as the pressure of the water and the normal force N.

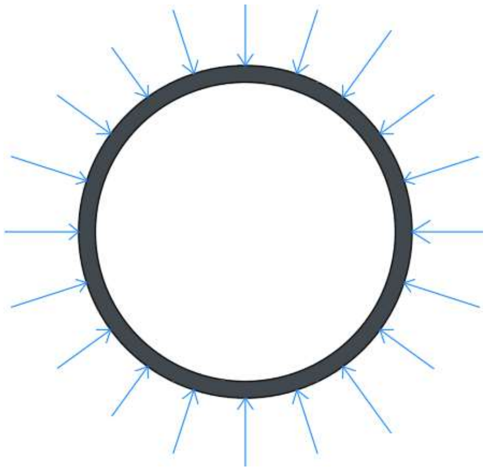

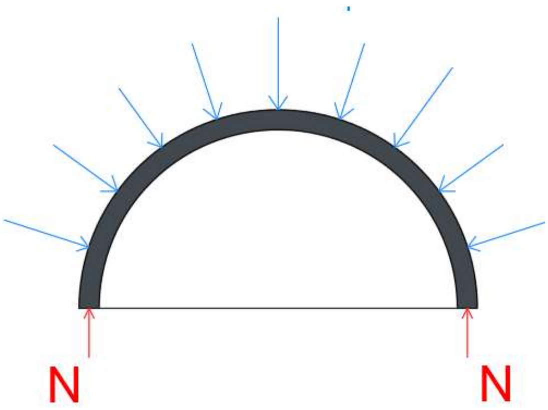

Writing the balance of forces in the vertical direction:

$$2 * N = p_{water} * 2 * R$$

$$N = p_{water} * R$$

But N is also given by σ, allowable tension which is equal to 1400 kg/cm^2 for steel, multiplied by s, the thickness of the bell:

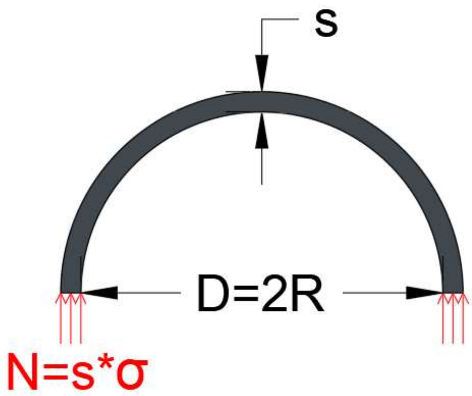

By equating the two formulations of N, it is possible to obtain the minimum thickness s needed to withstand the required water pressure:

$$\sigma * s = p_{water} * R$$

$$s = \frac{p_{water} * R}{\sigma} = 0.5\ cm$$

Where

- p_{water}= 3.5 kg/cm^2
- R= 200 cm
- σ= 1400 kg/cm^2

Since the bell must be able to withstand other possible stresses, due to the marine environment, but also to the laying phase, during which the holding cable will exert a tension on the bell, and to the actual working phase, when the excavator will be drilling or hammering a pile in the seabed, seems wiser to consider a greater thickness of 3 cm.

Considering the thickness and the water pressure, It is now possible to evaluate the deformation ε that could occur:

$$\varepsilon = \frac{\sigma}{E}$$

The deformation can also be expressed as a function of the diameter D of the bell:

$$\varepsilon = \frac{\Delta D}{D}$$

And being the area $A \propto D^2$, and consequentially dA=2*D*ΔD, it is possible through some substitutions to obtain the area variation dA, which appears to be negligible.

$$dA = 2\frac{p\,R}{s\,E}D^2 = 0.004\;m^2$$

Where

- p= 3.5 kg/cm^2
- R= 200 cm
- E= 2100000 kg/cm^2
- s= 3 cm

Considering the bell dimensions and thickness, it possible to estimate the steel volume necessary and it is equal to a maximum volume of 4 m^3. Being γ_{steel}= 80 kN/m^3, the dry weight of the steel is equal to 320 kN≈ 32 tons.

Since being submerged in water, the bell will be subjected to an upward push of Archimedes equal to the weight of the fluid displaced:

$$S = \gamma_w * V = 761.5\;kN \approx 76.15\;tons$$

Where

- γw= 10.1 kN/m^3 seawater density
- V= bell volume = $(\pi R^2) * H = (\pi * 2^2) * 6 = 75.4\;m^3$

- S= upward Archimedes push [kN]

So in order to sink the bell is necessary to placed inside the bell at least 45 tons, which can be easily reached considering the weight of the excavator, the piles and all the necessary equipment, at the same time paying attention not to exaggerate or the bell will become too heavy to hold by the boat.

10.1 Pile Anchors (PA): preliminary design for GEMSTAR

1.Pre-dimensioning of the diameter. A preliminary pile diameter is proposed, based on the designer's experience or on practical recommendations.

$$D_p = 530\ mm$$

2. Pile wall thickness. The thickness of the pile, tP, is determined using the following Equation API RP2A-WSD:

$$t_p = \left[6.35 + \frac{D_p}{100}\right] = 11.65\ mm$$

where DP is the pile diameter in mm and tP is the thickness of the pile wall in mm.

3. Embedded length. The embedded length, Lr, is computed with the formula of Poulos and Davis:

$$L_r = 4\left(\frac{E_s I_P}{n_h}\right)^{\frac{1}{5}} = 3.5\ m$$

where Lr is the embedded length in m; Es= 200 GPa is Young's modulus of the steel, IP, is the second moment of area, and nh= 80 MN/m^3 is the horizontal coefficient of the subgrade reaction.

$$I_P = \frac{1}{8}\left(D_p - t_p\right)^3 t_p = 2 * 10^8 mm^4$$

4. Axial capacity (structural). Anchors for floating structures are only loaded by tension stresses. The structural capacity to axial loads is determined, based on API RP 2A-LRFD:

$$Q_{RASP} = \phi_{t,y} F_y A_p = 5240\ kN$$

where Fy= 25 MPa is the yield stress of the steel, Ap, is the cross-sectional of the anchor, and φt, y is the resistance factor for axial tensile strength, which can be taken as 0.95 API RP 2A-LRFD.

5. Lateral capacity (structural). The shear capacity, QRLSP, of the pile can be determined, using the following expressions:

$$Q_{RLSP} = \frac{\phi_{vs} F_{cr} A_p}{2} = 1489.2\ kN$$

With

$$F_{cr} = max(F_{cr1}, F_{cr2})$$

$$F_{cr1} = \frac{1.60\ E_s}{\left(\frac{D_p}{t_p}\right)^{\frac{5}{4}} \sqrt{\frac{L_r}{D_p}}}$$

$$F_{cr2} = \frac{0.78\ E_s}{\left(\frac{D_p}{t_p}\right)^{\frac{3}{2}}}$$

Fcr is the maximum value between Equations and must not exceed 0.6 Fy. The resistance factor for lateral strength, φvs is 0.90 LRFD.

6.Revision of structural capacity. To satisfy the design requirements, the total force on the mooring system (Vd, Hd) must not exceed the axial (QRASP) and lateral capacities (QRLSP). If the above requirements are not fulfilled, the pile geometry must be modified, and the revision procedure restarted.

$$H_d = S_1 \cos 40° = 1480.4\ kN$$

$$V_d = S_1\ \text{sen}\ 40° = 1242.2\ kN$$

Where S1= 1932.5 kN considering the same two lines configuration already analysed for the dead weight anchor.

7. The geotechnical capacity of piles on rock. Rock Socket Interface: a significant amount of research has been undertaken regarding the pile-rock interface for rock socket piles. The roughness and cleanliness of the rock socket are important factors in determining the pile-rock adhesion and have a significant influence on pile load capacity. The limiting skin friction for grouted rock sockets is often governed by the rock strength as follows:

$$Q_f = \alpha q_u A_f = 49694\ kN$$

where α is the adhesion factor, which depends on socket roughness but is generally taken as 0.1 for a smooth socket, Af=$\pi L_r D_p$.

The axial geotechnical capacity, QRAGP, of piles driven into rock depends on the resistance of the pile shaft, Qf, and the submerged weight of the pile, Wp.

$$W_p = L_r A_p(\gamma_s - \gamma_w) = 52.77\ kN$$

$$Q_{RAGP} = Q_f + W_p = 49747\ kN$$

The lateral geotechnical capacity, QRLGP, is calculated using the so-called P–Y curves.

8.Geotechnical design revision. The acting design loads on the pile, Vd, Hd, must not exceed the geotechnical capacity. Otherwise, the diameter must be reviewed and adjusted.

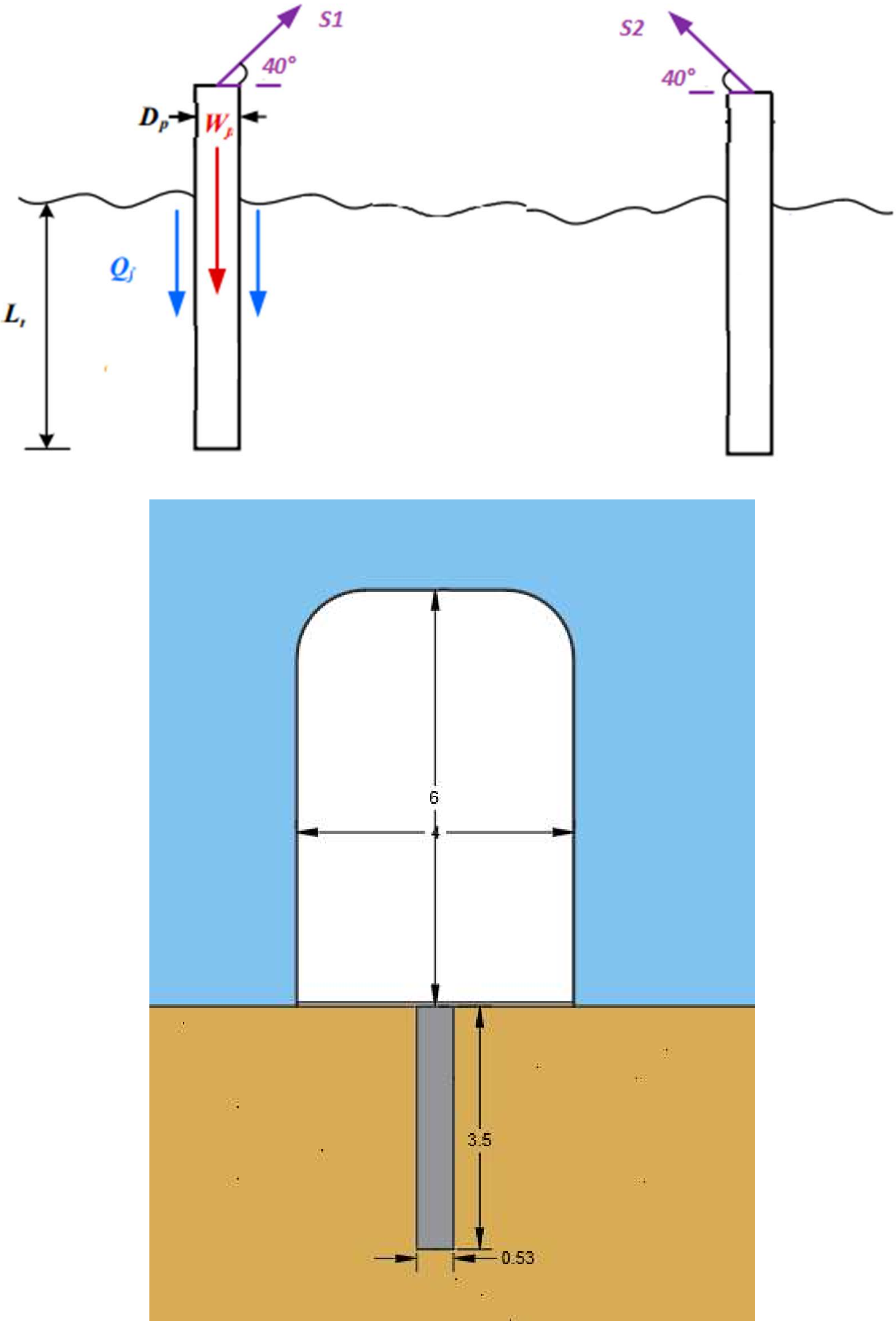

Figure 75:Piles anchorage configuration (first) and bell scheme and dimensions(second)

10.2 Potential forces acting on the bell

If this system would be used in the Messina Strait, it would be potentially exposed to strong sea current, reaching 3 m/s. These currents exercise a force on the bell, so it's important to find them in order to see if the bell would be able to withstand to them without risking any damages.

The pressure forces have been calculate through an OpenFOAM numerical simulation as for the dead weight anchor case. The coordinate system chosen is the one showed in the figure below and negative values indicate a force acting in the direction opposite to the arrows shown. The following results were obtained:

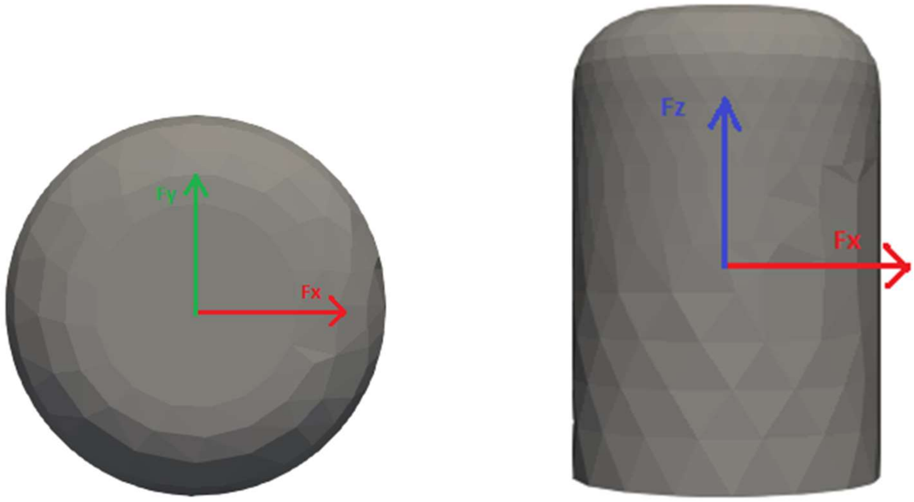

	Fx	Fy	Fz
Pressure force	37.46 kN (3.8 tons)	14.86 kN (1.5 tons)	38.04 kN (3.9 tons)

Knowing these results, it's possible to schematize the action of the pressure forces and so see their contribution on the proposed design. More precisely there are: a drag force Fx of 3.8 tons, which is acting on the front face of the bell and pushing against it, a lift force Fz of 3.9 tons, which is acting on the top face of the bell and it tends to lift up the structure and so not contributing to its stability on the seabed, and a lateral force Fy of 1.5 tons.

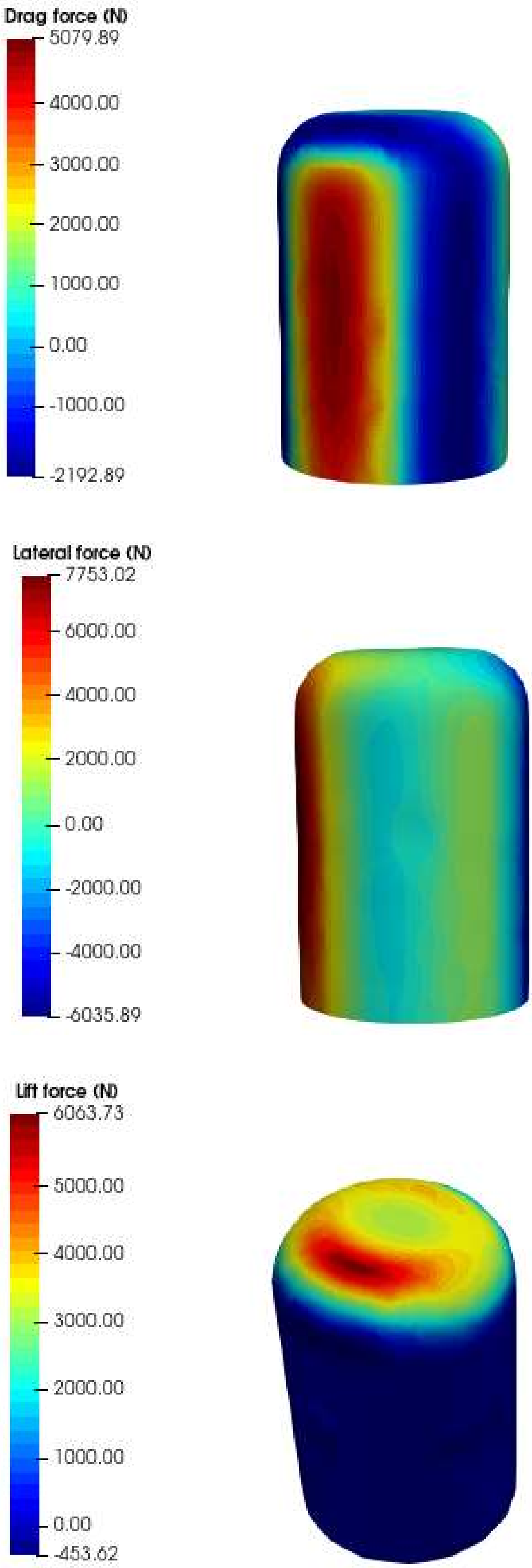

Figure 76:Drag force (first), Lateral force (second) and Lift force(third) acting on the bell

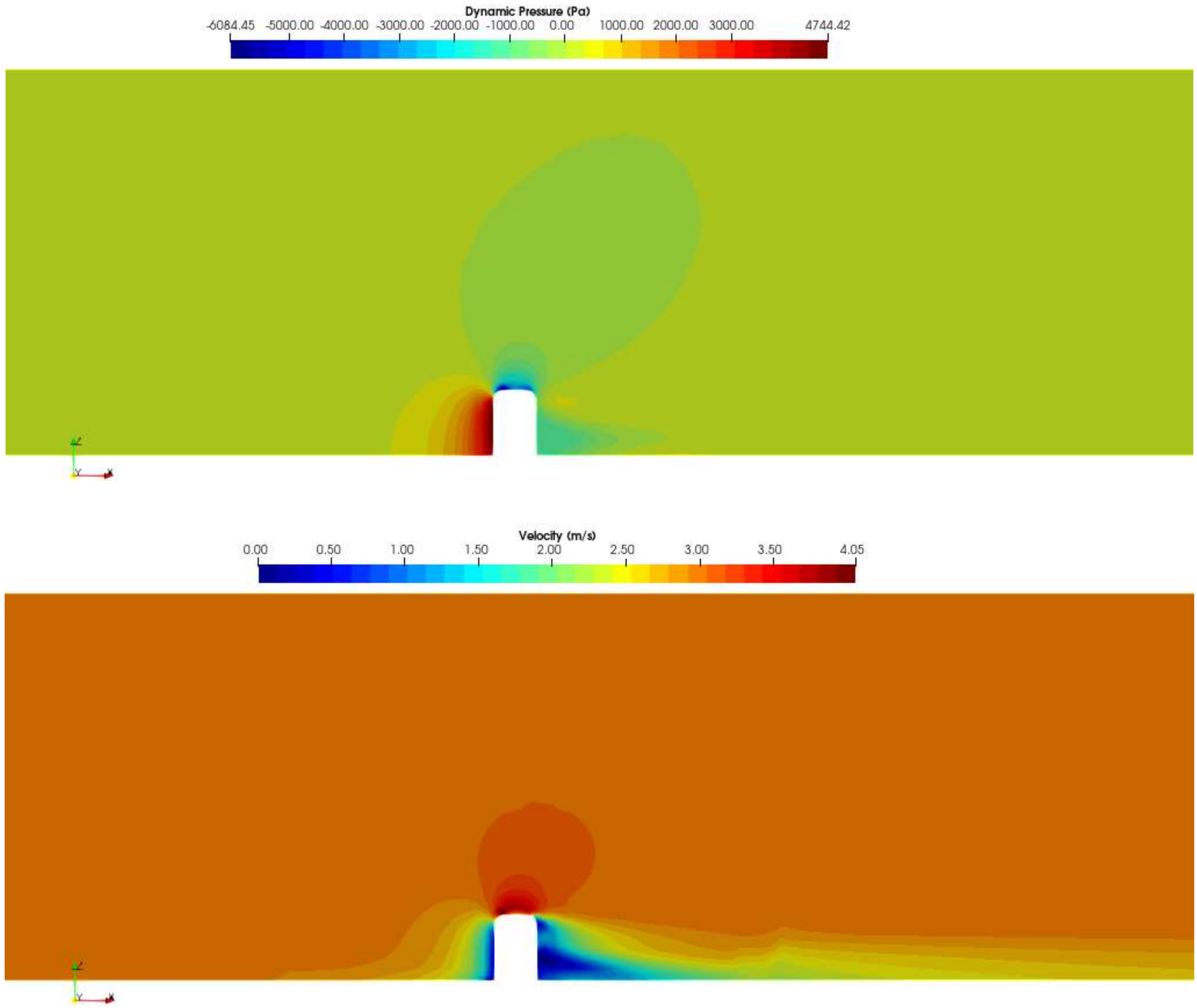

Figure 77:Pressure field(first) and velocity field(second)

Chapter XI

ENVIRONMENTAL ASSESSMENT

This chapter provides a brief overview of the potential environmental impacts of a marine renewable energy device, focusing then on the case study device.

11.1 The amended EIA directive

The concept of ecology is that of an all-inclusive living system, ranging from microorganisms to whales and including humankind. Any disruption of this system may have a chaotic effect, causing extensive negative effects throughout the system.

Works are bound to cause an impact, and when they are carried out on an unknown environment, difficult to monitor and to control, the hazard is larger since it is unclear what the extent of the impact may be.

Together with the additional impacts, the benefits must be assessed.

It is not infrequent that the building of renewable energy plants in place of traditional ones may become advantageous, but it's necessary to mitigate the impact in the long run and to do so an environmental impact assessment is required.

EIA (=environmental impact assessment) is the process to understand and evaluate the potential effects of a project from concept to decommissioning, and implement mitigation measures to attenuate the adverse impacts. EIA has been a requirement in EU law since 1988 and, since its implementation, it has undergone four amendments (i.e. 1997, 2003, 2009 and 2014).

EIA must be intrinsic with the project (not after the project), and public in order to allow the consultation to ensure interested parties or stakeholders are participating and contributing with concerns and opinions to the decision-making. So it's important to obtain public input into decisions by providing information.

EIA should be approved/rejected within 90 days. Therefore, it is a recommendation (not mandatory) to engage with the Regulators and its consultees prior to submitting an application.

The EIA is developed in 3 phases:

- **Screening:** determine whether an EIA is required;
- **Scoping:** determine content and extent of the matters that should be covered;
- **Impact analysis:** characterization or the analysis of the existing environmental and socioeconomic conditions in the impact area.

EIA is needed where the public or private project has some significant impact and where the Member Authorities have the discretion to decide based on a "Screening" procedure in projects such as: industrial installations for the production of electricity, installations for the harnessing of wind power (wind farms), construction of harbours, port installations and marinas. So it’s reasonable to think that also MRE devices (WECs and TECs) are between them.

So focusing on MRE devices, the project’s impact is produced:

- <u>During the installation and dismissal of a project:</u> such as the damage to the bed due laying of the power cable and mooring system, etc...
- <u>During the operation phase:</u> physical Impact (waves, currents, downstream sediment dynamics,…), impact on biota (turbines striking mammals and fishes); noise impact,
- continuous vibration; direct or indirect impact on birds migration path; impact on population (damage to fishing activity; use of space,...)
- <u>During maintenance:</u> direct impact of operations; production of waste materials,...
- <u>Impact in case of failure:</u> oil spill, direct damage, etc...

As said, the EIA contains the description of the project, the adopted mitigation measures, but also the description of the aspects of the environment likely to be significantly affected by the project, including (Art 3, Paragraph 1):

a) population and human health; b) biodiversity; c) land, soil, water, air and climate; d) material assets, cultural heritage and the landscape; e) the interaction between the factors referred to in points (a) to (d).

So the following information must be collected:

- Physical aspects: Soil, water, air, climate and the landscape (wave, current, sediment transport, with possible deposition/erosion, turbidity, erosion);
- Population, socio-economic aspects, fauna and flora, noise, continuous vibration, electromagnetic fields, visual impact. Effect on marine life (main threat is to alter bird / fish migration due to vibrations), but also on shipping (transportation) and on commercial fishing; pollution from machinery (oil, paintings, toxic antifouling coating).
- Material assets and the cultural heritage (old relics buried under the sediments);

- Interactions (e.g. documented effect of turbidity on marine life).

Let’s see more in detail the MRE devices environmental assessment.

11.2 MRE environmental assessment

Tidal energy converter devices, as all the kind of marine renewable energy (MRE), harnesses energy from the ocean and provides a low-carbon sustainable energy source. The MRE industry is in the early stages of development and although it supports climate change mitigation, there are concerns that MRE devices and systems could affect portions of the marine environments.

The researchers examining MRE interactions with animals, habitats, and ecosystem processes has generally coalesced around two terms:

- **stressors** (i.e., those parts of an MRE system that can cause stress, injury, or death)
- **receptors** (i.e., marine animals, habitats, and ecosystem processes).

After about a decade of research, the stressors that appear to present the greatest risk include the moving blades on turbines, as well as potential interactions with mooring lines, anchors or foundations, power export cables, and the emissions and interactions that can result from any of these parts. The receptors include the marine animals living in and traversing the vicinity of an MRE development; the habitats into which the devices are deployed; and oceanographic processes, such as the natural movement of waters, wave heights, sediment transport, and the concentrations of dissolved gases and nutrients that support marine life.

It is the interaction of stressors and receptors that can be examined.

The stressor-receptor interactions considered are those for which researches have been directed to assess the level of risk to animals, habitats, and natural processes, and to attempt to decrease the level of uncertainty around these interactions.

Interactions that needs to be taken into account are:

1. Collision risk with turbine blades;
2. Effects of underwater noise on animals;
3. Effects of electromagnetic fields (EMF) on animals;
4. Changes in benthic and pelagic habitats;
5. Changes in oceanographic processes;

6. Entanglement of animals with mooring systems;
7. Sediment resuspension;
8. Chemical pollution;
9. Social and economic impact;
10. Archaeological concerns.

Let's see them more in detail.

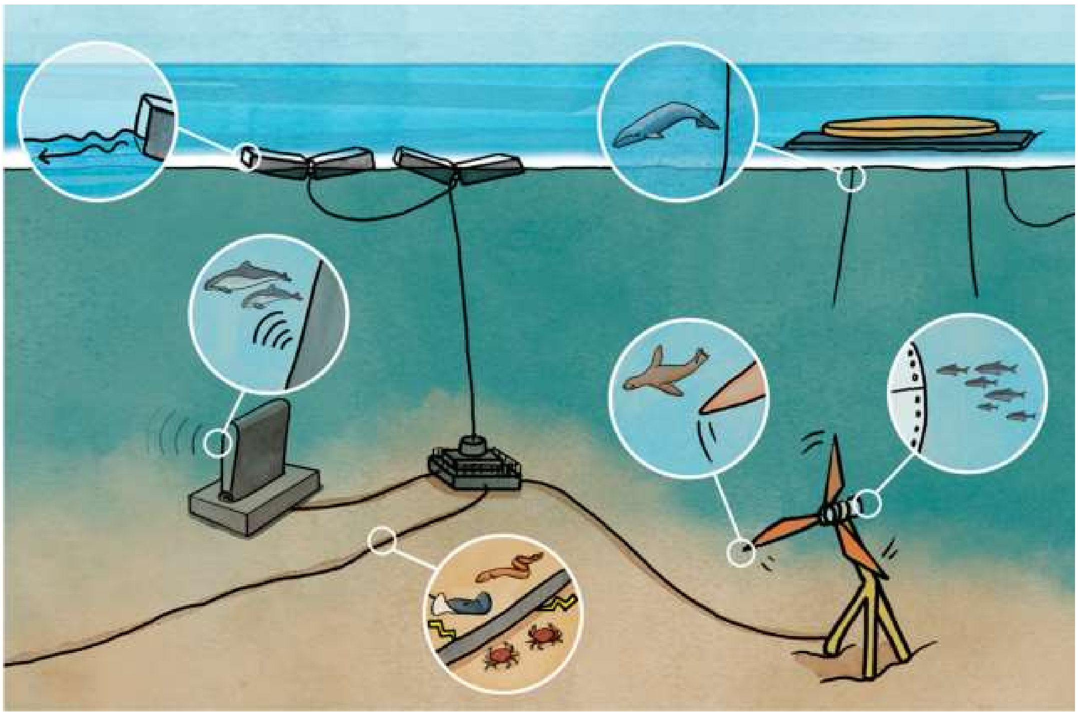

Figure 78:MRE environmental impacts

1. Collision risk with turbine blades

The potential for marine animals to encounter and collide with tidal turbines continues to present challenges for permitting developments due to the associated uncertainty and knowledge gaps related to collision risk. To date, knowledge of the actual risk of collision to marine mammals, fish, and seabirds with turbines is limited because the frequency of occurrence and consequences are unknown.

Much of the research that focuses on collision risk examines marine mammals and fish in the vicinity of turbines, although challenging oceanographic conditions in turbulent and often murky tidal waters make direct observations very difficult.

The probability of "serious injury" from collision risk to marine animals varies by species and the amount of space the turbine takes up in a passage.

To date, even if no collisions of marine mammals or seabirds have ever been observed, and only a few observations have shown fish in contact with turbines or other MRE infrastructure, the collision risk remains a key issue.

Studies on tidal energy turbines showed that if the blades are moving under certain velocity (3-4 m/s), collision risk is minimum, so the fishes are able to avoid them. While the most dangerous area is the red one and the risk can be mitigated by removing sharp edges (Figure 76).

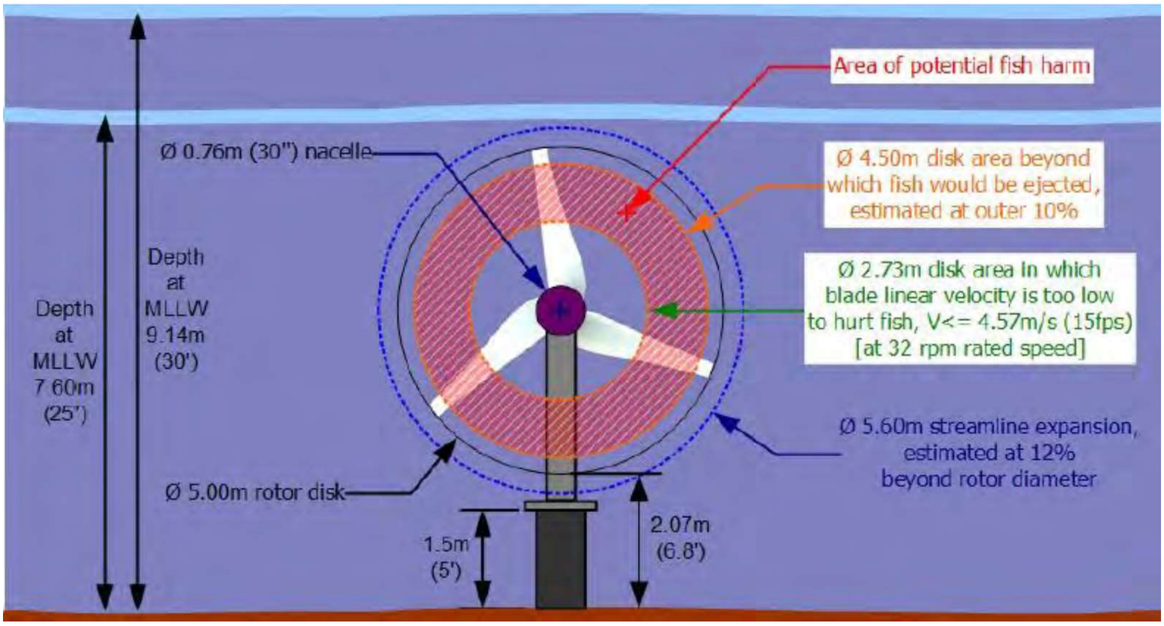

Figure 79:Collision risk with turbine blades

2. Effects of underwater noise on animals

Turbines produce operational underwater noise, most commonly from the power take-off systems or generators, although some sound may be produced from mooring systems in the water column as well. Noise emissions coming also from offshore construction activities, such as pile driving, may cause considerably more stress to marine animals.

These anthropogenic sounds in the marine environment may affect the way that many marine animals interact with their surroundings and may also affect communication, social interaction, orientation, predation, and evasion. Impacts may include auditory masking, stress, behavioural changes, acoustic responses or injuries, and, in extreme cases, barotrauma or death. Risks to marine animals from anthropogenic sounds, including the operation of MRE devices, vary with the amplitude, frequency, and directionality of the noise source, as well as propagation losses, prevailing ambient noise, animals' hearing thresholds, and possible behavioural responses.

To date, there is no evidence that operational noise from MRE devices harms marine animals physically or behaviourally, although there is a need to characterize the sound output from additional types and designs of turbines.

3. Effects of electromagnetic fields (EMF) on animals

The several anthropogenic activities create altered or additional sources of EMF, including those from MRE power export cables carrying electricity to shore. Export cables are commonly buried or laid on the seabed, while inter-device cables may be suspended in the water column. Measurements of the magnetic and induced electrical fields emitted from cables and energized devices are used to evaluate EMF emissions.

The response of marine animals to EMFs depends on the electro- and magneto-sensitivity of the animal. The probability of an encounter with an EMF depends on the animal's movement and distribution, life stage, and spatio temporal use of the environment where the EMF occurs.

Individual species' responses may include altered avoidance or attraction behaviour, and a variety of other behavioural, physiological, developmental, and genetic responses. So effect on the migratory and feeding habits of mammals and fish such as sharks, eels and rays, which use the Earth's geomagnetic field for navigational purposes.

The levels of EMF reported in many field and laboratory studies are much higher than those expected from MRE export cables and the evidence to date suggests that the levels are unlikely to keep animals away from their preferred habitats or affect migration patterns. There is a need, however, to better understand the likely EMF emissions from MRE cables, based on the configuration and electricity loads of specific cables, to identify potential effects, particularly as the MRE industry scales up to large-scale arrays. Although burial of cables and other measures such as placement of concrete mattresses are not considered to be effective ways to mitigate magnetic emissions into the marine environment, burial separates most sensitive species from the source of the emissions.

The effects of Electromagnetic fields from the generating equipment and transmission lines on marine life remain a highly controversial topic.

4. Changes in benthic and pelagic habitats

The installation of MRE devices generally requires gravity foundations, pilings, or anchors that may alter benthic habitats, along with mooring lines, transmission cables, and mechanical moving parts in the water column that may affect pelagic habitats.

The presence of these structures on the seabed or within the water column has the potential to alter species occurrence or abundance at a localized scale and may lead to artificial aggregating of animals or changes in animal behaviour. These changes may theoretically lead to indirect effects such as recruitment of non-native invasive species. This is called **artificial reef effect**, and it may spread at the ecosystem scale, affecting the structure and functioning of local and regional food webs in unknown ways.

'Reef effect' is usually considered to be a positive anthropogenic impact, as artificial reefs generally have higher densities and biomass of fish and decapod crustaceans than surrounding soft bottoms. Also, when associated with a fisheries exclusion area, artificial reefs may function as refuges for these populations, with potential spill-over benefits for fisheries.

On the other hand, reef effect may potentially result in long-term negative effects if the structures facilitate the introduction of non-indigenous sessile species. Indeed, the number of non-native species present on new hard artificial substrate can be 2.5 times higher than on natural substratum. Thus, the presence of a new hard substratum, such as a cable or its protection structures, on soft sediment can potentially open a corridor to a new area for some hard-bottom sessile species.

During MRE device installation, the loss of benthic habitat caused by the footprint of anchors and foundations can be avoided or mitigated when vulnerable habitats have been identified and avoided during the siting process. Cable laying or burial may also disturb habitats, but studies have shown that the benthic communities and habitats recover at about the same rate as natural growth and any negative effects are quickly dissipated with distance from MRE structures. While the ecological footprint of a single deployed MRE device may be relatively limited, an array of devices may act as a network of interconnected artificial reefs.

MRE projects may also act as **marine reserves**, which can promote the recovery of local species because their presence reduces fishing activity.

5. Changes in oceanographic processes

Tidal energy power generation devices will increase turbulence in the water column, which in turn will alter mixing properties, sediment transport and, potentially, wave properties. In both the near field and far field, extraction of kinetic energy from tides will decrease tidal amplitude, current velocities, and water exchange in a region in proportion to the number of units installed, potentially altering hydrography and sediment transport.

Moving rotors and foils have been shown to increase mixing in systems where salinity or temperature gradients are well defined. Tidal energy turbines may also modify wave heights by extracting energy from the underlying current.

6. Entanglement of animals with mooring systems

Many MRE devices require mooring systems (i.e., mooring lines, anchors) to maintain their position on or within the water column, and draped inter-array cables to connect devices to one another or to offshore substations. These mooring systems and cables may present entanglement or entrapment hazards for some marine animals.

The probability of an encounter between marine animals and MRE mooring systems and subsea cables is a function of the line or cable configuration and depth, and the animal's size and behaviour.

The animals considered to be most at risk of encounters with MRE mooring systems and subsea cables are large migratory baleen whales because of their migratory patterns and feeding behaviours.

MRE mooring lines and cables have no loose ends and are sufficiently taut that no looping can occur, and entanglement has not been considered a significant issue of concern within permitting processes for small numbers of MRE devices. However, the risk of animal entanglement in anthropogenic debris caught in MRE device moorings and subsea cables persists.

7. Sediment resuspension

Depending on the nature of the seafloor, sediment reworking by installation, maintenance or decommissioning of a MRE device and power cables can lead to turbid plumes that can reach several tens of hectares, with suspended particulate matter concentrations that can reach several dozen mg/l. Decrease in water transparency and deposition of the re-suspended material may limit light for primary producers and impact feeding ability of fish that detect their prey visually. The efficiency of invertebrate filter-feeding could also be temporarily modified.

8. Chemical pollution

The main chemical risk is the potential release of sediment-buried pollutants (e.g., heavy metals and hydrocarbons) during sediment re-suspension caused by cable burial, decommissioning or repair works. The highest contaminant concentrations are generally located in coastal areas due to human activities. A preliminary analysis to assess the level of sediment toxicity should be performed in potentially polluted areas to select a cable route which avoids the remobilisation and dispersion of pollutants.

9. Social and economic impact

MRE development can bring social and economic benefits to a region, including the stimulation of economic development, production output, regional development, along with the generation of employment and revenue. However, if not carefully and sensitively sited and implemented, MRE development could have adverse social and economic impacts including conflicts with existing marine uses (such as with local fishing and recreation), visual obstruction, and economic effects. All Marine Converters must be mapped, and all vessels, large and small, are required to keep clear for a space of usually 1000 m in diameter.

10. Archaeological Concerns

Civilization arise mostly along coasts. These seas were 100 m lower 15'000 years ago, and so the coasts that existed are now submerged, so many relics lie buried in coastal sediments. Pipeline excavation is critical in such areas very likely for stream-type TECs projects, in places where the strong currents may have caused shipwrecks. In case of a discovery, the national laws require that work be ceased until the local archaeologists have removed the relic.

11.3 GEMSTAR's environmental assessment

As previously said this device is positioned under the waters of the Strait of Messina, where a small submerged ecosystem is hidden, so peculiar as to represent "a natural laboratory of the whole Mediterranean", thanks above all to its function as a "crossroads" between the two basins of the Mediterranean Sea and to the particular hydrodynamic and chemical-physical.

Furthermore, its particular shape and position on the border between the Ionian Sea and the Tyrrhenian Sea make the Strait an exceptional observation point for the migratory flows of numerous species moving between the two basins. Among these are the "great swimmers" such as tuna, bonito, imperial garfish and swordfish. The Strait is also a privileged passage point for numerous cetaceans, what Cetologists define as a "whale gate", i.e. an obligatory passage and a natural bottleneck that dolphins, fin whales and sperm whales cross to reach the area of the Aeolian Islands to reproduce. Also present in the Strait are the flat cap shark, some rare specimens of white shark or the sea eagle.

The high hydro-dynamism of the waters of the Strait and the particular currents that characterize it, with a continuous and incessant movement and slow mixing of waters, make this environment rich in fish species that now prefer warmer, now colder, now saltier waters, for reproduce and live. As mentioned before, the characteristic currents of the Strait, the "upright" (from North to South) and the "descending" (from South to North), are born thanks to the encounter/clash between the two Ionian and Tyrrhenian seas, which present different chemical-physical characteristics, and represent a fundamental factor in the diffusion of the species in this area.

The particular geomorphology of the Strait and the phenomena resulting from the currents, such as the upwelling of deep waters, combined with the strong sirocco winds and the favourable lunar conditions also give rise to the phenomenon of "beaching" of bathypelagic species. These species, which normally live at great depths (well below 200 metres) also due to their migrations along the water column mainly for the search for food, find themselves on the surface and then end up stranded by the wind, of wave motion and surface currents.

Knowing these informations, it's clear that is necessary to do the appropriate environmental considerations when proceeding with the device installation, in order to evaluate the possible solutions for mitigating the potential consequences on the marine environment, and so flora and fauna.

To assess the potential environmental impact of the GEMSTAR device and of its proposed mooring system, let's see which impacts needs to be taken into account and when it's possible how to mitigate them.

- <u>Changes in oceanographic processes:</u>

  The GEMSTAR, as tidal energy device, may increase turbulence in the water column, which in turn may alter mixing properties, sediment transport and, potentially, wave properties. The tidal energy turbines may also modify wave heights by extracting energy from the underlying current.

  The underwater anchorage leads to the creation of high turbulence zones around the structure itself, due to the high velocity currents that are present there, as showed through the OpenFOAM simulation.

  These recirculating areas could be dangerous for fishes and marine life, that's one of the reasons why a blunter anchor shape is preferable to a more angular one, since it allows to reduce areas of turbulence and mitigate the environmental impact.

  In addition, the combination of a such big anchorage and high velocity currents generates vertical velocities, which can be disturbing too.

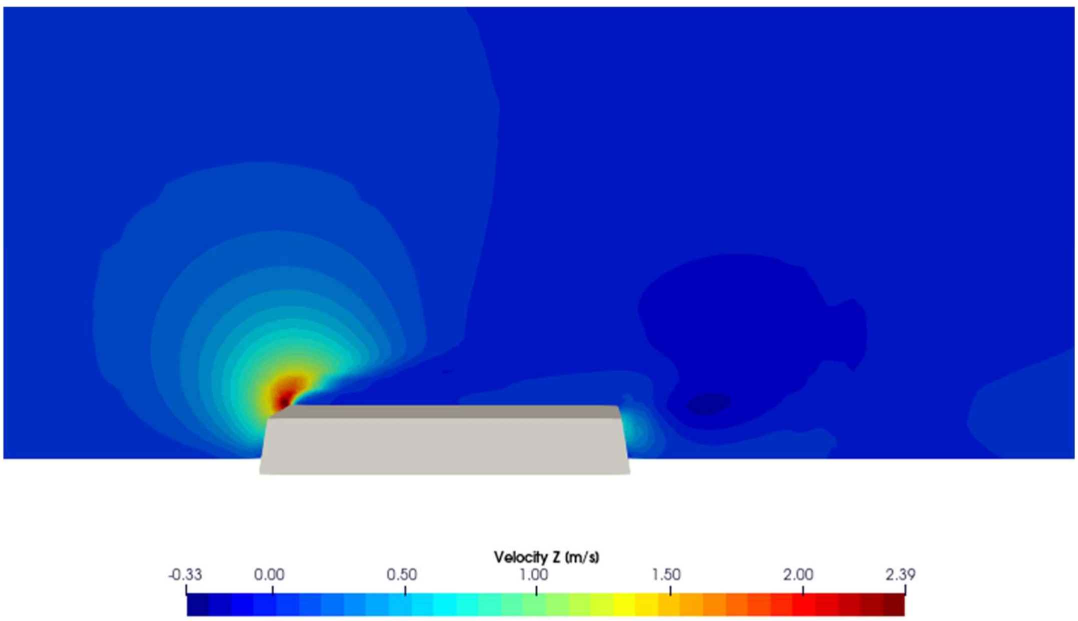

Figure 80:Veltical velocity field

- Entanglement of animals with mooring systems:

  The GEMSTAR device requires a mooring systems (i.e., mooring lines, anchors) to maintain its position within the water column, and power export cables. These mooring systems and cables may present entanglement or entrapment hazards for some marine animals, but being just a single device, the entanglement has not been considered a significant issue.

  The proposed mooring system is a taut line system, and not a catenary one. This configuration does not lay on the seabed, so the avoidance of contact with the seabed of the taut mooring system has benefits: the mooring line does not damage the seabed and the benthic environment, and the seabed does not damage the line. This benefits both environmental concerns and maintenance requirements of the line.

- Changes in benthic and pelagic habitats:

  The footprint of the anchorage can lead to substratum alterations, and it may affect related benthic communities by direct impacts such as displacement, damage or crushing of organisms.

  The substratum alterations are created by equipment used for cable route preparation and installation of the cable too. However, such effects are restricted to a limited area, the intensity of disturbance, depending on the installation method.

  It could be avoided or mitigated identifying the possible presence of vulnerable habitats, and so avoiding them during the siting process.

  Like for other immersed objects, the anchorage, the unburied submarine power export cables and associated protection/stabilisation can create artificial reefs, inducing the ‘reef’ effect with its positive and negative aspects, as explained previously.

- Power export cables and the effects of electromagnetic fields (EMF) on animals:

  Also for the GEMSTAR, the power export cables are necessary to carry electricity to shore.

  Before any deployment, the cable route must be chosen, depending on the bathymetry, seabed characteristics and economic activities of an area. The route must first be prepared, sometimes with adjustment of the slope and depth, or removal of obstacles before the passage of the cable-laying device.

During installation, maintenance and decommissioning phases, these effects may include physical habitat disturbances, sediment resuspension, chemical pollution and underwater noise emission. More long-term effects may occur during the operational phase, with changes in electromagnetic fields, risk of entanglement, chemical pollution, and creation of artificial reef and reserve effects.

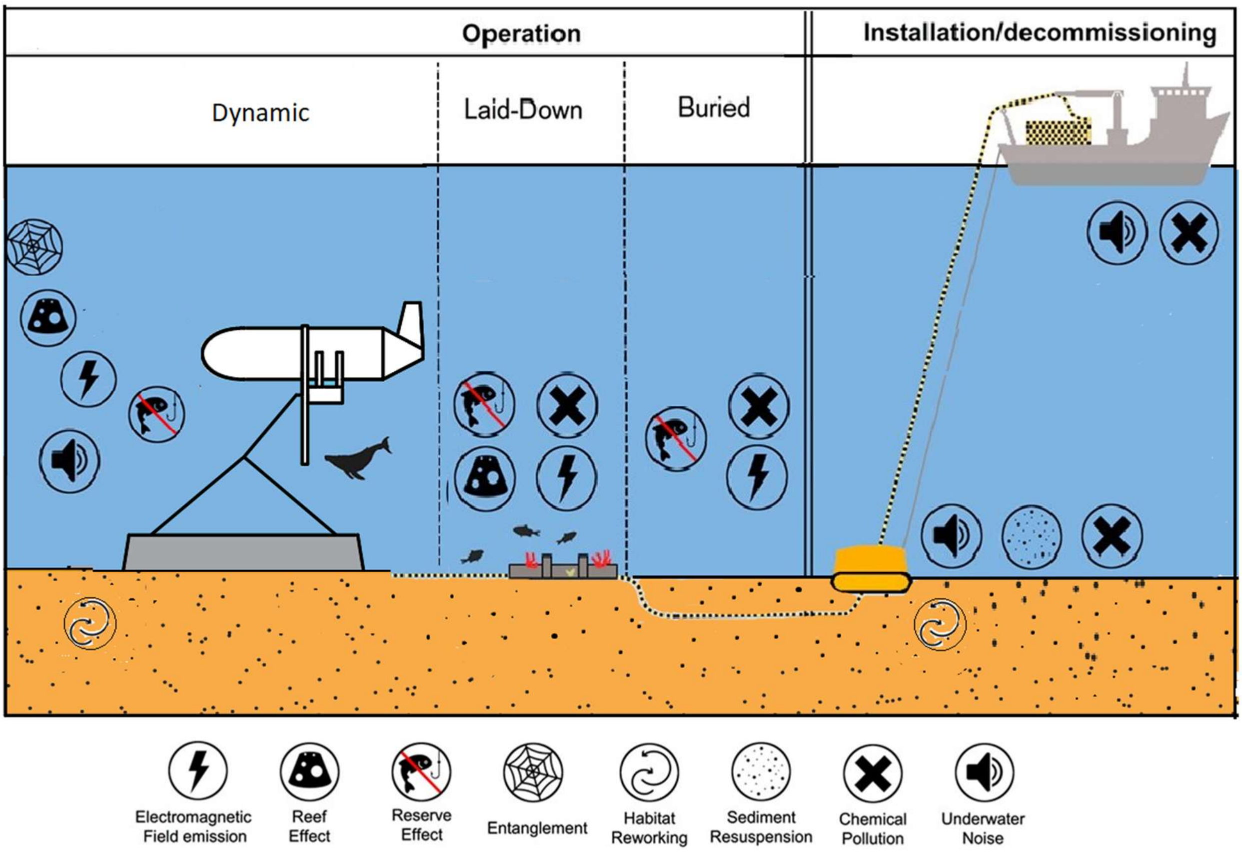

Figure 81:Power export cables impact on the different phases

The potential ecological impacts of EMF are of particular concern. Many marine species around the world are known to be sensitive to electromagnetic fields. Thus, submarine power cables can possibly interact in a negative way with sensitive marine species, especially benthic and demersal organisms through: effects on predator/prey interactions, avoidance/attraction and other behavioural effects, effects on species navigation/orientation capabilities, and physiological and developmental effects.

Moreover, the physical presence of an unburied cable, a cable that is simply laid on the seabed, can result in both the creation of a new artificial habitat and the alteration of the surrounding natural habitat. Alternatives to the unburied cables are the various associated protection or stabilising structures, such as: concrete mattresses, riprap and protection shells, and they could provide a new substrate that is subject to biological colonisation.

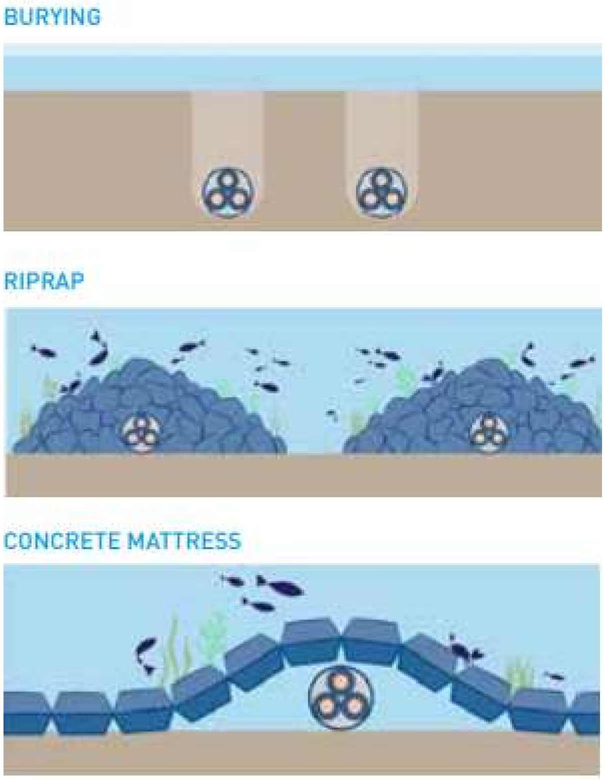

Figure 82:Main laying techniques for subsea power cables

- <u>Effects of underwater noise on animals:</u>

The installation of the GEMSTAR mooring system doesn't require pile driving, since it is a dead weight anchor and so laid on the seabed, but still, noise emissions coming from the construction activities, may cause a considerable stress to marine animals.

The two turbines produce operational underwater noise, and although there is no evidence that operational noise from turbine devices harms marine animals physically or behaviourally, there is a need to characterize the sound output from this device.

- <u>Social and economic impact:</u>

The GEMSTAR could bring social and economic benefits to a region, including the stimulation of economic development, production output, and regional development. As for all the MRE devices, it could have adverse social and economic impacts too if it includes conflicts with existing marine uses, such as with local fishing and recreation.

A positive aspect of this device is that being a submerged structure, it doesn't interfere with the naval traffic of the strait, and only during the maintenance phase it is raised to the water surface. Furthermore, it is also an attractive alternative in locations where keeping a good aesthetics is a constraint.

- Archaeological concerns:

The bathymetric and stratigraphic results don’t show the presence of archaeological remains on the concession area.

Chapter XII

CONCLUSIONS

Thanks to this work of thesis, it was possible to determinate the pressure forces acting on the considered mooring system, through OpenFOAM. These forces must be considered on the design process of the anchor, and so verify if the proposed structure is actually able to resist to them during its operative life time, without risking any structural problem.

Through the shape design analysis, it’s clear that a blunter and with inclined faces (trapezoidal profile) shape structure can better satisfy:

- the structural requirements, contributing to the stability of the underwater body thanks to the inclined frontal faces, through which it was possible to obtain a down force exploiting the water current;
- the hydrodynamic requirements, reducing the recirculating zones and so the vortexes on the frontal, top and rear areas around the structure, thanks to the blunt edges of the structure.

So a more hydrodynamic shape, and so with a low drag coefficient, is the best resulting shape for the analysed case study, considering also the imposed from the limitations in the realizing phase of the anchor.

The environmental assessment allows to be more aware of what installing a big structure in a certain environment means, and at the same time trying to find the best solutions to mitigate the potential consequences on the environment itself. The environmental assessment made will gain even more meaning if the project will be spread on large scale in the future, building an energy farm.

The relevance of this thesis is that it was able to develop a method and tool, through OpenFOAM, applicable to any structure, not only calculating the forces but also reproducing the hydrodynamic conditions at which the structure is subjected to, and so making the best design choices about the shape and the realizing process of the structure itself.

Chapter XIII

BIBLIOGRAPHY

Chaplin C. R. (2001). Torsional failure of a wire rope mooring line during installation in deep water. Failure analysis case studies II, 45-60.

Coiro D., Coppola M., Di Noia L. P., Troise G., Bizzarrini N., Lazzerini G. (2019), Coupling fixed pitch rotor design to PMG de-fluxing control for GEMSTAR marine current turbine. IEEE, 680-689.

Coiro D., De Marco A., Scherilo F., Maisto U., Familio R., Troise G. (2009), Harnessing marine current energy with tethered submerged systems: experimental tests and numerical model analysis of an innovative concept. IEEE, 76-86.

Coiro D., Troise G. (2012), Stima della produzione energetica da correnti marine nello Stretto di Messina. Ricerca di Sistema Elettrico, 23-35, 42, 43.

Coiro D., Troise G., Ciuffardi T., Sannino G. (2013), Tidal current energy resource assessment: the Strait of Messina test case. IEEE, 213-220.

Copping, A. E., Hemery, L. G., Overhus, D. M., Garavelli, L., Freeman, M. C., Whiting, J. M., ... & Tugade, L. G. (2020). Potential environmental effects of marine renewable energy development—the state of the science. *Journal of Marine Science and Engineering*, *8*(11), 879.

Cucco, A., Quattrocchi, G., Olita, A., Fazioli, L., Ribotti, A., Sinerchia, M., ... & Sorgente, R. (2016). Hydrodynamic modelling of coastal seas: the role of tidal dynamics in the Messina Strait, Western Mediterranean Sea. *Natural Hazards and Earth System Sciences*, *16*(7), 1553-1569.

Davidson J., Ringwood J. (2017), Mathematical modelling of mooring systems for wave energy converters – a review. Energies, 6.

Frid, C., Andonegi, E., Depestele, J., Judd, A., Rihan, D., Rogers, S. I., & Kenchington, E. (2012). The environmental interactions of tidal and wave energy generation devices. *Environmental Impact Assessment Review*, *32*(1), 133-139.

GEM | SeaPower (seapowerscrl.com)

GEMSTAR – LIGHTING UP THE FUTURE TOGETHER

Harris, R. E., Johanning, L., & Wolfram, J. (2004). Mooring systems for wave energy converters: A review of design issues and choices. *Marec2004*.

Longhitano, S. G. (2018). Between Scylla and Charybdis (part 1): the sedimentary dynamics of the modern Messina Strait (central Mediterranean) as analogue to interpret the past. *Earth-Science Reviews*, *185*, 259-287.

Longhitano, S. G. (2018). Between Scylla and Charybdis (part 2): The sedimentary dynamics of the ancient, Early Pleistocene Messina Strait (central Mediterranean) based on its modern analogue. *Earth-Science Reviews*, *179*, 248-286.

Maree (Ocean Tides: Introduction, Origin and Types | Ocean Tides | Geography (geographynotes.com))

Maree (What are tides? (noaa.gov))
Marine Power Project :: Marine Current Energy (strath.ac.uk)

MarineTraffic (www.marinetraffic.com).

Martinelli, slides

OpenFOAM user guide

Perri, F., Dominici, R., Le Pera, E., Chiocci, F. L., & Martorelli, E. (2016). Holocene sediments of the Messina Strait (southern Italy): relationships between source area and depositional basin. *Marine and Petroleum Geology*, *77*, 553-566.

Stretto di Messina. Wikipedia. (https://it.wikipedia.org/wiki/Stretto_di_Messina).

Taormina, B., Quillien, N., Lejart, M., Carlier, A., Desroy, N., Laurans, M., ... & Barillier, A. (2020). Characterisation of the potential impacts of subsea power cables associated with offshore renewable energy projects. SPECIES project (2017-2020): Review and perspectives.

The future of renewable energy | Minesto

Tidal devices : EMEC: European Marine Energy Centre

Tidal Energy - Definition, Characteristics, Uses, Advantages and Disadvantages (vedantu.com)

Tidal Power - Tidal Stream Generator
Tidal Power as a Predictable Energy Resource (alternative-energy-tutorials.com)